

**Surface water inundation mapping
By remote sensing for
Milingimbi Island, Northern Territory**

W. C. Nadeeka Wickramasinghe

Supervisors Prof. Okke Batelaan

Dr. Edward Banks

Thesis submitted in partial requirement for the degree of Masters of Science

(Water Resources Management)

16 November 2017

College of Science and Engineering

Flinders University



CONTENTS

Contents	ii
List of Tables	v
List of Figures.....	vi
Abbreviations	viii
Abstract	x
Declaration	xii
Acknowledgements	xiii
1. Introduction	1
1.1 Background	1
1.2 Problem statement.....	1
1.3 Objective of the research	4
1.4 Anticipated outcome of the study.....	5
2. Literature Review.....	6
2.1 Remote sensing of water	6
2.2 Spectral characteristics of water	10
2.3 Methods of water detection with satellite remote sense images	16
2.4 Accuracy assessment.....	26
3. Data and Methods	30
3.1 Study area	30

3.2	Data source	30
3.2.1	Remote sensing data.....	30
3.2.2	Rainfall data	33
3.2.3	Sea level data	40
3.3	Methodology	43
3.3.1	Data preparation.....	43
3.3.2	Image analysis and data processing.....	43
3.3.3	Unsupervised image classification	43
3.3.4	Supervised image classification	44
3.3.5	Normalised Differential Water Index.....	46
3.3.6	Modified Normalised Differential Water Index.....	47
3.3.7	Water area extracted from European Commission Joint Research Centre's Global Surface Water dataset (EC JRC-GSW).....	48
3.3.8	Accuracy assessment of identifying inundation area	49
3.3.9	Correlation between rainfall and inundation area	51
4.	Results and discussions	52
4.1	Extraction of water area on 01 Feb 2010	52
4.1.1	Investigating the spectral signature.....	53
4.1.2	Water extraction with different methods	54
4.1.3	Comparison of water extraction by different methods.....	56

4.1.4	Comparison of water extraction by supervised classification and $NDWI_{ref}$	58
4.2	Extraction of water area on 28 Oct 2003	62
4.2.1	Investigating the spectral signature	62
4.2.2	Water extraction with different methods	64
4.2.3	Comparison of water extraction by different methods	64
4.2.4	Comparison of water extraction by supervised classification and $NDWI_{ref}$	67
4.3	Discussion on surface water extraction	69
4.4	Performance of water extraction on multiple images	72
4.5	Accuracy assessment	75
4.5.1	Overall accuracy	75
4.5.2	Kappa coefficient	77
4.5.3	Figure of merits	78
4.5.4	Discussion on accuracy assessment	80
4.6	Correlation between rainfall and inundation area	82
4.7	Correlation between sea level and inundation area	86
4.8	Frequency of inundation	88
4.8.1	Frequency of wet season inundation	88
4.8.2	Frequency of dry season inundation	88
5.	Conclusion	92

5.1	Research findings.....	92
5.2	Limitations of the study.....	94
5.3	Outcome of the study.....	95
5.4	Recommendations for future researches.....	96
6.	Appendices	98
7.	References	114

LIST OF TABLES

Table 1. Band details of Landsat sensors	32
Table 2. Landsat images used for the study.....	33
Table 3. Comparison of daily rainfall between BOM and SILO data	34
Table 4. Rainfall data for the study area	36
Table 5. Comparison of extracted water area on 01 Feb 2010.....	58
Table 6. Comparison of extracted water area on 28 Oct 2003.....	67

LIST OF FIGURES

Figure 1 : Interaction of radiance and water features	8
Figure 2 : Spectral reflectance pattern of water, soil and grass	11
Figure 3 : Spectral reflectance curves of different objects on the ground	11
Figure 4 : Percent reflectance of clear and algae-laden water	13
Figure 5 : Percent reflectance of algae-laden water with suspended sediment	13
Figure 6 : Average spectral reflectance curves of water in five lakes.....	15
Figure 7 : Average spectral reflectance curves of water for different water quality.	15
Figure 8 : Spectral reflectance curves of lake water, vegetation and built-up land ..	18
Figure 9 : Spectral reflectance curves for typical water and shadow pixels.....	22
Figure 10 : Location of the study area, Milingimbi Island, NT.....	30
Figure 11 : Graph of daily SILO rainfall vs daily BoM rainfall	35
Figure 12: Daily rainfall available for Milingimbi Island in BoM and generated rainfall in SILO database from 1987 to 2016	38
Figure 13 : Daily rainfall used for the study from 1987 to 2016	38
Figure 14 : Daily rainfall distribution in four years.....	39
Figure 15 : Monthly mean sea level at Darwin.....	40
Figure 16 : Monthly mean sea level at Groote Eylandt.....	41
Figure 17 : Location map of SEAFRAME stations	41
Figure 18 : Sea surface height trend around Australia.....	42
Figure 19 : Spatial modeller for NDWI classification.....	46
Figure 20 : Spatial modeller for MNDWI classification	48
Figure 21 : Selection of ground data for accuracy assessment.....	50

Figure 22 : Spectral reflectance curves of different land features	53
Figure 23 : Spectral reflectance curves of different water features	55
Figure 24 : Extraction of surface water area on 01 Feb 2010	57
Figure 25 : Comparison of surface water area extracted on 01 Feb 2010 image	59
Figure 26 : Investigation of spectral reflectance curves at random pixels	60
Figure 27 : Comparison of spectral reflectance curves on 01 Feb 2010 image	61
Figure 28 : Investigation of Spectral reflectance curves on 28 Oct 2003 image	63
Figure 29 : Comparison of water area extracted on 28 Oct 2003	66
Figure 30 : Comparison of spectral reflectance curves on 28 Oct 2003 image	68
Figure 31: Extraction of inundation area on thirteen images	72
Figure 32: Overall accuracies of different methods	75
Figure 33: Kappa coefficients of different methods	77
Figure 34: Estimation of Figure of Merits	79
Figure 35 : Extracted surface water inundation areas by supervised classification ..	82
Figure 36 : Investigating surface water inundation areas and rainfall	83
Figure 37 : Correlation between inundation area and cumulative rainfall	84
Figure 38 : Daily rainfall and extracted surface inundations in 2014	85
Figure 39 : Average monthly sea level variation recorded at Darwin tidal gauge and dry season surface water inundation area in Milingimbi Island for years 2003, 2011, and 2016	87
Figure 40 : Average monthly sea level variation recorded at Groot Eylandt tidal gauge and dry season surface inundations in Milingimbi Island for years 2003, 2011, and 2016	87
Figure 41 : Wet season inundation areas and the frequency	89
Figure 42 : Dry season inundation areas and the frequency	90

ABBREVIATIONS

ASTER	-Advanced Spaceborne Thermal Emission and Reflection Radiometer
AWEI	- Automatic Water Extraction Index
BoM	- Bureau of Meteorology
DN	- Digital Number
EC JRC-GSW	- European Commission Joint Research Centre Global Surface Water
EMR	- Electromagnetic Radiation
ETM	- Enhanced Thematic Mapper
FoM	- Figure of Merits
GEE	- Google Earth Engine
ISO DATA	- Iterative Self Organizing Data Analysis Technique
NASA	- National Aeronautics and Space Administration
NDWI	- Normalized Difference Water Index
NDWI _{ref}	- Water index NDWI applied on the surface reflectance image
NDWI _{DN}	- Water index NDWI applied on the DN image
NIR	- Near Infra-red
nm	- Nanometre
NWI	- New Water Index

m	- Metre
MIR	- Mid Infrared
MNDWI	- Modified Normalized Difference Water Index
OLI	- Operational Land Imager
SEAFRAME	- SEA-level Fine Resolution Acoustic Measuring Equipment
SWIR	- Short wave Infrared
TCW	- Tasseled Cap Transformation
TM	- Thematic Mapper
USGS	- United States Geological Survey
WRI	- Water Ratio Index
μm	- Micrometre

ABSTRACT

Surface water is the most accessible source of water for humans. It is affected by both climate change and human activities. In situ data are not regularly available for detecting the changes in surface water. Satellite remote sensing and GIS techniques facilitate the investigation of surface water changes and overcome the lack of in situ data. The goal of this study was to use images of Landsat 5 Thematic Mapper (TM), Landsat 8 Operational Land Imager (OLI) and inundation maps from European Commission Joint Research Centre Global Surface Water (EC JRC-GSW) monthly water history database to extract and assess accuracy of mapping surface water in Milingimbi Island, Northern Territory, Australia during the period from 1987 to 2016. On the island, the spatial distribution of shallow surface water inundation of salty land is changing frequently. No previous study has been performed on surface water inundation on Milingimbi Island. Initially, surface water area was extracted from thirteen images by unsupervised and supervised image classifications, Normalised Difference Water Index (NDWI), and Modified Normalised Difference Water Index (MNDWI). Surface water for each respective month was also extracted from the EC JRC-GSW monthly water history maps. Then surface water area was extracted by supervised classification from another 11 images for both wet season (Dec- April) and dry season (May- Nov). During the wet season, cloud cover has affected almost all the wet images and the possibility to extract inundation areas during the wettest moments was limited.

The extracted water area from unsupervised, supervised classifications and MNDWI methods was very similar, while the area based on the NDWI method and EC JRC-GSW corresponded closely. There were significant differences in area between the two groups. The accuracy assessment showed the highest accuracy for the supervised classification. One of the study objectives of using EC JRC-GSW data as a time series of monthly surface water area for investigating the surface inundation process was not successful.

For wet season inundations, the correlation (although relatively low) between surface water area and rainfall was comparatively best with sixty days cumulative rainfall. Most of the dry season inundations were observed on days with zero or insignificant rainfall. Spatial distribution of inundations were mapped separately for wet and dry seasons. The inundation areas of higher frequency are different in wet and dry season. There is no sea level monitoring station in Milingimbi to investigate the correlation of sea level and dry season inundations. When referred to nearest SEAFRAME (SEA-level Fine Resolution Acoustic Measuring Equipment) station in Darwin, the sea level is the highest during the months of October and November. This study recommends use of non-optical satellite remote sensing for improving future inundation mapping in Milingimbi Island in investigating wet season characteristics and monitoring the sea level, and establishing accurate elevation data to investigate dry season inundation.

Key words

Surface water, Remote sensing, Unsupervised / Supervised Classification, NDWI, MNDWI

DECLARATION

I certify that this thesis does not incorporate without acknowledgment any material previously submitted for a degree or diploma in any university; and that to the best of my knowledge and belief it does not contain any material previously published or written by another person except where due reference is made in the text.

Signed : W. C. N. Wickramasinghe

Date : 16/ 11 /2017

ACKNOWLEDGEMENTS

I would like to express my gratitude and respect to my supervisor Prof. Okke Batelaan and co-supervisor Dr. Edward Banks for their invaluable guidance, support and encouragement. This study is an outcome of their valuable insights, constructive comments, and the time spent on reviewing my work. It is indeed a pleasure to work with them.

I would like to express my sincere thanks to Mr. Robert Keane for the guidance on GIS processing, Mr. Lanre Abiodun for guidance in using SILO data and Mr. David Langdon for language editing. I would like to acknowledge the use of data from BoM, USGS and EC JRC/Google for this study. This study acknowledges the traditional owners and custodians of the lands of Milingimbi Island.

I would like to express my sincere thanks to all the lecturers in the Masters of Water Resources Management programme and would like to mention Prof. Andrew Milington, Mr. Stephen Fildes and Dr. David Bruce for introducing me the remote sensing techniques. This knowledge was a great resource in this study. Also, I would like to express my gratitude to the Government of Australia and the Government of Sri Lanka for granting this valuable opportunity for me to study in Flinders University.

I appreciate all my friends for sharing memorable time during this period. Finally, thanks to my family; father, brothers and sisters for their wishes and encouragement, my late mother for her shadow with us. Thanks to my lovely sons, Harindu and Randil for their understanding and love during my studies. My deepest gratitude to my loving husband Kithsiri, without his continuous support and encouragement this study would not be possible.

1. INTRODUCTION

1.1 Background

The integrated influence of climate change and anthropogenic activities have considerably affected the water cycle (Lawford 2008; Pekel et al. 2016; Xia et al. 2017). Such impacts influence the environmental evolution of soil and water (Chahine 1992; Herrick, Sala & Karl 2013; Oki & Kanae 2006). Sea level rise is a major impact of climate change (Mimura 2013). McInnes et al. (2013) say since 1800 the sea level has been rising at an increasing rate. Two major threats caused by the changes in sea levels are the inundation of coastal land and degradation of fresh water resources (Mimura 2013).

1.2 Problem statement

Milingimbi Island is in the Arafura Sea in the Northern Territory and is the largest island of the Crocodile Island Group. The island covers approximately 50 km² of area in which the highest elevation is about 16 m above mean sea level in the central part of the island. Extensive saline mud flats surround the higher parts of the island (Woodgate 2013). The central part of the island is covered with vegetation. There are several tidal creeks, which are bounded by mangrove forest. Surface water exists within the tidal creeks and a brackish billabong. There are no fresh water features (Woodgate 2013). Currently, 1600 Indigenous people live on the island. Water is a scarce resource on the island and the drinking water supply depends solely on a shallow fresh water aquifer beneath the island (Batelaan et al. 2015).

There are three main aquifers beneath the island: a near surface aquifer, central aquifer and a deep aquifer separated by two aquitards. The near surface aquifer is too small and shallow for water supply. The central fresh water aquifer is shallow and current community water supply depends on this aquifer. The deep aquifer is more saline. According to present data, the central and the deep aquifers are present only in the central portion of the island. There is noticeable increase in the salinity level in the central aquifer, according to groundwater samples from the monitoring network. If the pumping is increased, there is a possibility of contaminating the central aquifer due to upward leakage from the saline aquifer. Also the central aquifer is vulnerable to saltwater intrusion from the sea (Batelaan et al. 2015).

Milingimbi Island is in a tropical climate zone with distinct wet and dry seasons. The island receives a high rainfall in the wet season from November to April with an average annual rainfall of 1090 mm. Almost no rainfall occurs during the dry season from May to October. Groundwater recharges mainly during the wet season. The proportion of groundwater recharge, evapotranspiration loss and lateral flow to the coast is unknown (Batelaan et al. 2015).

People of 'Yolngu' group has been living on Milingimbi Island for over 40,000 years. In 1923, the Methodist Overseas Mission established the settlement. When Milingimbi Island was bombed during World War II, the residents moved to Elcho Island. The settlement was re-established in 1951. Currently, the majority of the people live on the eastern side, in a small township and there is also a small out station in the central northern part of the island (Woodgate 2013).

Other than the tidal creeks and the brackish billabong called 'Nalajrwa', seasonal surface water exists over the mud flats (Woodgate 2013). Spatial and temporal

distribution of surface water on the island has not been studied. According to Augustine (1960), 'Nalajrwa' water hole is very deep and tested sodium chloride content of the water was very close to sea water. Woodgate (2013) says the billabong is expected to be connected to the adjacent aquifer. Billabong water has Na-Cl type signature and its high salinity may be a result of evaporative concentration of salts. According to a Charles Darwin University (2010) report on 'Milingimbi water' prepared by consulting Milingimbi residents, the small surface water areas, which are called wells, have fresh water in the wet season and the water gradually changes to saltier in the dry season. The limited knowledge on surface inundation areas, which have saline water, has created a potential risk of contaminating the fresh water aquifer.

Seasonal surface inundation in the coastal area has contributed to the degradation of the limited land resources of the island. Extending the area of saline mud flats into the recharge area of the aquifer lead to contamination of the groundwater. In addition, the projected population will be 2300 by the year 2030 (Batelaan et al. 2015). The quantity and the quality of the groundwater will be critical to meet the demands of the future population. Woodgate (2013) says that some years it was difficult to meet the water demand during the driest months. The increasing population will face difficulties in the future with the already limited fresh water resources of the island. According to Batelaan et al. (2015) desalinisation projects are not feasible to meet the fresh water requirement. Milingimbi residents highly respect and value their traditional land and water. They believe their ancestors secured water for generations with their traditional knowledge (Charles Darwin University 2010). As a consequence of these developing circumstances, there are high social, cultural and

economic aspects in investigating the water resources in Milingimbi Island to develop better water management plans.

1.3 Objective of the research

The objective of this study is to identify the surface water inundation process of the island during the 30 years period from 1987 to 2016 and determine if rainfall and/or tidal waves were the cause of surface water inundation.

To achieve this objective, Landsat images from the United States Geological Survey (USGS) are used to identify water areas by applying image classification or water indices in order to identify the spatial and temporal distribution of surface water area. The surface water inundation of Milingimbi Island from the monthly water history maps of the European Commission Joint Research Centre – Global Surface Water (EC JRC-GSW) are used to compare with the extracted inundation areas from this study. The suitability of EC JRC-GSW data will be assessed for use as a data source for monthly surface water inundation areas in Milingimbi Island.

1.4 Anticipated outcome of the study

With this study, it is expected:

- To assess the suitability of EC JRC-GSW monthly water history data to estimate the surface water inundation of Milingimbi Island;
- To gather comprehensive knowledge on the behaviour of seasonal surface water in Milingimbi Island, which has not been explored so far;
- To identify the possible risk of contaminating the fresh water aquifer from surface water inundation;
- To identify future research areas on the surface water inundations.

2. LITERATURE REVIEW

2.1 Remote sensing of water

Surface water is the most accessible water resource for the human population (Pekel et al. 2016). Surface water has been a vital resource for the development and the existence of human civilization (Lawford 2008). It is equally important for the sustainability of the environment and the ecosystem (Huang et al. 2016). Surface water is affected by both climate change and human activities (Lawford 2008; Pekel et al. 2016; Vorosmarty et al. 2000). The knowledge of the location, extent and the recurrence of surface water is required in water allocation and resource management (Khawlie et al. 2005). The change in surface water has many impacts on the human social behaviour, related to domestic needs, agricultural production, urbanization, water management and eco system balance.

Lawford (2008) says in-situ data are the best reliable source in analysing the impacts on surface water. Sometimes in-situ data are collected through specific studies and not regularly available due to lack of technology. Satellite remote sensing augments ground-based data, with earth surface observations for many decades. It has overcome the time-consuming traditional manual work and high cost in detecting the spatial distribution of water. During the last twenty years, Satellite remote sensing has been widely used to monitor the distribution and the changes in surface water (Gao et al. 2016; Wang et al. 2011).

In different countries, researchers have used remote sensed data to study long term changes in surface water bodies (Gautam et al. 2015; Henry et al. 2006; Idol, Haack & Mahabir 2015; Mereuta 2015.; Rokni et al. 2015; Wu & Liu 2014) and surface inundation areas during floods (Henry et al. 2006; Zhou et al. 2000). According to

Leng et al. (2016), few studies have investigated the change detection of surface water and the possible impacts due to climate change. Spatial and temporal variation in the surface water extent should be a research strand of climate change impact (Prigent et al. 2012). Pekel et al. (2016) have studied the changes in global surface water for 32 years, using satellite images. Alsdorf, Rodríguez and Lettenmaier (2007) says remote sensing is the only source of data to study the spatial and temporal distribution of global surface water.

According to the Centre for Remote Imaging, Sensing and Processing, at the National University of Singapore (CRISP 2001), remote sensing is a technology of observing objects at distance by the sensors that are not in direct contact, normally by using the electromagnetic radiation for carrying the information. In satellite remote sensing Earth objects are observed with electromagnetic radiation captured by the sensors in the satellite and resulting products are images. The information about the ground objects is extracted by analysing and interpreting these images (Jensen 2014).

When the radiation from the sun (E_{Sun}) reaches a water body, a part of the radiation is reflected from the water surface (L_s). Some of the radiation penetrates the air-water interface, interacts with the constituents in the water and exits the water surface (L_v). Some radiation penetrates the water, reaches the bottom, and then propagates back and exits the water-air interface (L_b). Some radiation is scattered in the atmosphere without reaching the water surface (L_p). Figure 1 illustrates the water radiance interaction. The energy L_s carries spectral information about the surface characteristic. L_v has the characteristics of water column. L_b is important in bathymetric mapping of water bodies (Jensen 2014).

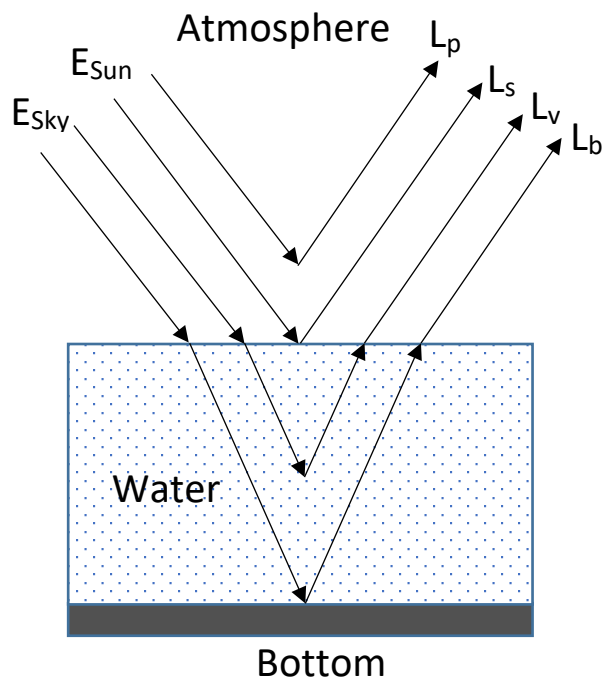


Figure 1 : Interaction of radiance and water features
(Jensen 2014)

In remote sensing of water, the radiance recorded by the remote sensor records the energy from all four sources L_s , L_v , L_b and L_p . The electromagnetic radiation is changed due to scattering and absorption by aerosols and gases when transmitting through the atmosphere from the Earth surface to the satellite sensor. The atmospheric effect is different in different wave bands, as both Rayleigh and Mie scattering depends on the wavelength (Richards & Jia 1998).

Recorded image data by sensors contains geometric and radiometric errors. Image pre-processing is done for corrections before an image is used for classifications (Richards & Jia 1998). Geometric errors are caused by the relative motion of the satellite, scanners and the earth, and curvature of the earth (Richards & Jia 1998). For the geometric corrections a standard geographic coordinate system is used to develop the geometric relationship with the image by selecting geometric ground control points on the image (Du, Teillet & Cihlar 2002) and typically corrected by the vendor.

Radiometric error is the change in measured brightness value of the pixel due to effect of the atmosphere, variations in the solar illumination angles, Earth-sun distance and the instrumentation used for recording data (Chen, Vierling & Deering 2005). There are two methods of radiometric corrections absolute and relative. Absolute radiometric correction uses sensor calibration data and an atmospheric correction algorithm based on modelling the atmospheric attenuation at the time of image acquisition to convert the image data in Digital Numbers (DN) to the reflectance at the surface (Du, Teillet & Cihlar 2002). Relative radiometric correction uses a base image to adjust the radiometric properties of the other images to reduce the atmospheric effect among multiple images. It is an image based method, which can correct the noise due to the atmosphere, sensor and other sources in one process and is simpler than the absolute method (Chen, Vierling & Deering 2005).

Accurate measurements of the atmospheric optical properties at the time of image acquisition is required for the correction of the atmospheric effect and these measurements are frequently unavailable (Richards & Jia 1998). According to Song et al. (2001), requirement of atmospheric correction depends on the analytical method for the information extraction and the atmospheric correction is not required when a single date image is classified with maximum likelihood classifier if the training data are derived from the image. However, it is required in the applications of multi-temporal images, such as change detection with image differencing. Also, atmospheric correction is required for indices, such as Normalized Difference Vegetation Index (NDVI) and Simple Ratio (SR), as the atmospheric effect is different in different bands (Song et al. 2001). In post-classification change detection,

atmospheric correction is not required as the resulting images are used to detect changes after the classification of the images separately.

In literature, both optical (passive systems) and radar (active systems) remote sensing have been used to detect surface water, with challenges for both systems (Martinis et al. 2015). In optical remote sensing, electromagnetic radiation (EMR) is captured by the sensors usually in visible, near infrared (NIR) and short wave infrared (SWIR) regions of the electromagnetic spectrum. Passive, visible infrared (VIR) and short wave infrared (SWIR) sensors are widely used due to data accessibility, and interpretability (Li et al. 2016). Landsat satellite images have been widely used in literature for water detection as the images are of medium spatial and moderate temporal resolution and provide continuous data for long-term analysis (Zhou et al. 2017).

2.2 Spectral characteristics of water

The reflectance of solar radiation depends on the objects on the ground. In optical remote sensing, objects are distinguished with the spectral reflectance pattern of the objects (Jensen 2014). Therefore, identifying spectral characteristics of different land cover types is important to distinguish water from other land features such as vegetation, soils, and buildings (Haibo et al. 2011). The spectral reflectance curve gives the percentage of energy that an object reflects in different wavelengths. Figure 2 shows the spectral reflectance pattern of water with grass and soil taken from the ASTER (Advanced Space borne Thermal Emission and Reflection Radiometer) spectral library. Figure 3 shows spectral reflectance curves of common ground objects extracted from Landsat ETM⁺ by Wen and Yang (2011). The spectral curves show that

water absorbs most of the radiation and show very low reflections in all wavelengths compared to other objects.

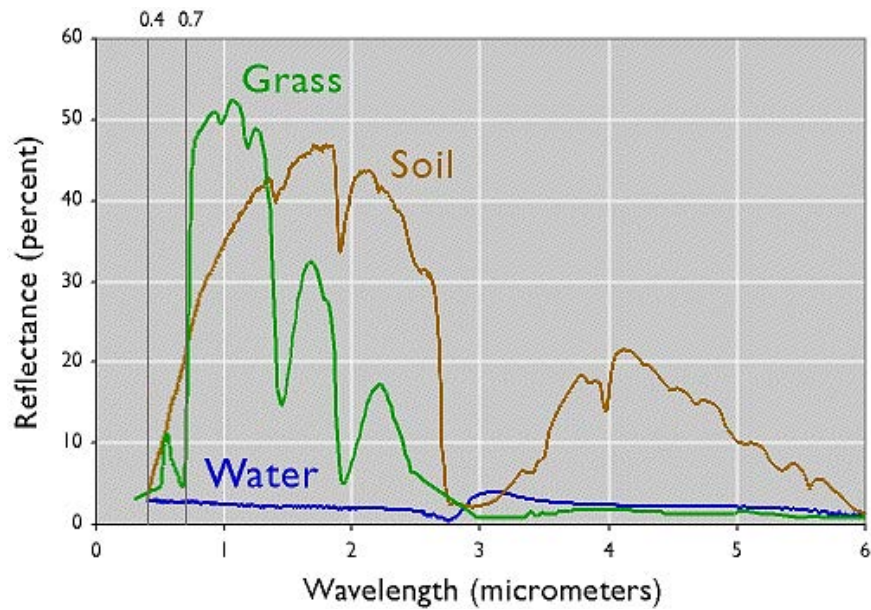


Figure 2 : Spectral reflectance pattern of water, soil and grass observed by ASTER sensor (<https://www.e-education.psu.edu> 2017)

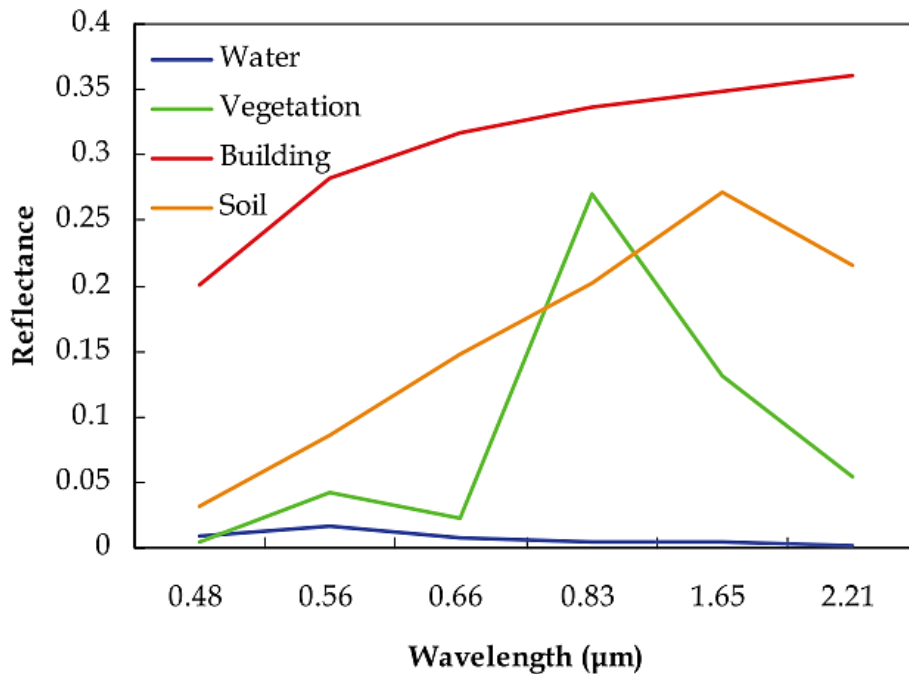


Figure 3 : Spectral reflectance curves of different objects on the ground extracted from Landsat ETM+ image (Wen & Yang 2011)

According to Jensen (2014), there are three important spectral characteristics of water. The least amount of absorption and scattering is in the blue wavelength (400-500 nm). Relatively little scattering and higher absorption takes place in green and yellow light (520-580 nm). Absorption is high and scattering is insignificant in orange and red wavelength energy (580-740 nm). Almost all the incident near infrared (NIR) and Middle infrared (MIR) (740-3000 nm) is absorbed in deep pure water. Therefore, the best wavelength to distinguish pure water from land features is the NIR and MIR wavelengths. At these wavelengths, the reflectance of vegetation and bare soil contrasts significantly to that of water.

The spectral reflectance of water changes due to the constituents in water. Organic and inorganic constituents of water, especially near the surface dramatically increase the NIR radiance leaving the water surface (Jensen 2014). Algae floating near the water surface reflect highly in NIR (Lillesand, Kiefer and Chipman (2004). Jensen (2014) shows that chlorophyll-a changes the spectral characteristics of water at four noticeable spectral regions. Figure 4 shows that algae-laden water has high absorption of blue light between 400-500 nm and red light at approximately 675 nm. There is a prominent reflectance peak around 690-700nm and another peak around 550 nm. There are dramatic changes in spectral reflectance when both suspended sediments (red loam for these curves) and chlorophyll occur in the water with significant increase in the green wavelength (Figure 5). It shows that peak reflectance in the visible region shifts towards longer wavelengths particularly increase at 700nm as shown in Figure 5.

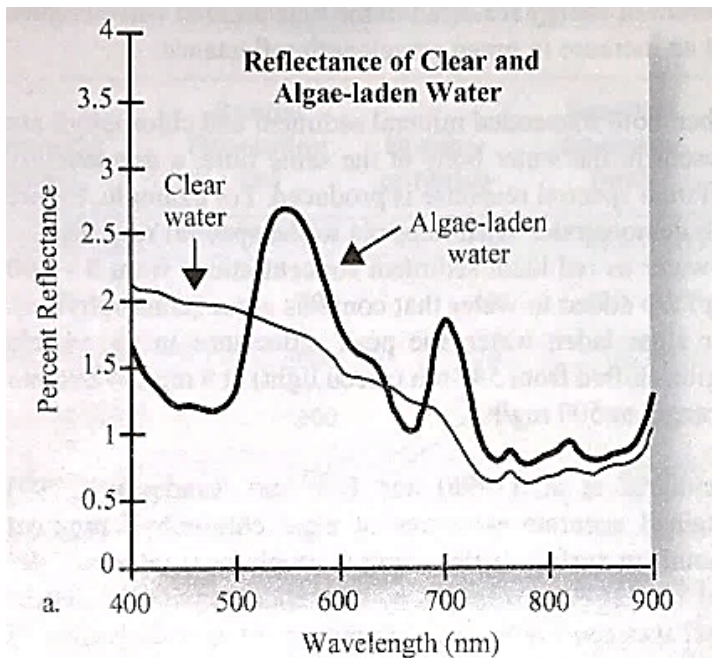


Figure 4 : Percent reflectance of clear and algae-laden water based on in situ spectroradiometer measurement (Jensen 2014)

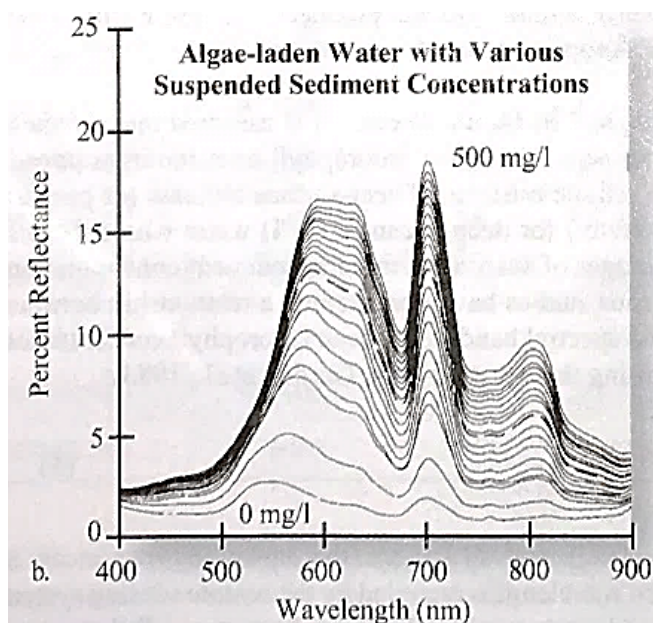


Figure 5 : Percent reflectance of algae-laden water with suspended sediment in various concentration ranging from 0-500 mg/l (Jensen 2014).

Spectral characteristics of water varies with hydrological, biological and chemical characteristics of water (Seyhan & Dekker 1986). The transmittance of water is high

in all visible wavelengths. It increases when the wavelength decreases and almost all incident radiation in NIR and then SWIR is absorbed by water. Van Der Meer and De Jong (2001) argue that suspended sediments, plankton and pigments in water increase the reflectance.

Many researchers have used Landsat images for monitoring constituents in water for assessing the water quality. According to Lavery et al. (1993), many researchers, such as Lathrop and Lillesand (1986), Dwivedi and Narain (1987), and Bagheri and Dias (1990), have found that there is a significant correlation between Landsat TM band 1, 2, and 3 with chlorophyll concentration in coastal and inland water bodies. Lavery et al. (1993) observed high correlations in algorithms developed with multiple regression analysis to monitor salinity in two estuaries using Landsat TM band 4 and band 7. Alparslan et al. (2007) derived formulae through regression analysis using the reflectance values of band 1, 2, 3, and 4 of Landsat 7 ETM images to assess the water quality parameters of Omeli reservoir. According to Pekel et al. (2016) the spectral properties of water vary according to the suspended solids and dissolved organic matter, chlorophyll concentration, depths and water body bottom material in shallow water at the wave lengths used by Landsat sensors.

Wen and Yang (2011) used stepwise multiple linear regression analysis in monitoring water quality in five lakes in China using Landsat ETM+ images. The average spectral reflectance curves for water in five lakes of different water quality are given in Figure 6. It shows that the spectral reflectance of water dramatically changes due to constituents of water.

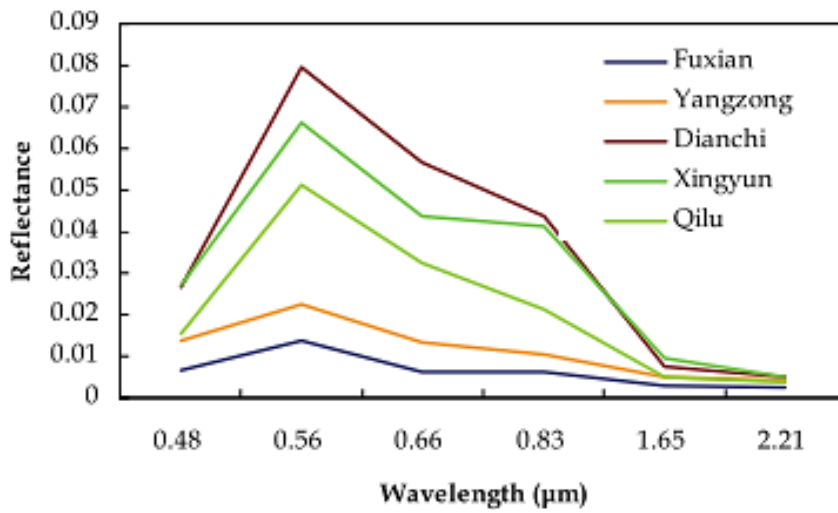


Figure 6 : Average spectral reflectance curves of water in five lakes of different water quality, extracted from a Landsat ETM + image (Wen & Yang 2011)

Figure 7 shows that the average spectral curves of water used for training data in defining different levels of water quality. The sixth level represents the average spectra of a lake with alga.

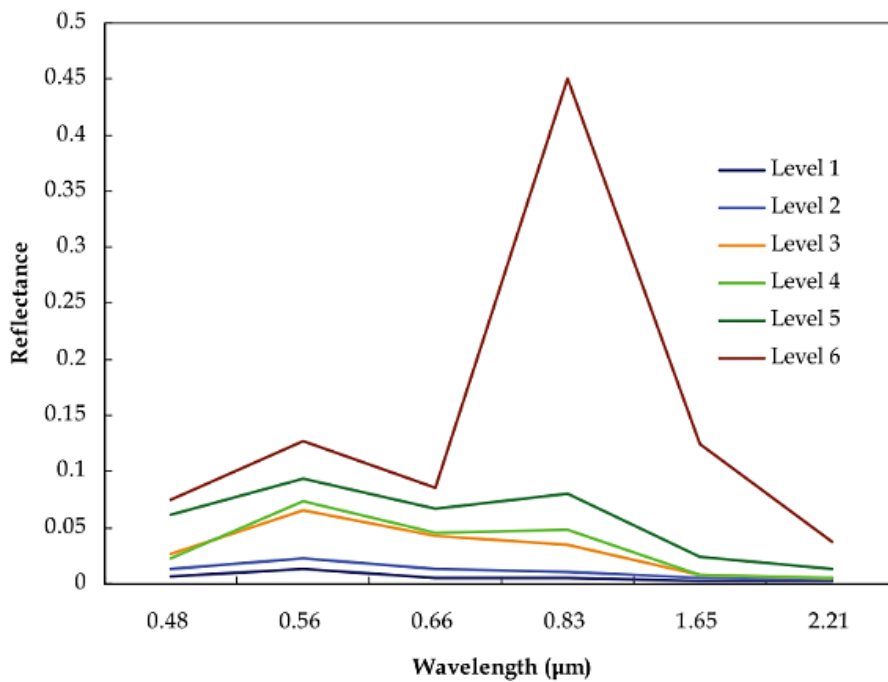


Figure 7 : Average spectral reflectance curves of water for different water quality levels collected for training data (Wen & Yang 2011)

2.3 Methods of water detection with satellite remote sense images

Image classification is the method used to categorise all the pixels in an image into themes or land cover types using a numerical basis for the spectral pattern of the data for each pixel. The method for a particular classification depends on the nature of the data and the applications of the classified data (Lillesand, Kiefer & Chipman 2004).

McFeeters (1996) reviewed the methods to detect open water features in practice and found that the researchers have used either a single band or a ratio of two bands to detect open water bodies. Single band method used reflected NIR radiation as NIR is strongly absorbed by water and strongly reflected by dry soil and terrestrial vegetation. However, single band threshold may introduce error through the decision of the analyst to discriminate water from land and may lead to over or under estimation of water, as has been identified by many researches such as McFeeters (1996), Xu (2006), Haibo et al. (2011), and Liu, Yao and Wang (2016). Water contaminants such as suspended sediment, algae, etc. will increase the reflectance in the NIR and MIR region thus the distinction between water and land becomes more difficult to delineate.

The band ratio methods use the ratio of the reflections in visible bands, such as green or red, to the NIR and MIR bands. Soil and terrestrial vegetation show high reflectance in NIR band thus are suppressed with the band ratio. Open water bodies are enhanced as the reflectance in NIR band is low. McFeeters (1996) argued that the band ratio is an improvement to distinguish water from non-water features though it is unable to eliminate all non-water features. Therefore, McFeeters (1996)

proposed the Normalized Difference Water Index (NDWI) to eliminate the vegetation and land features enhancing the water features in the image.

$$\text{NDWI} = \frac{\text{Green} - \text{NIR}}{\text{Green} + \text{NIR}} \quad (\text{Eq. 1})$$

Where green is the reflectance of the Green band and NIR is the reflectance in Near Infrared band.

The reflectance of water is maximum in the green wavelength and is lower in NIR wavelength. Therefore, incorporating Green band maximises the reflectance of water features. NDWI is a dimensionless index, which ranges from -1 to +1. Water bodies are enhanced in the image as NDWI has positive values for water. In contrast, vegetation and soil features are suppressed with zero or negative NDWI values.

Later, Xu (2006) studied the performance of the algorithm NDWI in three image subsets of Landsat ETM⁺ in lake, river, and sea environments with built-up lands. Xu (2006) showed that the Green band (band 2) has higher reflection than the NIR band (band 4), in both water and built up area as shown in Figure 8. Then, NDWI shows positive values for both built-up land and water. In an urban environment, extracted water bodies applying NDWI are mixed with noise from built up lands. Hence, NDWI is not efficient to suppress the built up lands.

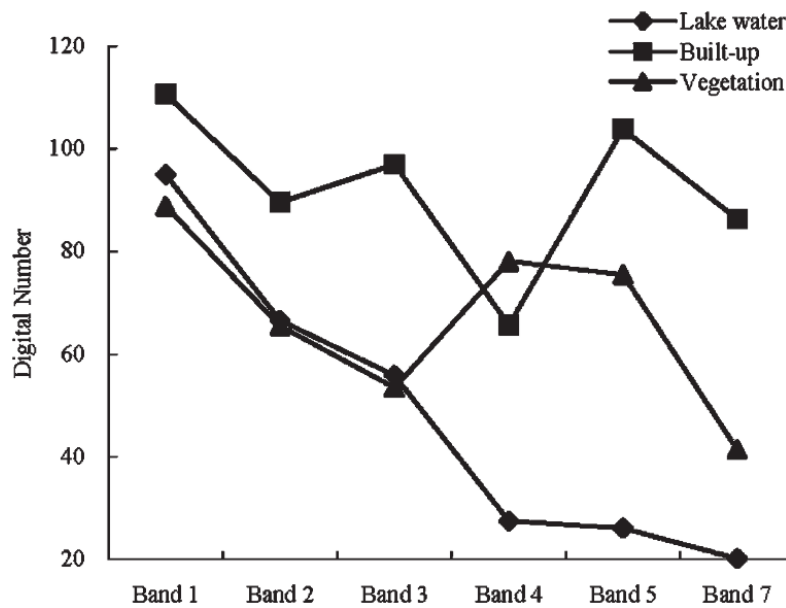


Figure 8 : Spectral reflectance curves of lake water, vegetation and built-up land extracted from a Landsat ETM+ image for Fuzhou city (Xu 2006)

Xu (2006) showed that average DN number for built up area is greater in MIR band (Band5) than the green band (band 2) and introduced Modified Normalized Difference Water Index (MNDWI).

$$\text{MNDWI} = \frac{\text{Green} - \text{MIR}}{\text{Green} + \text{MIR}} \quad (\text{Eq. 2})$$

Where green is green band (band 2 in Landsat TM) and MIR is Middle Infra-Red band (band 5 in Landsat TM) in the raw Landsat image.

MNDWI has a negative value for built-up areas as DN is greater in MIR than Green band. Water absorbs more MIR light than NIR light, hence MNDWI has higher positive value for water than NDWI. Soil reflects more in MIR than in NIR and soil has a negative MNDWI value. The reflectance of vegetation in MIR is lower than NIR though it is higher than Green. Hence, MNDWI of vegetation is still negative. Consequently, MNDWI suppresses the vegetation and soil, enhances the water features and increases the contrast between water and built up area.

Later, Shen and Li (2010) studied the performance of the spectral characteristics of Landsat TM bands in different environments and proposed a new algorithm named as Water Ratio Index (WRI). They found that the performance of WRI is favourable compared with NDWI in two environments; built up area in the mountains covered with vegetation, and bare area with mountain shadows.

$$WRI = \frac{Green+R}{NIR+MIR} \quad (Eq. 3)$$

As the reflectance of water bodies in green and red bands are greater than NIR and MIR bands, WRI gives a value greater than 1 for water bodies.

Following the work by Shen and Li (2010), Haibo et al. (2011) proposed the New Water Index (NWI) based on the DN values of water and other ground features on the Landsat ETM image where C is a constant.

$$NWI = \frac{Band\ 1-(Band\ 4+Band\ 5+Band\ 7)}{Band\ 1+(Band\ 4+Band\ 5+Band\ 7)} * C \quad (Eq. 4)$$

Haibo et al. (2011) used supervised classification, unsupervised classification, single band threshold in band 5 (MIR band), NDWI, MNDWI, and NWI to extract water bodies from a Landsat ETM, DN value image and used the supervised classification as the base line to compare the methods. In this study Haibo et al. (2011) found that NWI is able to extract water features but it is not efficient in distinguishing water and built up areas. Meanwhile, Haibo et al. (2011) found that MNDWI has the highest accuracy in extracting small water bodies in comparison to NDWI in built up areas and single band threshold in band 5 has more noise.

In the above study, Haibo et al. (2011) showed that the image classification methods such as unsupervised and supervised classifications which are already been used for satellite image analysis, can be used to detect water in the images other than the methods described above. Unsupervised and supervised classification are spectrally oriented classification systems (Jensen 2014). Unsupervised classification could be used where there is no prior knowledge about the area. It is a cluster analysis where the analysis software forms several feature classes by clustering similar pixels depending on the parameters specified by the analyst. Then the clusters forming water features are identified by comparing with ground data. The selection of initial class parameters and the iterative adjustments is an issue in unsupervised classification (Haibo et al. 2011).

For the supervised classification, prior knowledge of the ground features is required (Lillesand, Kiefer & Chipman 2004). The pixels of water features are identified on the image and a classification model is built to enable the computer to automatically identify the pixels with the same spectral characteristics. The water and other land cover classes are classified based on the spectral signatures of the selected training pixels. Supervised classification has limited usage in large scale or reproducible mapping mainly due to the time constraints (Zhou et al. 2017).

Fang-fang et al. (2011) applied NDWI, MNDWI, and single band threshold of MIR band on reflectance values after pre-processing of Landsat TM and ETM⁺ images, to detect water in different environments such as built up area, dense vegetation area, mountain area, bare ground, and lake area. The study found that the performance accuracies of indices were different in various environments. MNDWI appeared to have a high accuracy for built up areas and bare grounds. Gautam et al. (2015) detect

surface water bodies in an urban environment applying NDWI, MNDWI, WRI, and supervised image classification. According to their study, they found that the MNDWI, WRI, show closely matching outcomes with supervised classification.

Feyisa et al. (2014) proposed the Automatic Water Extraction Index (AWEI) to extract water especially in areas under shadow and dark surfaces. $AWEI_{nsh}$ is proposed for situations where shadow is not a major problem, while $AWEI_{sh}$ is for situations with shadow.

$$AWEI_{nsh} = 4 * (\rho_{band2} - \rho_{band5}) - 0.25 * \rho_{band4} + 2.75 * \rho_{band7} \quad (Eq. 5)$$

$$AWEI_{sh} = \rho_{band1} + 2.5 * \rho_{band2} - 1.5 * (\rho_{band4} + \rho_{band5}) - 0.25 * \rho_{band7} \quad (Eq. 6)$$

where ρ is the reflectance value of spectral bands of Landsat 5 TM; band 1, band 2, band 4, band 5 and band 7.

Li et al. (2016) highlight that the water extraction is not accurate with available indices in areas with low-albedo surface backgrounds, such as in cities with asphalt roads, under the shadows of clouds, mountains, and buildings, and then proposed NDWI-DB. Based on the spectral curves of typical water and shadow pixels in Landsat 8 OLI (Figure 9), NDWI-DB is proposed as

$$NDWI - DB = \frac{DN_D - DN_S}{DN_D + DN_S} \quad (Eq. 7)$$

Where DN_D is the DN of the dark blue band 1 and DN_S is the DN of the SWIR-7 band.

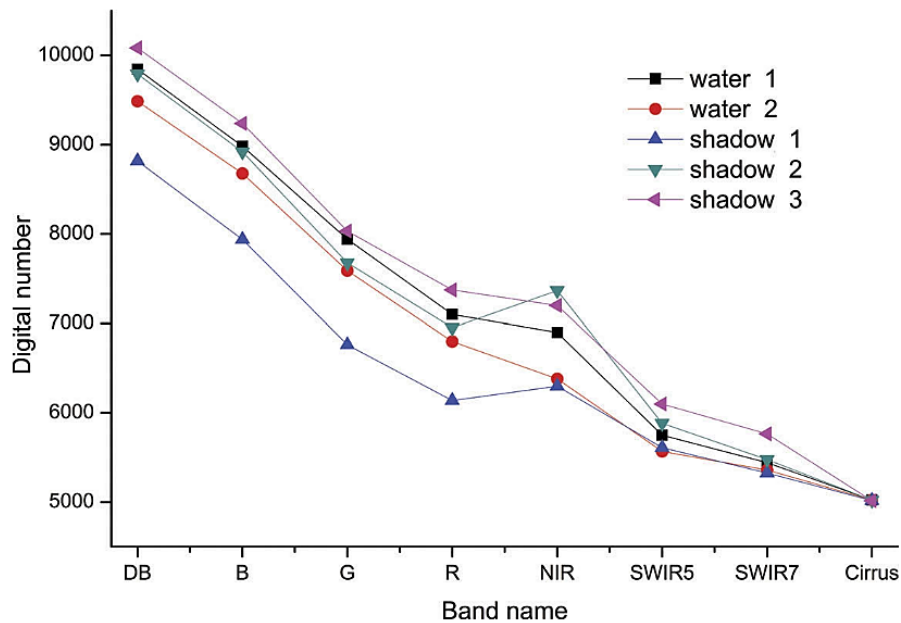


Figure 9 : Spectral reflectance curves for typical water and shadow pixels extracted from Landsat 8 OLI image (Li et al. 2016)

Li et al. (2016) extracted waterbodies by applying NDWI–DB, MNDWI, and AWEI in natural mountainous area, plain city and plain country and showed that NDWI–DB has the best ability to extract water whereas other indices were not able to extract small water areas, such as narrow rivers and small ponds. However, the accuracy of AWEI was higher in natural mountains and lower in plain region when compared to NDWI–DB. The study further found that MNDWI extracts most water in natural mountainous area though it is not successful in removing the shadow.

The improvement of radiometric resolution in Landsat sensors from 8 to 12 bits in Landsat 8 OLI, increases the grey scale levels of data. It avoids the saturation in extreme dark regions and facilitates discriminating subtle features in water bodies (Gao et al. 2016; Li et al. 2016; Zhou et al. 2017).

In DN images of Landsat 8 OLI, Gao et al. (2016) extracts water bodies in a mountain area and a relatively flat plateau area using NDWI and wetness component of

Tasseled Cap transformation (TCW). They concluded that NDWI was able to eliminate mountain shadow though it was weak in extracting small water bodies. TCW is able to extract more water bodies but includes noise from shadow areas.

Some studies use DN value images, whereas other studies use the reflectance images to calculate NDWI (Liu, Yao & Wang 2016). Liu, Yao and Wang (2016) evaluate NDWI and MNDWI using both Landsat 8 DN value image and reflectance image. Green, NIR and MIR bands for Landsat OLI images are bands 3, 5 and 6 respectively. Therefore, McFeeters (1996) NDWI is applied with band 3 and 5 as NDWI35 and Xu (2006) MNDWI is applied with band 3 and 6 as NDWI36 for Landsat 8 OLI images. According to the definitions, NDWI uses reflectance values and MNDWI uses DN values. The study concludes that the performance of NDWI35 is better with reflectance images whereas the performance of NDWI36 is better with DN value images. Liu, Yao and Wang (2016) conclude that NDWI35 with reflectance images is the best method and complies with the original definition, while NDWI36 with DN images is preferred when compared to single band threshold for identifying water with Landsat 8 OLI images.

Zhou et al. (2017) studied the performance of water indices TCW, NDWI, MNDWI, and AWEI in an environment of shallow and deep fresh water bodies. Surface reflectance data images of Landsat 7 ETM⁺, Landsat 8 OLI, and Sentinel-2 MSI were used in this study. The study shows that NDWI has the higher accuracy in all three sensors. TCW shows the lowest accuracy with the highest commission error and the lowest user accuracy identifying built-up lands as water.

According to the literature, there are multiple methods available for water body extraction, such as thematic classification methods of supervised and unsupervised

classifications, single band thresholds, spectral relationship methods, and water index methods (Li et al. 2016; Zhou et al. 2017). Threshold based water detection and water index methods have undergone a succession of evolutions (Zhou et al. 2017) and many techniques and methods for water extraction are investigated by researchers (Shen & Li 2010). Some water indices are originally proposed to be based on DN values and some other water indices are originally based on reflectance. Apart from this fact, some researchers (Gao et al. 2016; Li et al. 2016) have used DN value images to extract water bodies with water indices, which are originally defined to be used with reflectance values.

According to (Li et al. 2016), although some indices and methods are used for water extraction today, there is a lack of accurate, efficient and automatic extraction methods. Fang-fang et al. (2011) argue that there are no universal acceptable indices for detecting surface water and each index has different performance on the background environment. Zhou et al. (2017) argue that water indices are the most common methods due to easiness and high accuracy. Li et al. (2016) conclude that MNDWI is the most common water index used by the researchers.

The review of available methods for detecting the surface water features from satellite images shows that the performance of each method depends largely on the background environment. The finding in the above studies may not be simply applicable to other areas. Many other factors, including water constituents with sediment, salinity, and phytoplankton, may affect the performance of the indices.

Supervised classification is effective in detecting water bodies with background knowledge of land cover types by the researchers. Some researchers, such as Haibo et al. (2011), use the supervised classification image as the base map to compare

other classifications. However, it is a time consuming method when compared to the water index methods. Also, some researchers such as Gautam et al. (2015) shows that water extraction with MNDWI closely matches with the result of supervised classification. Many studies (Fang-fang et al. 2011; Haibo et al. 2011; Li et al. 2016) show higher accuracy in extracting water with MNDWI and some other studies show higher accuracy with NDWI. For NDWI the main problem was the noise from built up area. MNDWI has shown better performance in extracting small water bodies (Haibo et al. 2011).

The study area of Milingimbi Island covers a small area, has a flat terrain and low rising residential buildings in the southern corner of the island. Therefore, there is no effect from mountain or building shadows in this study area. However, the shadow from heavily vegetated areas could be a challenge. The surface water areas change rapidly from wet season to dry season with various levels of inundations and may consist of small water areas. The water inundation is mostly over the salty mud flat area. The water quality may change from fresh to saline during the inundation period and lead to different spectral reflectance patterns. Due to the unknown variation of the characteristics of water, unsupervised classification is suitable to identify clusters of similar spectral characteristics and to distinguish water. Considering the accuracy of identifying and extracting changing water areas, unsupervised classification, supervised classification, and indices NDWI, and MNDWI were selected to find the best performance method for the study area. A classification system should be mutually exclusive in the sense that any area should fall into one category, and it should classify every area in the image; this highlights the importance of identifying a suitable classification system at the beginning of a study (Congalton 1991).

2.4 Accuracy assessment

Once an image classification is completed, it is necessary to assess the accuracy of the image to check the degree of confidence of the result (Richards & Jia 1998). Classification accuracy is the main measure of the quality of the map prepared by applying various image classification techniques on remote sense images. Accuracy assessment evaluates the suitability of a map for operational applications (Foody 2008). The accuracy is assessed by comparing the sample pixels of the classified map against the reference ground data (Lillesand, Kiefer & Chipman 2004). Classification accuracy seems a simple concept but is a very difficult to assess due to many problems (Foody 2008).

The most widely used methods for assessing the accuracy of image classification are based on the error matrix (Comber et al. 2012; Congalton 1991; Foody 2002). The comparison of the ground data and the classification is given in a tabular form, which is referred to as confusion or error matrix. Error matrix shows the number of correctly identified pixels and the number of erroneously identified pixels for each class in the classified map.

There are many factors to consider in an accuracy assessment to represent the classification with the error matrix. They are the collection of ground data, spatial auto correlation, sample size, sampling scheme, and classification method (Congalton 1991). Collection of ground data could be difficult depending on the level of classification. Although no ground data set is completely accurate, the assessment of the accuracy is critically affected by the accuracy of the reference data. When there is an influence from the presence, absence or degree of a certain characteristics of a

pixel for the presence, absence or degree of a certain characteristics of neighbouring pixels is referred as spatial auto correlation.

The sample size should be large enough to maintain the accuracy assessment statistically valid. The sample size should be kept minimum, as the sample collection is expensive. Congalton (1991) introduces a rule of thumb to use a minimum of 50 samples for each land use category for the error matrix. Further recommendations are to increase the sample size up to 75 or 100 samples per category when there are more than 12 land use categories and the area is larger than approximately 4000 km². According to Lillesand, Kiefer and Chipman (2004) the samples of the category of interest can be increased and the samples of low importance categories can be decreased considering the practical limitations of the time and the cost. Few samples can be taken for the categories of low variability such as water. More samples should be considered for categories with a high degree of variability such as uneven aged forests. When the classification is good or number of samples are insufficient, the error matrix has many zeroes at off diagonal values. Richards and Jia (1998) note that choosing random samples of individual pixels across the thematic map is more statistically significant in excluding the correlated near-neighbouring pixels.

Overall accuracy is the ratio between total number of correctly classified pixels and the total number of reference pixels. Omission error and commission error show the exclusion or inclusion to the proper land cover type respectively. User's accuracy is the ratio of the number of correctly classified pixels to the total number of pixels in each category. Producer's accuracy is the ratio of the number of correctly classified pixels to the number of reference pixels in each category (Lillesand, Kiefer & Chipman 2004). The overall accuracy is perhaps the most simple descriptive statistic calculated

with the error matrix (Congalton 1991). Richards and Jia (1998) indicate that the distinction between the producer's accuracy and user's accuracy is important; the user's accuracy has a potential to be mostly adapted for assessing the required accuracy of a classification.

Kappa is a discrete multivariate technique used for accuracy assessment which is a statistical test done on the error matrix. This method is appropriate on remotely sensed data as the data is discrete and binomially or multinomially distributed (Congalton 1991).

$$\hat{k} = \frac{N \sum_{i=1}^r x_{ii} - \sum_{i=1}^r (x_{i+} * x_{+i})}{N^2 - \sum_{i=1}^r (x_{i+} * x_{+i})} \quad (\text{Eq. 8})$$

Where,

\hat{k} - Kappa Coefficient

r - number of rows in the error matrix

x_{ii} - number of observations in row i and column i (on the major diagonal)

x_{i+} - total of observations in row i (shown as marginal total to right of the matrix)

x_{+i} - total of observations in column i (shown as marginal total at bottom of the matrix)

N - the total number of observations included in matrix

(Lillesand, Kiefer & Chipman 2004).

It is important to define the minimum level of required overall accuracy in order to reduce the potential for subjective post classification evaluation in thematic mapping with remote sensed images. In literature, an accuracy value of over 85% has been widely used as the target for overall accuracy and explicitly as a standard for thematic

mapping with remote sensed imagery. However Foody (2008) argues that the target accuracy is a function of variables, such as spatial and spectral resolution of remotely sensed data, the number of classes defined in the classification, and the users requirements, such as tolerance to error and impacts of variations due to severity of the error. In assessing the acceptability of the map, the map accuracy is compared with the target accuracy.

However, the accuracy measurements calculated on the error matrix provide accuracy measures based on the total area only. It does not provide any information about the spatial distribution of the error. The overall accuracy measured from the error matrix may differ in sub regions of the study area. The error in local areas may be much higher or smaller than the overall accuracy. On the other hand, errors in local regions may cancel out, which may lead to erroneous high overall accuracy. The spatial error of classification is important and, therefore, Foody (2002) says a land cover map should include a map of the spatial distribution of the error.

Perica and Fougoula-Georgiou (1996) use spatial measure with the “figure of merit” index in comparing the spatial patterns of two images. Figure of merit measures the ratio of the intersection and the union of the areas in two Boolean maps. It is a dimensionless index, which has a theoretical range between 0 for ‘no agreement’ and 1 for ‘perfect agreement’ of the two corresponding maps.

3. DATA AND METHODS

3.1 Study area

The study area is Milingimbi Island in Northern Territory, Australia (Figure 10). The geographical extent of the island is 134°50'-134°56' E, 12°02'-12°09'S and the total area is about 50 km². The highest elevation is about 16 m above sea level at the central area of the island.

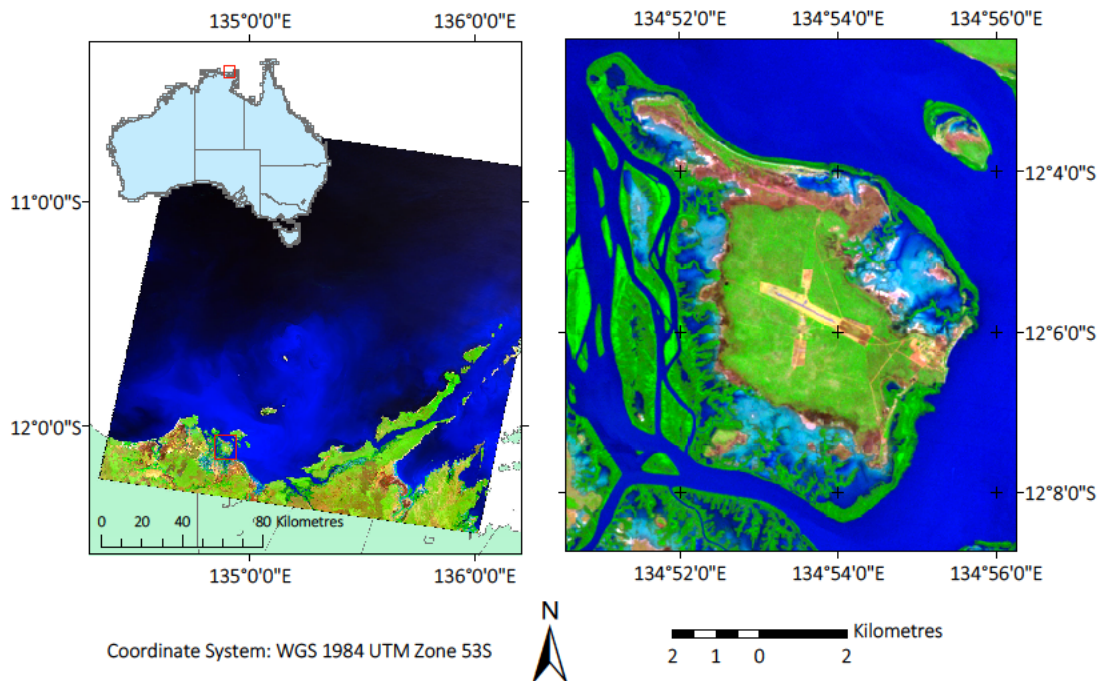


Figure 10 : Location of the study area, Milingimbi Island, NT

3.2 Data source

3.2.1 Remote sensing data

Landsat data was chosen for the study because of the continuous dataset for the study area that are available from 1987 to present. Landsat satellites are sun synchronous satellites of near polar orbiting at an altitude of 705 km above the earth.

The repeat cycle of a satellite is 16 days and two satellites operate concurrently with an 8-day cycle (Pekel et al. 2016) observing 183 km wide swath of the earth in each pass. Landsat 5 Thematic Mapper has operated from March 1984 to Nov 2011. Landsat 5 consists of seven spectral bands of band 1 to 5 and band 7 of spatial resolution of 30m (Table 1). Thermal band 6 is of 120m spatial resolution and images are resampled to 30m (USGS 2017).

Landsat 8 was launched in Feb 2013. It has two instruments on board Operational Land Image (OLI) and Thermal Infrared Sensor (TIRS). Landsat 8 consists of nine spectral bands. Bands 1 to 7 and band 9 are of spatial resolution of 30m and panchromatic band 8 is of 15 m spatial resolution (USGS 2017). Ultra Blue band 1 senses deep blue and designated for coastal and aerosol studies. Band 9 is designated for cirrus clouds (NASA 2013). Liu, Yao and Wang (2016) say that the band composition of both sensors in visible and NIR bandwidths are within close ranges but with slight differences.

Table 1. Band details of Landsat sensors
Landsat 5 TM and Landsat 8 OLI (USGS 2017)

Satellite/Sensor	Bands	Wavelength (μm)	Resolution (m)
Landsat 5 TM	Band 1 - Blue	0.45-0.52	30
	Band 2 - Green	0.52-0.60	30
	Band 3 - Red	0.63-0.69	30
	Band 4 - Near Infrared (NIR)	0.76-0.90	30
	Band 5 - Shortwave Infrared (SWIR) 1	1.55-1.75	30
	Band 6- Thermal	10.40-12.50	120 (30)
	Band 7 - Shortwave Infrared (SWIR) 2	2.08-2.35	30
Landsat 8 OLI	Band 1 - Ultra Blue (coastal/aerosol)	0.435 - 0.451	30
	Band 2 - Blue	0.452 - 0.512	30
	Band 3 - Green	0.533 - 0.590	30
	Band 4 - Red	0.636 - 0.673	30
	Band 5 - Near Infrared (NIR)	0.851 - 0.879	30
	Band 6 - Shortwave Infrared (SWIR) 1	1.566 - 1.651	30
	Band 7 - Shortwave Infrared (SWIR) 2	2.107 - 2.294	30
	Band 8 - Panchromatic	0.503 - 0.676	15
	Band 9 - Cirrus	1.363 - 1.384	30
	Band 10 - Thermal Infrared (TIRS) 1	10.60 - 11.19	100 (30)
	Band 11 - Thermal Infrared (TIRS) 2	11.50 - 12.51	100 (30)

All images of both Landsat 5 and Landsat 8 sensors were checked in the “Glovis” website to scrutinised suitable images for the study. The images of no cloud cover on the study area or with clouds not affecting the inundation area were selected. From the Landsat archive, a limited number of images showing inundation in the study area could be used for the study due to the heavy cloud cover during the wet season. The selected images of the study area are of Path 103 and row 068. The Landsat DN images (L1T products) in the USGS remote sensing archive were downloaded through the “Glovis” viewer. The Surface Reflectance (LEDAPS) products of Landsat TM 5 and

LASRC products of Landsat 8 OLI were received through Landsat archive data sets in “Earth Explorer”. Table 2 shows the images used for the study.

Level 1 Terrain (corrected) L1T are radiometrically and geometrically corrected top of atmosphere radiance products (USGS 2016). Top of atmosphere reflectance is corrected for scattering and absorbing effect of the atmosphere in Surface Reflectance products (Vermote et al. 2016). Landsat 8 surface reflectance products are 30m spatial resolution images delivered from band 1 to band 7 with condition specific files (USGS 2017).

Table 2. Landsat images used for the study

No.	Sensor	Date	No.	Sensor	Date
1	Landsat 5 TM	1988 Aug 31	16	Landsat 8	2014 Apr 01
2	Landsat 5 TM	1989 Sep 19	17	Landsat 8	2014 APR 17
3	Landsat 5 TM	1990 Oct 8	18	Landsat 8	2014 May 03
4	Landsat 5 TM	1992 Mar 19	19	Landsat 8	2014 July 22
5	Landsat 5 TM	1995 Nov 23	20	Landsat 8	2014 Aug 23
6	Landsat 5 TM	1998 Jan 31	21	Landsat 8	2014 Nov 11
7	Landsat 5 TM	1998 Aug 11	22	Landsat 8	2014 Nov 27
8	Landsat 5 TM	2003 Oct 28	23	Landsat 8	2015 Sep 27
9	Landsat 5 TM	2004 Apr 05	24	Landsat 8	2016 Nov 16
10	Landsat 5 TM	2004 Nov 15			
11	Landsat 5 TM	2008 Jan 27			
12	Landsat 5 TM	2009 Aug 25			
13	Landsat 5 TM	2010 Feb 01			
14	Landsat 5 TM	2010 Apr 22			
15	Landsat 5 TM	2011 Oct 02			

3.2.2 Rainfall data

Measured daily rainfall data for Milingimbi Island from January 1987 to Dec 2016 was taken from the Bureau of Meteorology (BoM) website. Weather station 14402 (latitude 12.12° S and longitude 134.91° E) was operated from 1923 to March 2003. Weather station 14404, (latitude 12.09° S and longitude 134.89° E) has been in

operation since July 2003 to the present date (BoM, 2017). Where there were periods of missing measured BoM rainfall data, the database of Scientific Information for Land Owners (SILO) maintained by the Department of Science Information Technology and Innovation (DSITI) was used. SILO provides gridded datasets for fifteen climate variables in grid resolution of 0.05° latitude by 0.05° longitude. It is approximately a 5 km by 5 km grid. Daily rainfall for Milingimbi Island was extracted from the SILO gridded dataset for the study period. Point rainfall data for each day was estimated with a Thiessen polygon method.

A comparison of BoM and SILO data was done for the period from 01 Jan 1999 to 18 Nov 2014, as continuous daily rainfall was available in both datasets. Days when there was no rain were not considered to avoid the bias with many zero values in the data (Table 3). Figure 11 shows the graph of daily rainfall of SILO vs BoM data. The RMSE value of the distribution is 0.89.

Table 3. Comparison of daily rainfall between BOM and SILO data

Sum of daily rainfall in SILO data (form 01 Jan 1999 to 18 Nov 2014)	= 15890 mm
Sum of daily rainfall in BoM data (form 01 Jan 1999 to 18 Nov 2014)	= 16100 mm
Percentage difference between sums	= 1.3 %
Mean of (SILO daily rainfall – BoM daily rainfall)	= -0.12 mm
Sum of (SILO daily rainfall – BoM daily rainfall)	= - 210 mm
Mean of absolute (SILO daily rainfall – BoM daily rainfall)	= 2.12 mm
Sum of absolute (SILO daily rainfall – BoM daily rainfall)	=3640.5 mm

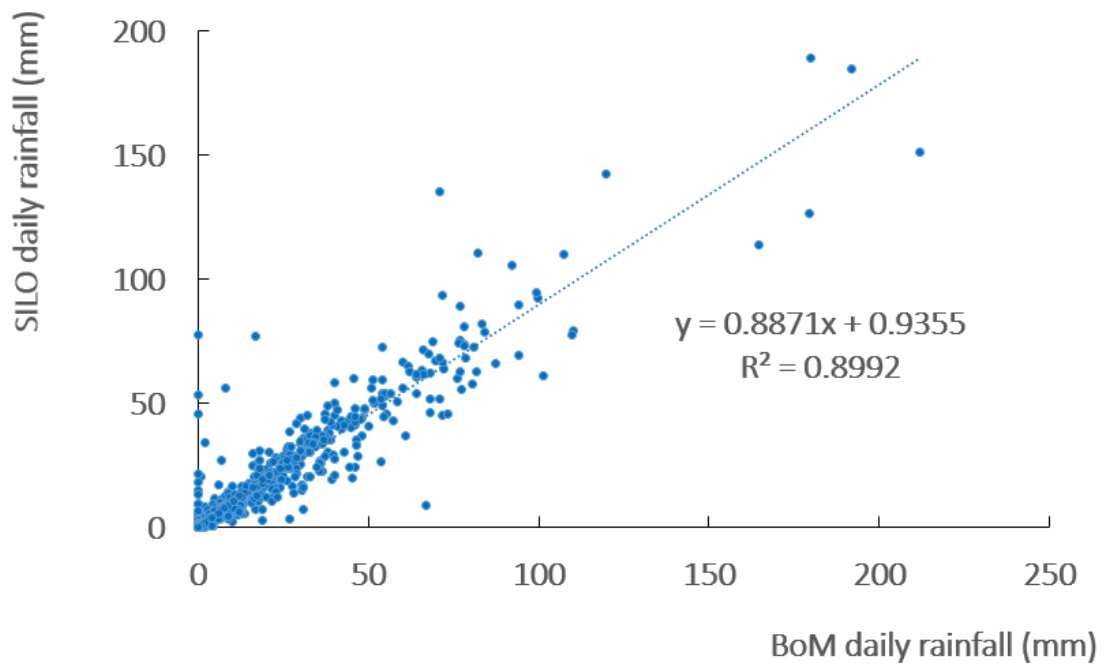


**Figure 11 : Graph of daily SILO rainfall vs daily BoM rainfall
from 01 Jan 1999 to 18 Nov 2014**

The data gaps of BoM daily rainfall data were filled with the SILO data to provide a continuous daily rainfall record for the study period (Table 4).

Table 4. Rainfall data for the study area

Year	BoM Data		SILO Data	Annual Rainfall considered for the study (mm)	Maximum Daily Rainfall (mm)	Date of maximum daily rainfall
	Annual Rainfall (mm)		Annual Rainfall (mm)			
	Station 14402	Station 14404				
1987	NA		1665.8	1665.8	134.9	11-Feb
1988	NA		1172.5	1172.5	111.1	28-Mar
1989	NA		1539.8	1539.8	112.2	12-Mar
1990	NA		563.5	563.5	54.6	10-Jan
1991	NA		956.8	956.8	49.1	12-Jan
1992	NA		1150.6	1150.6	94.3	7-Jan
1993	NA		1311.7	1311.7	82.4	20-Dec
1994	NA		914.3	914.3	71.1	18-Mar
1995	916.8*		1740.6	1740.6	101.7	17-Jan
1996	733.6*		1219.9	1219.9	94.4	2-Apr
1997	457.6*		1103.2	1103.2	61.8	4-Jan
1998	NA		1604.5	1604.5	71.6	26-Jan
1999	NA		1853.2	1853.2	135.6	25-Nov
2000	NA		1737.7	1737.7	110.9	11-Nov
2001	1351.8*		1758.5	1758.5	89.5	10-Jan
2002	758*		743	758	81.0	2-Jan
2003	NA	NA	1698.8	1698.8	185.0	6-Jan
2004		993.2	1244.8	993.2	211.8	31-Dec
2005		586.2	989	586.2	120.0	13-Mar
2006		745.2	1524.1	745.2	101.6	14-Mar
2007		1354.4	1353.7	1354.4	81.6	28-Feb
2008		1160.2	1295.4	1160.2	71.8	18-Feb
2009		882.2	1159.8	882.2	179.8	18-Feb
2010		1227.4	1501	1227.4	78.6	5-Jan
2011		1726.4	2339.8	1726.4	110.2	30-Mar
2012		301.8*	819.6	819.6	69.2	20-Apr
2013		1387.8	1203.5	1387.8	179.6	30-Mar
2014		1218.0		1218.0	109.8	2-Feb
2015		1494.4		1494.4	140.0	24-Mar
2016		839.6		839.6	82.2	31-Jan

* annual rainfall is not completed and not correct.

Figure 12 shows the graphs of daily rainfall for the study area from both measured BoM data and generated SILO data. Visual inspection of BoM and SILO data shows the strong seasonality in rainfall between the wet and dry season. Figure 13 shows the combined data sets of daily rainfall from 1987 to 2016.

Rainfall seasonality for the study area

The period of available measured rainfall data from 2004 to 2016 was considered to study the seasonality over the study area. During this period, the highest annual rainfall was 1726.4 mm in 2011. The lowest annual rainfall of 586.2 mm was in 2005. When the highest daily rainfall is compared between year 2005 and 2011, it was 110.2 mm in 2011, and 120.0 mm in 2005. In year 2005, the annual total rainfall is lower and the highest daily rainfall is higher. The annual total rainfall does not indicate the temporal distribution of daily rainfall throughout the year. The highest daily rainfall in each year was considered from 2004 to 2016. The highest daily rainfall of 211.8 mm in year 2004 is the maximum and 69.2 mm in year 2012 is the minimum during the period.

The daily rainfall in years 2004, 2005, 2011 and 2012 were plotted to observe the variability in rainfall between years for the study area. The rainfall distribution graphs in Figure 14 show that the rainy season in dry and wet years in the study area is from December to April. Accordingly, December to April is considered to be the wet season, while from May to November is considered to be the dry season.

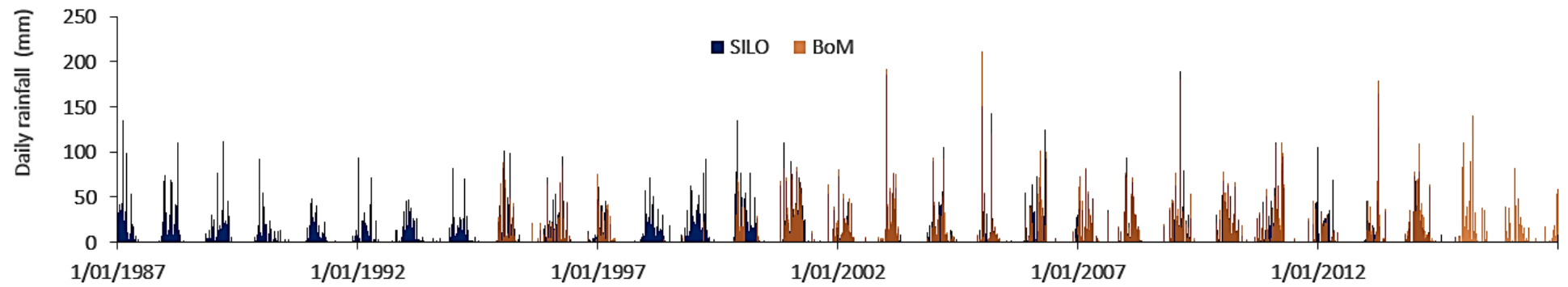


Figure 12: Daily rainfall available for Milingimbi Island in BoM and generated rainfall in SILO database from 1987 to 2016

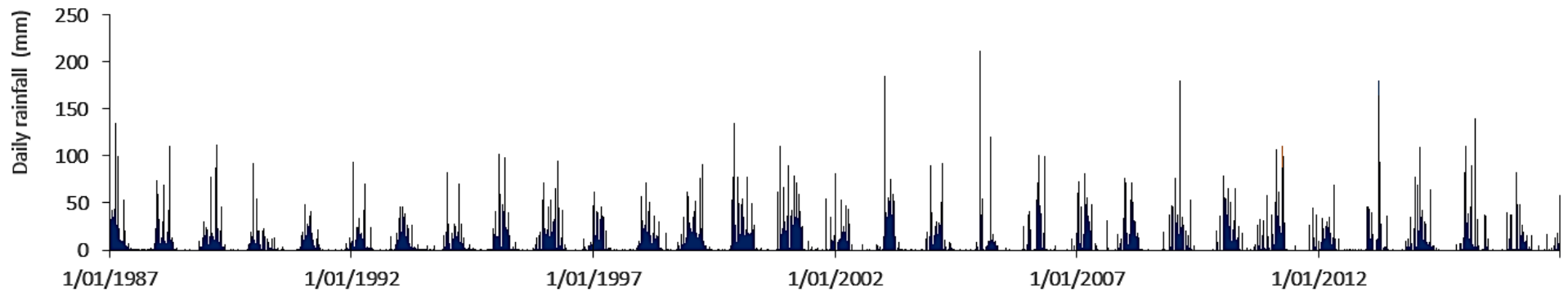


Figure 13 : Daily rainfall used for the study from 1987 to 2016

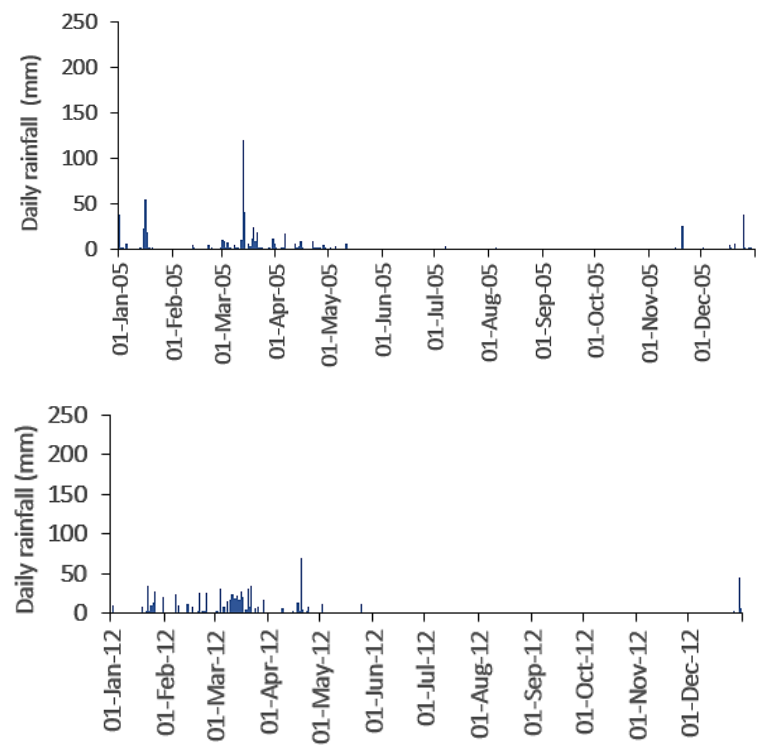
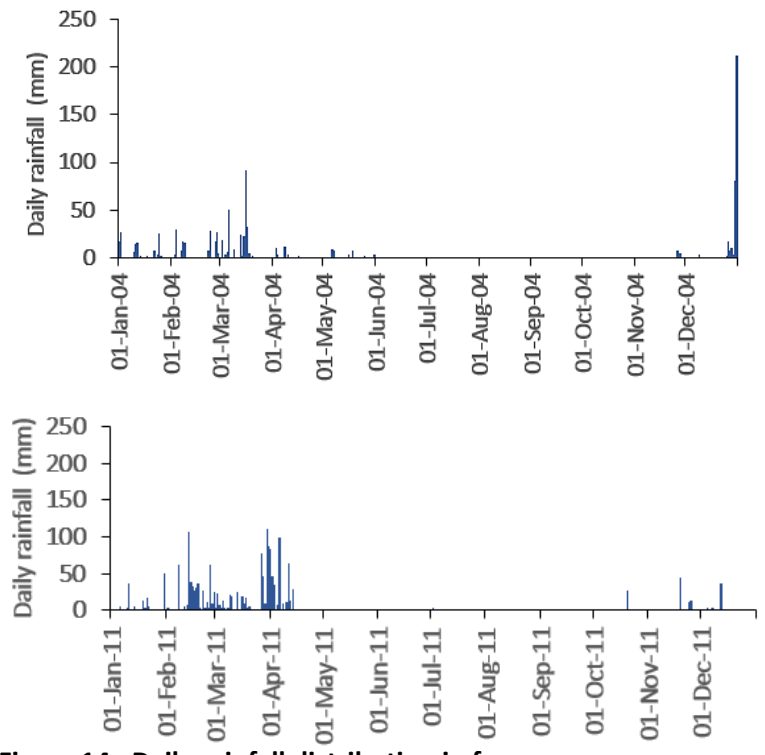


Figure 14 : Daily rainfall distribution in four years 2004, 2005, 2011, and 2012 in the study area

3.2.3 Sea level data

There is no sea level monitoring station at Milingimbi Island; however, there are monthly sea level measurements recorded at SEAFRAME (SEA-level Fine Resolution Acoustic Measuring Equipment) stations in Darwin and Milner Bay- Groote Eylandt, which are available from Bureau of Meteorology (BoM) website. Figure 15 and Figure 16 show the monthly maximum, minimum and mean sea level data for Darwin and Groote Eylandt from 1990 and 1993 respectively. Zero sea level represents an arbitrary fixed offset from the zero of the tide gauge (BoM 2017). Figure 17 shows the locations of SEAFRAME stations.

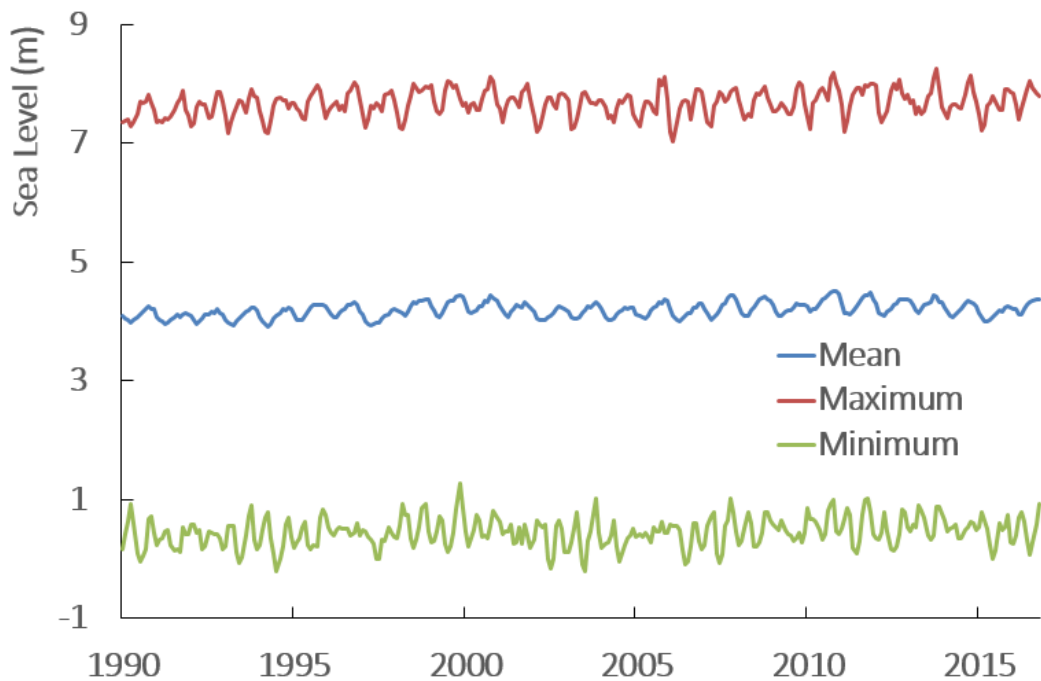


Figure 15 : Monthly mean sea level at Darwin from 1990 to 2016 (BoM 2017) zero sea level represents an arbitrary fixed offset from the zero of the tide gauge

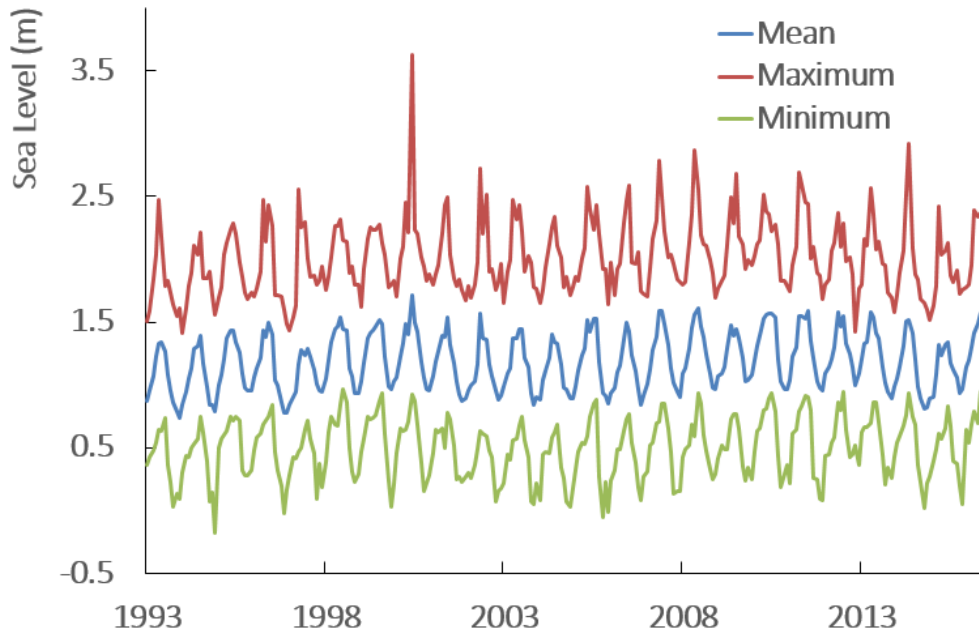


Figure 16 : Monthly mean sea level at Groote Eylandt from 1993 to 2016 (BoM 2017)
 zero sea level represents an arbitrary fixed offset from the zero of the tide gauge

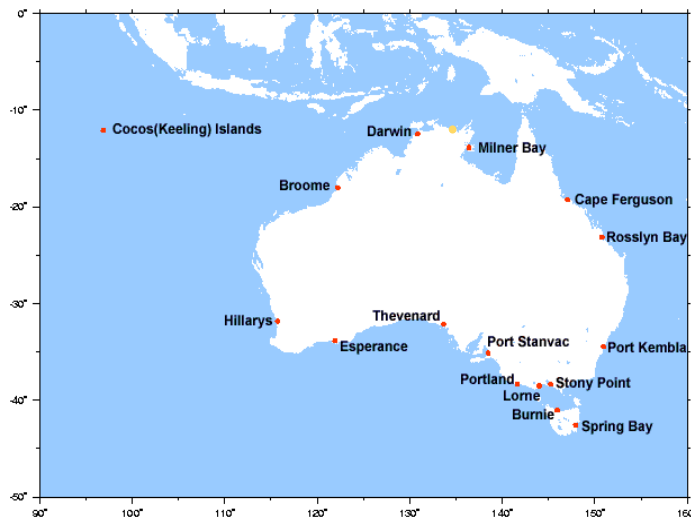


Figure 17 : Location map of SEAFRAME stations
 Showing the Darwin and Milner Bay- Groote Eylandt stations (BoM, 2017)

According to BoM (2016), the rate of sea level rise observed in North of Australia is between 5 to 7 mm/year (Figure 18).

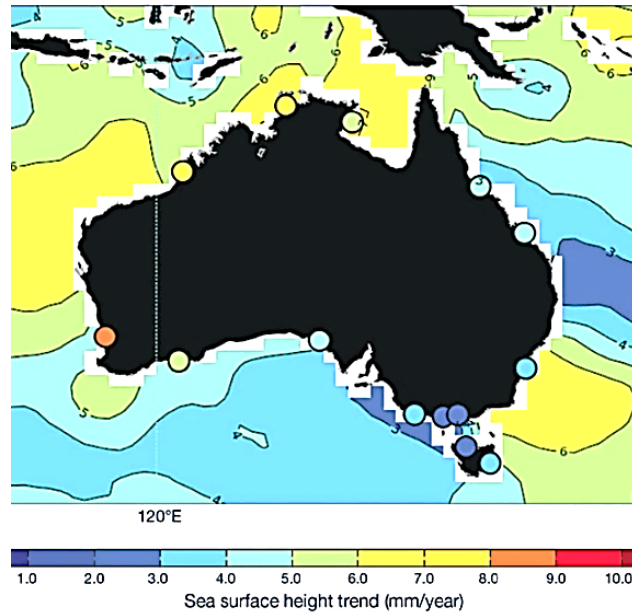


Figure 18 : Sea surface height trend around Australia (BoM 2016)

3.3 Methodology

3.3.1 Data preparation

The downloaded images were combined by layer stack in Erdas Imagine to get the multispectral image. A subset image covering the study area was cut out from each image for this study. The downloaded images were georeferenced in WGS84 UTM projection zone 53.

3.3.2 Image analysis and data processing

Image classifications and water indices were applied to distinguish water from non-water features. Different methods and different indices behave differently in different environments. Initially four methods were used to select the most suitable method to detect water in the environment of the study area to develop a time series of water availability. Unsupervised and supervised image classifications, indices of NDWI and MNDWI, was performed on the selected Landsat images. The software Erdas Imagine was used for image analysis and to develop the thematic maps of 'Water' and 'Non Water'. The thematic images were converted into vector files and polygon features in ArcGIS software for extracting areas.

3.3.3 Unsupervised image classification

In unsupervised classification, image data are classified into spectral groups or clusters by the classification software based on the given parameters and then the image analyst assigns a land cover type for each spectral group with ground reference data. The ISO DATA (Iterative Self Organizing Data Analysis Technique) method was applied with 25 to 30 classes and two standard deviations. This was done to keep a small distance between pixels in the same class and to make a large distance between pixels from different classes. A maximum iteration of 20 was selected with a convergence threshold of 0.95. The convergence threshold specifies to stop the

processing when 95% or more pixels stay in the same cluster between iterations (Erdas 2010). The computer-generated clusters were assigned to classes by visual interpretation.

When clouds occurred over the area, dry salty flats and the clouds were classified into one cluster. The cloud shadow and water were also classified into one cluster. According to Pekel et al. (2016), shadows may overlap with water because spectral characteristics of surface underlying shadows are not identified. Water area was estimated in ArcMap using the vector form of the classified image.

3.3.4 Supervised image classification

In supervised classification, the analyst controls the classification specifying the algorithm and the numerical description of the spectral attributes of each land cover type by selecting training areas in the image. Each pixel is classified to the most closely resembling land cover type.

Parallel-piped classifier and Gaussian maximum likelihood classifier are the most commonly used algorithms in supervised classification. Maximum likelihood classifier uses both variance and the covariance to classify any unknown pixels.

Training data is used in the classification to develop a set of statistics for each land cover type based on the spectral response pattern. Training data should be collected to represent all variations of the one land cover type and be sufficient in number to determine the statistical parameters. The number of training samples to represent spectral variability of one cover type depends on factors such as information classes and complexity of the geographic area (Lillesand, Kiefer & Chipman 2004).

Selection of training samples throughout the image for one cover type will increase the representativeness of all the variations. According to Lillesand, Kiefer and Chipman (2004) the theoretical minimum number of pixels for a training set is $n+1$, where n is the number of spectral bands. In practice, the number of pixels for a training set is used as a minimum of $10n$ to $100n$ pixels to improve the mean vectors and the covariance matrices.

Training data are refined to identify that all the important spectral classes are included and to avoid redundancies in the collected training sample. This improves the accuracy of the classification. The training data is analysed to include normally distributed and spectrally separable data. Hypothetical histograms for all cover types in all bands are visually checked to identify the normal distribution. It shows the distribution of an individual category. A bimodal distribution shows that two subclasses of slightly different spectral characteristics are included in the sample. To improve the classification, each sub class is taken as a separate category. The original training data set is refined to get a normally distributed, spectrally separable data set by merging, deleting and adding.

The training samples for the supervised classification were collected from the image by visual interpretation and using the Area of Interest tool (AOI) in Erdas Imagine. Three land cover classes were considered water, vegetation and soil. A separate class for residential area was not considered as the area was in one class with soil during unsupervised classification and the classification was to identify water and non-water. The Maximum Likelihood classifier was used for the supervised classification and the classified image was recoded into two land cover types of 'Non water' and 'Water'.

3.3.5 Normalised Differential Water Index

The Normalized Difference Water Index (NDWI) proposed by McFeeters in 1996 was

$$\text{NDWI} = \frac{\text{Green} - \text{NIR}}{\text{Green} + \text{NIR}}$$

Green is the reflection in green wavelength and NIR is the reflection in NIR wavelength. In the images of Landsat TM, band 2 and band 4 correspond to the green and NIR wavelength respectively. For the images of Landsat 8 OLI, band 3 and band 5 correspond to the green and NIR wavelength. Spatial modeller (Figure 19) was used in Erdas Imagine to perform the NDWI classification.

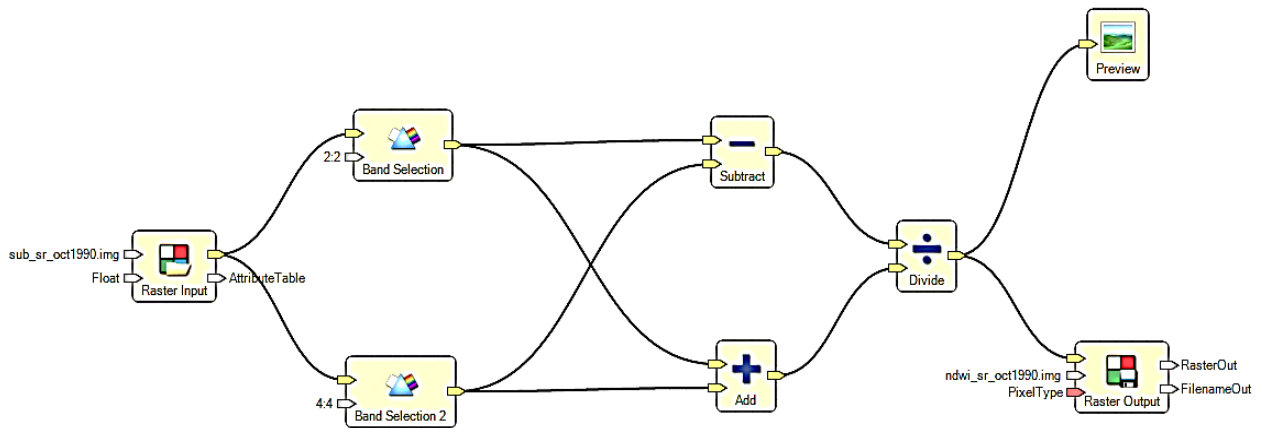


Figure 19 : Spatial modeller for NDWI classification used in Erdas

For NDWI_{ref} , Landsat surface reflectance products were used. According to the original proposal by (McFeeters 1996) the optimal threshold for NDWI_{ref} would be zero, where surface water areas are typically shown with positive pixel values and not-water areas with negative pixel values in the output NDWI_{ref} image. With a threshold of zero, the water area on the image included the billabong in many images and no water areas appeared in high ground area for NDWI_{ref} .

In this study DN image was used to model $NDWI_{DN}$ using the same model for $NDWI_{ref}$. A threshold value of zero for the $NDWI_{DN}$ model identified many areas in the central high ground of the island as water areas in the output image which are not-water areas. Liu, Yao and Wang (2016) note threshold selection is important in identifying water bodies, as the threshold value can lead to under-estimation or over-estimation of the water area with an empirical or arbitrary selected value. The optimum threshold for indices depends on the background environment. The threshold estimation for each image was performed in Arc Map and the optimum threshold values were selected by looking at the ground conditions to exclude impossible inundation areas, and not to exclude 'Nalajrwa' billabong. Then all the pixels with a value higher than the threshold were assigned to water with the raster calculator tool. For NDWI the threshold values varied between +0.02 to +0.1.

3.3.6 Modified Normalised Differential Water Index

Modified normalized difference water index (MNDWI) proposed by Xu (2006) was also used to detect water. MNDWI is given by

$$MNDWI = \frac{Green - MIR}{Green + MIR}$$

Green is the reflectance in green band and MIR is the reflectance of Middle Infra-Red band. Landsat TM, band 2 and band 5 correspond to the green band and MIR band respectively. For Landsat 8 OLI, band 3 and band 7 are correspondent to the green band and MIR band. Spatial modeller (Figure 20) was used in Erdas Imagine to perform the MNDWI classification.

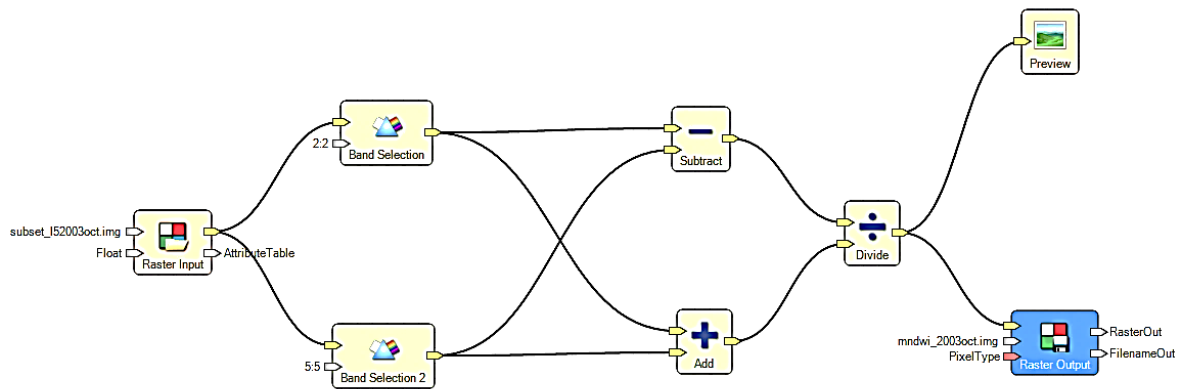


Figure 20 : Spatial modeller for MNDWI classification used in Erdas

As a zero threshold for MNDWI did not show a suitable area with the visual inspection at the corresponding image, optimum threshold values were selected by visual inspection. Threshold values for MNDWI varied from +0.1 to +0.3. With the raster calculator, all the pixels with values higher than the threshold value were assigned to the class 'water'.

3.3.7 Water area extracted from European Commission Joint Research Centre's Global Surface Water dataset (EC JRC-GSW)

Pekel et al. (2016) have studied changes in global surface water over 32 years using Landsat satellite images. This study used orthorectified, top of atmosphere reflectance, and brightness L1T images, which were acquired between 16 March 1984 and 10 October 2015 by Landsat 5 (TM), Landsat 7 ETM + and Landsat 8 OLI. The water area larger than 30m by 30m open to the sky, including fresh and salt water, was classified as open water. Each pixel was assigned to either one of the classes 'water', 'not water', or 'no data' using an expert system, which was based on spectral reflectance characteristics of different land cover types. The expert system was run in Google Earth Engine (GEE). GEE is an application-programming interface

and a computational infrastructure, which is optimised for parallel processing of geospatial data.

The performance of the expert system was evaluated by omission and commission error using 40124 control points distributed both temporally and geographically and across all three sensors. Overall omission error was less than 5% and commission error less than 1%. The omission of seasonal water classes was higher than the permanent water classes. The study by Pekel et al. (2016) found that during the period from 1984 to 2015, permanent surface water in an area of approximately 90,000 square kilometres has disappeared and new permanent surface water bodies of an area of 184,000 square kilometres have formed in the world. Loss of surface water is linked with long-term drought conditions, damming, river diversions, and extensive withdrawals while the increase is related to new constructions of water bodies, or new inundations affected by changing climate (Pekel et al. 2016).

‘Monthly water history’ data developed in this study shows all the global water detections at monthly level. The collection of 380 images showing monthly water history is available in Google Earth Engine code editor (<https://code.earthengine.google.com/>). In this study of Milingimbi Island, surface water data for the required months were extracted from water availability maps through GEE.

3.3.8 Accuracy assessment of identifying inundation area

Four images from the dry and wet season were selected for the accuracy assessment of the different extent of inundation areas, distributed throughout the study period. The selected images were 19 Sep 1989, 31 Jan 1998, 28 Oct 2003 and 01 Feb 2010.

For accuracy assessment of each image, ground data was extracted by visual interpretation. The spectral resolutions of Landsat TM and OLI image were sufficient to distinguish water surface and land features visually on the true colour image. Two hundred ground data points were generated in ArcMap based on random sampling by excluding the training area to avoid the bias (Figure 21). The ground points were assigned manually to classes, water and not water. The points that could not be assigned to a class were deleted.



Figure 21 : Selection of ground data for accuracy assessment excluding training areas on image 28 Oct 2003

The same set of random ground points was used to extract the predicted land cover in each classification. Error matrices were developed using the Frequency and Pivot tools in Arc GIS. Based on the error matrix, Overall Accuracy and Kappa values for each classification were estimated. Considering the behaviour of Overall Accuracy

and Kappa values for the different classifications on the four Landsat images, the best suitable classification for the study area was selected.

3.3.9 Correlation between rainfall and inundation area

Extraction of surface inundation area using remote sense images provides the inundation area at a particular time for the study area. The daily rainfall for the preceding day is collected at 9.00 am next day. The preceding rainfall in the island up to the image acquisition day was considered to study whether the rainfall has contributed to the surface inundation. The preceding accumulated rainfall over the past 15 days, 30 days, 60 days and 90 days were calculated from the daily rainfall series. The surface inundation area and the rainfall were plotted separately for different periods. The inundations during wet and dry season were separated.

4. RESULTS AND DISCUSSIONS

Maps of water inundation area in 13 different images using various extraction methods are presented in Appendix 2. The figures show the inundation area extracted by unsupervised and supervised classifications, and water indices MNDWI and NDWI. Areas of water inundation extracted by NDWI using both surface reflectance image and DN image are shown. The water inundation area for the particular month, which is extracted from the EC JRC GSWE, is also presented in the same figure. The wet image, showing the maximum water area for a particular month was selected from the Landsat Archive. For a particular month, the selected image for this study was the available cloud free image showing the highest inundation area. EC JRC GSW data is developed based on the Landsat data. By visual inspection of the images for each month, it is apparent that EC JRC GSW has used the same image used in this study to extract maximum water area for that particular month. The visual inspection was made by separating wet and dry images, comparing the water spread area and the clouds over the image.

The water extraction by different methods is discussed below for two images. The image on 01 Feb 2010 with the highest inundation area and the image on 28 Oct 2003 with partially inundated area were selected for the discussion.

4.1 Extraction of water area on 01 Feb 2010

The DN image (L1T product) of Landsat 5 on 01 Feb 2010 was used for the extraction of inundation area by supervised, unsupervised, MNDWI, and $NDWI_{DN}$ method and the surface reflectance image was used for $NDWI_{ref}$ method.

4.1.1 Investigating the spectral signature

Figure 22 shows the extracted spectral reflectance curves for four major land features in the study area. The spectral reflectance curves show similar pattern of behaviour with typical curves for soil, water and vegetation. The spectral reflectance curve of water at billabong shows higher reflectance in band 4. Vegetation shows slight increase in reflectance in band 2, more absorption in band 3, red edge from band 3 to band 4 (NIR). The vegetation reflectance is maximum in band 4 and then decreases. The soil reflectance curve shows increase in reflectance in band 1 to band 4. The spectral signature of vegetated mud flat shows mixed behaviour of reflectance in vegetation and soil.

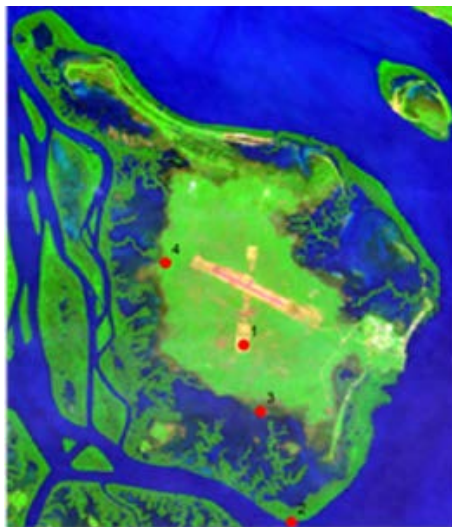
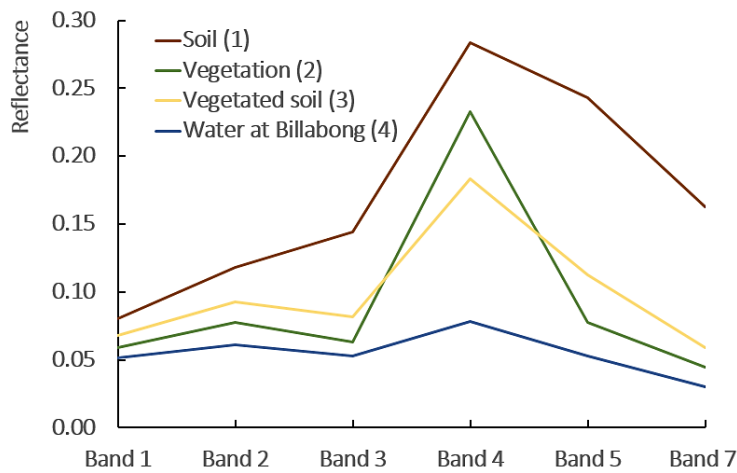


Figure 22 : Spectral reflectance curves of different land features extracted from Landsat 5 TM image

Figure 23 shows spectral signatures of water at different locations in the area. The spectral reflectance curves of water in the creek, the inundation area in the north, and the sea shows typical behaviour of water. Water in the billabong shows a different behaviour in band 4. The reflectance value in band 1, band 2, and band 3 dramatically changes in water at different locations. The change in band 3 shows the highest variability. The variability in band 2 is higher than band 1.

Water in the creek, the north inundation area and the sea show the highest reflectance in band 2 and then the absorption is increased from band 2 to band 3. The absorption is drastically increased from band 3 to band 5. The reflectance in sea water is slightly increased from band 5 to band 7. The reflectance of water in the creek and the north inundation area slightly decreased from band 5 to band 7.

The reflectance in water in the billabong is decreased from band 2 to band 3 and then is increased significantly in band 4. Then the reflectance is decreased from band 4 to band 7. The reflectance in billabong water in band 7 is higher than the water in other locations and matches more closely to the reflectance in seawater.

4.1.2 Water extraction with different methods

Figure 24 shows the extraction of inundation area by different methods and the image on 01 Feb 2010 in false colour composite in BGR 147. It shows a similar pattern of spatial distribution of inundation area in all the methods. The supervised, unsupervised, MNDWI and $NDWI_{DN}$ methods show higher inundation area than $NDWI_{ref}$ and EC JRC-GSW extraction. The supervised classification shows the highest inundation area.

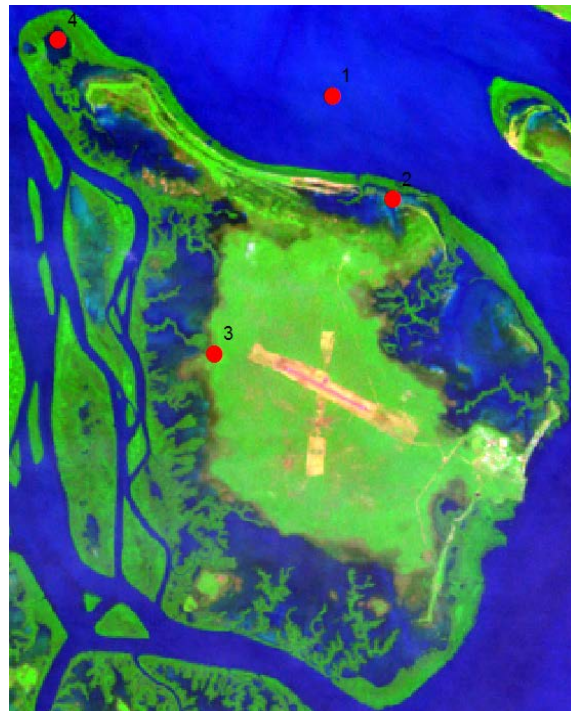
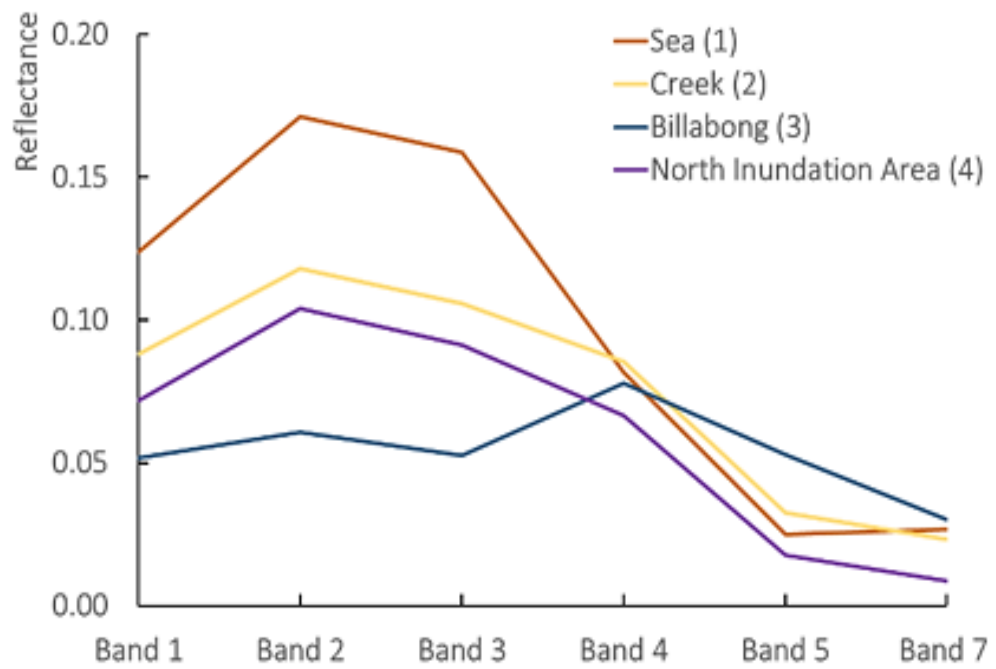


Figure 23 : Spectral reflectance curves of different water features in the study area extracted from Landsat 5 TM image

The permanent water feature, the billabong, is identified in the supervised classification, but as non-water in the unsupervised classification. The threshold in MNDWI and $NDWI_{DN}$ were at 0.07 and 0.05 to avoid water pixels in known non-water areas in the central area. At these thresholds, the billabong disappeared. The

threshold of $NDWI_{ref}$ was taken as zero and the billabong did not appear. In EC JRC-GSW classification also, the billabong area was not identified as water.

Referring to the accuracy assessment on image classification in section 5.3, supervised classification has the highest accuracy in the image on 01 Feb 2010. Therefore, the inundation area extracted by the supervised classification is used as the base map for the comparison with other methods.

4.1.3 Comparison of water extraction by different methods

Figure 25 shows the maps comparing the inundation area extracted by unsupervised, MNDWI, and $NDWI_{ref}$, methods with the supervised classification. The three methods were selected as they show higher accuracy on image classification as per the section 5.3. The comparison map for a method shows the pixels of similar identification as 'Water' in both the methods, the pixels of 'Water' according to supervised classification but 'Not-water' in the other method, and the pixels of 'Not-water' in supervised classification but 'Water' in the other method. The images of comparison show that most of the pixels identified as water in the other methods are identified as water in the supervised classification. The number of pixels, which are 'Not-water' in supervised classification but 'Water' in other classifications are very low.

Compared to the supervised classification the percentage of non-identified water pixels and newly identified water pixels are given in Table 5. Accordingly, unsupervised classification and MNDWI has not identified 5.65 % of area compared to the water area in supervised classification. This may be because the supervised classification often has over-classified pixels (fault positives). Both methods have identified 1.12% of other area as water. $NDWI_{ref}$ has not identified 34.97% of the area and has not identified other area as water.

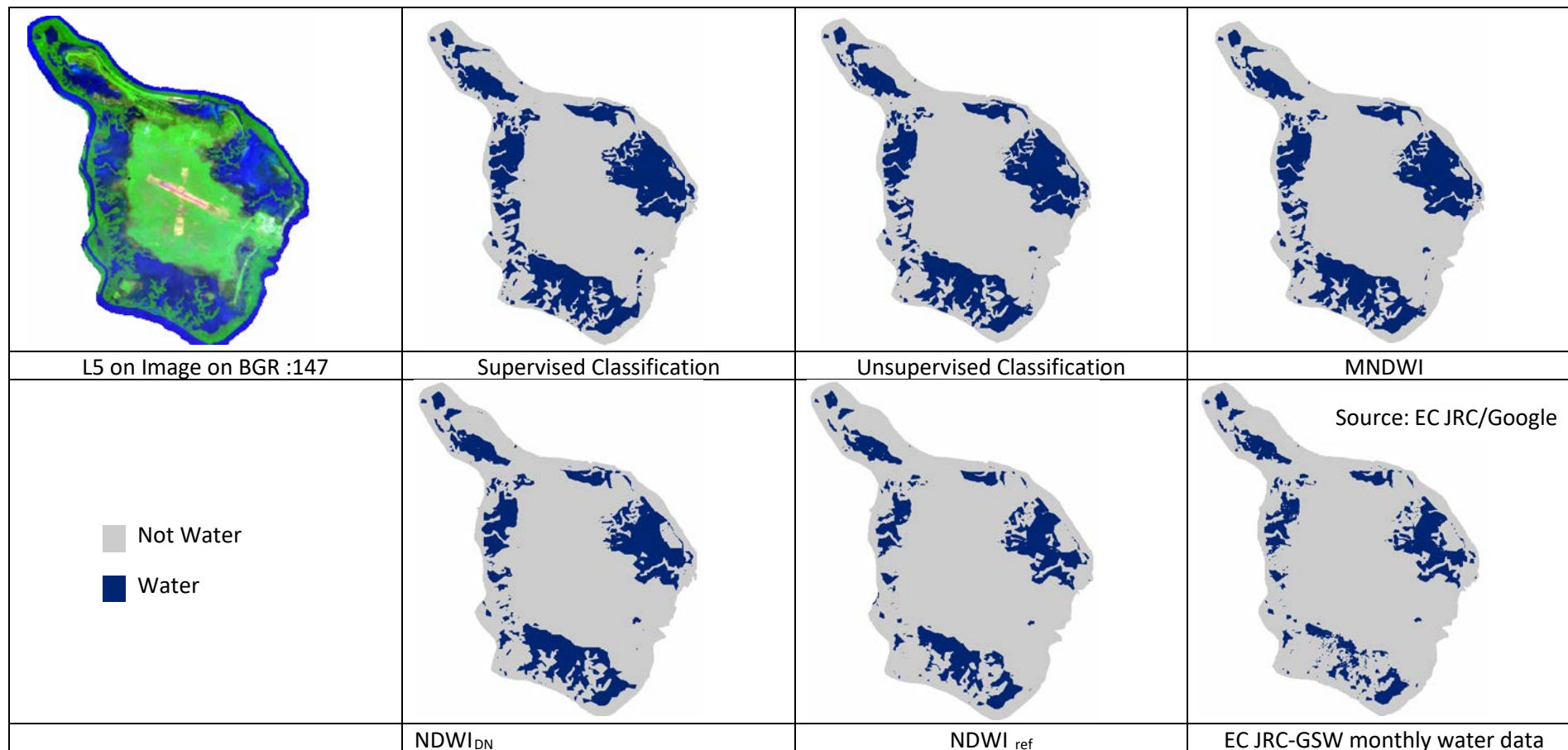


**Figure 24 : Extraction of surface water area on 01 Feb 2010
by different methods**

The spatial distribution of pixels not picked up by unsupervised classification as water shows similarity with MNDWI and the percentage of areas is similar in both methods not taken as water and newly identified as water compared to the supervised classification. Water pixels newly identified in other methods are most likely to be edge pixels and could be mixed pixels.

Table 5. Comparison of extracted water area on 01 Feb 2010 by different methods with supervised classification

	Unsupervised Classification	MNDWI	NDWI _{ref}
Area not identified as Water compared to water area in supervised classification (%)	5.65	5.65	34.97
Other area identified as Water compared to water area in supervised classification (%)	1.12	1.12	0.00

4.1.4 Comparison of water extraction by supervised classification and NDWI_{ref}

NDWI_{ref} has the highest area not identified as water but classified as water in supervised classification. The spectral signatures at three locations identified as 'Water' in supervised classification and 'Not-water' in NDWI_{ref} were investigated. The selection of three random points on the comparison map of supervised and NDWI_{ref} methods and overlaid random points on the map are shown in Figure 26.

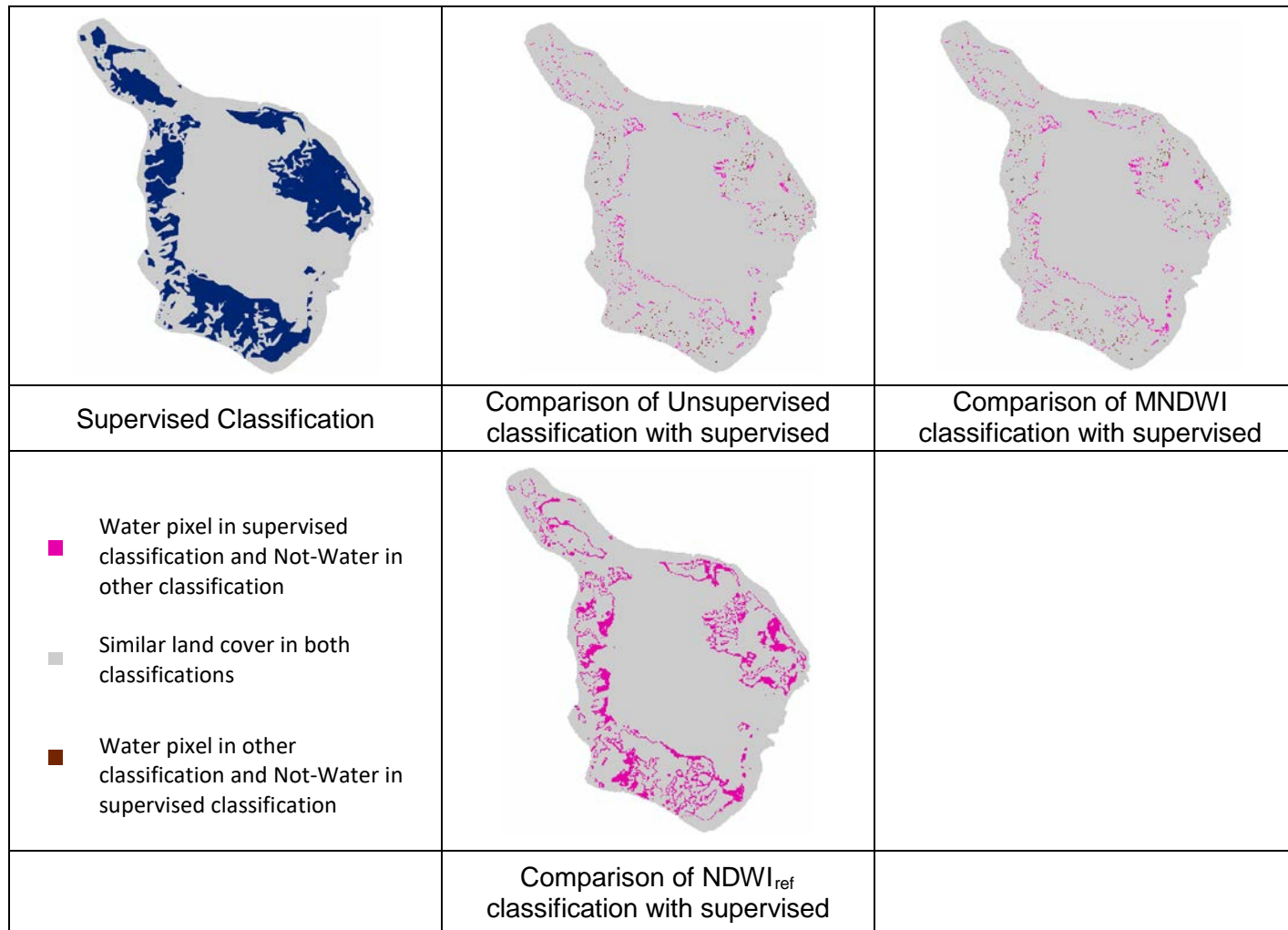
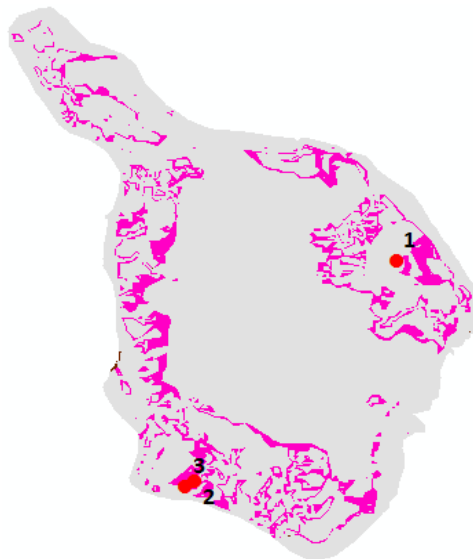
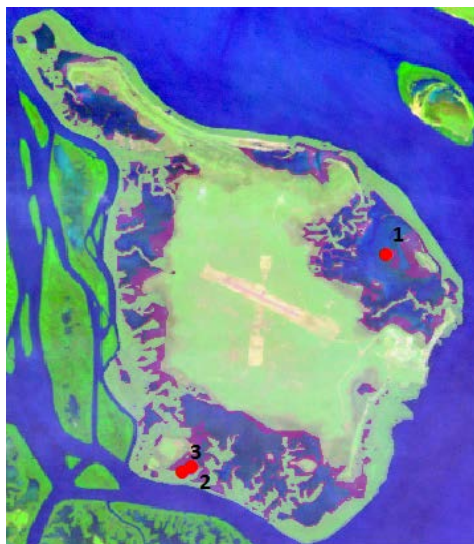
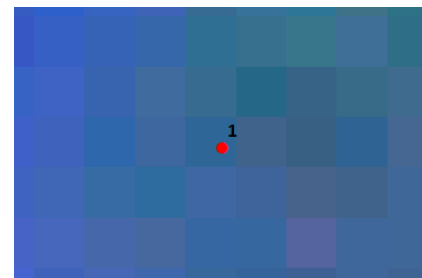


Figure 25 : Comparison of surface water area extracted on 01 Feb 2010 image by unsupervised classification, MNDWI, and $NDWI_{ref}$ with supervised classification

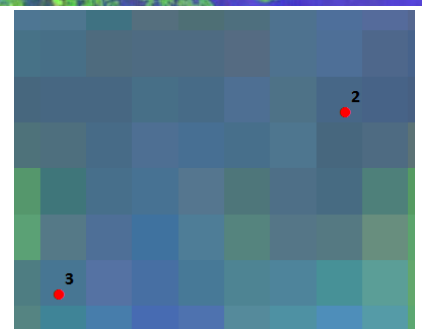
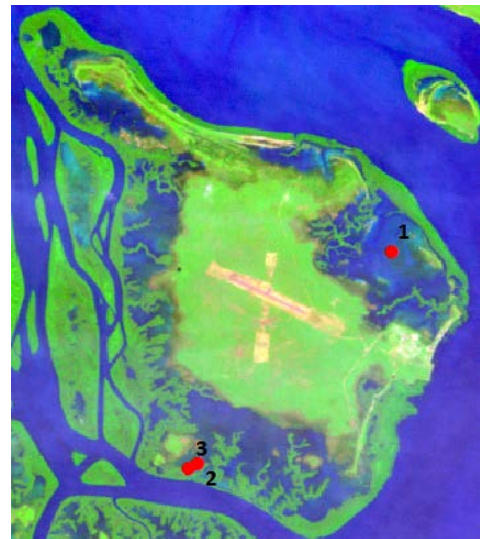


- Water pixel in supervised classification and Not-Water in $NDWI_{ref}$
- Similar land cover in both classifications
- Water pixel in $NDWI_{ref}$ and Not-Water in supervised classification

Map showing the variation of water area between supervised classification and $NDWI_{ref}$ classification.



Selection of random pixels in the variable area by overlaying on the image.



Investigating spectral reflectance curves at random pixels on the image (BGR : 147)

Figure 26 : Investigation of spectral reflectance curves at random pixels of water in supervised classification and non- water in $NDWI_{ref}$ on 01 Feb 2010 image

The plotted spectral reflectance curves at three points are shown in Figure 27. The spectral reflectance curves for water in creek and the billabong from the same image are also plotted in the graph.

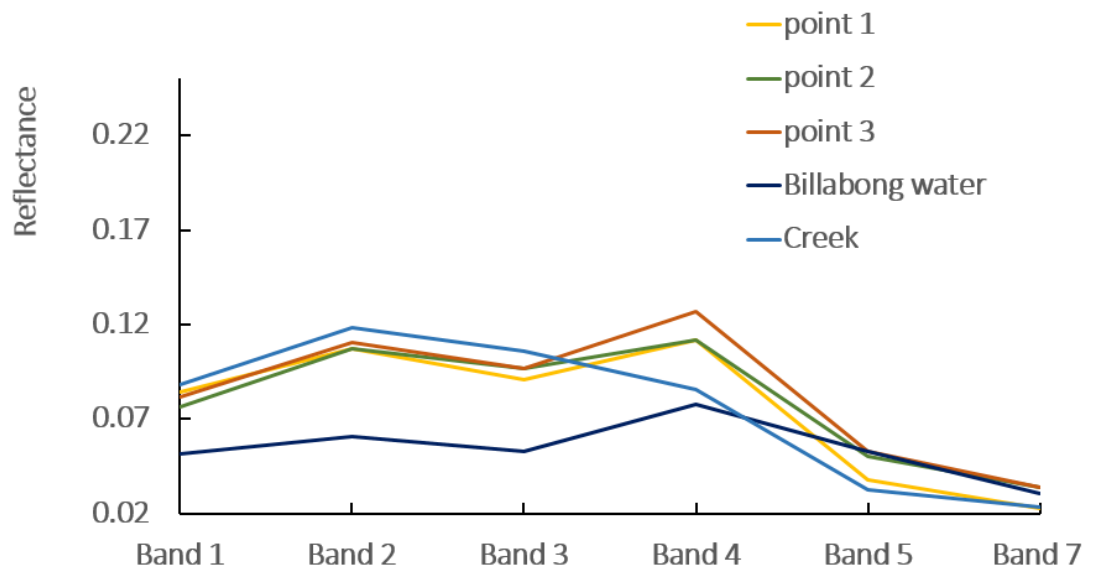


Figure 27 : Comparison of spectral reflectance curves on 01 Feb 2010 image at random points and water points

The spectral reflectance curves for three points behave in a similar way. The reflectance increases from band 1 to band 2 and then decreases slightly in band 3. The reflectance in band 4 is increased deviating the spectral reflectance curve of pure water. The reflectance in band 5 and band 7 are very low. The behaviour is similar to billabong water though the reflectance in band 1, 2, 3, and 4 are higher and in band 5 and 7 are marginally lower. The reflectance in NIR is higher than the reflectance in green at point 1, 2 and 3 thus NDWI is negative. The pixels, which behave similar to the pixels at these points are not classified as water in NDWI at zero threshold.

4.2 Extraction of water area on 28 Oct 2003

The DN image (L1T product) of Landsat 5 on 28 Oct 2003 was used for the extraction of inundation area by supervised, unsupervised, MNDWI, and $NDWI_{DN}$ method and the surface reflectance image was used for $NDWI_{ref}$ method.

4.2.1 Investigating the spectral signature

The colour composite BGR bands 1, 4, 7, in Figure 28, shows water in blue, vegetation in green and soil in brown colour. Points 1, 4, 5, and 6 are blue coloured pixels. The colour is heterogeneous when comparing the pixels. The point 2 is at the billabong, which is the permanent water feature in the island. The point 9 is at sea. The spectral reflectance curves at these different locations in inundation area, mud flat area, and the sea are also shown in Figure 28.

Spectral reflectance curves at point 1, point 3 (creek), and point 9 (sea) show a pattern similar to water, although the reflectance in band 1, 2, and 3 is comparatively higher than water. Point 2 (billabong) shows a slight increase in reflectance from band 1 to 2, then insignificant decrease in band 3, slight increase in band 4 and decrease in band 5 and band 7. The reflectance is low in billabong, however, the increase in reflectance in band 4, deviates from the behaviour of water. The reflectance at point 4 and 5 increases from band 1 to band 5, and then decreases in band 5 and band 7. The spectral reflectance curves behave differently, though the points seem to be water for this colour composite image.

The points 6, 7 and 8 are located in not-water area. The reflectance at these points increases significantly from band 1 to band 5 and decreases in band 7. There is sudden increase in reflectance from band 4 to band 5. The points 6 and 8 are located in salty area and the reflectance of about 0.4 in band 5 is very high. Point 7 is bare soil and

the spectral reflectance in band 5 is lower than 0.02. The curve behaves in a similar pattern with soil but the reflectance is lower. The reflectance values could be affected by the high moisture in the soil.

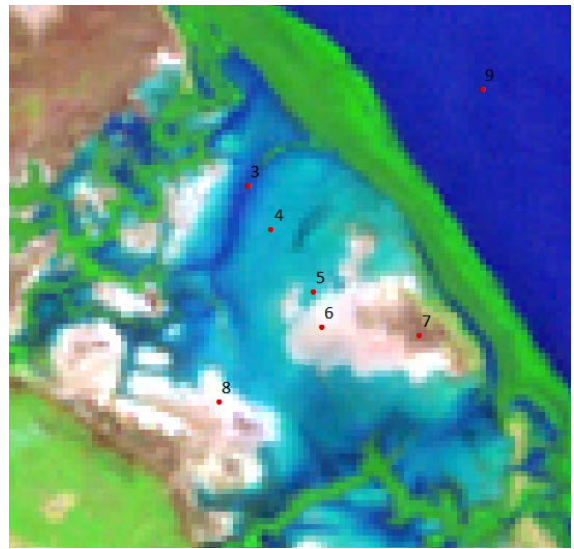
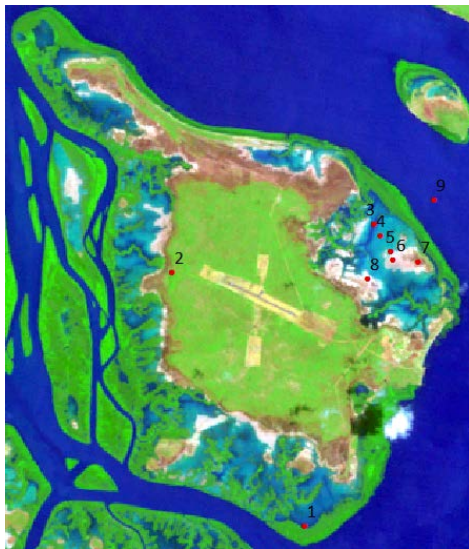
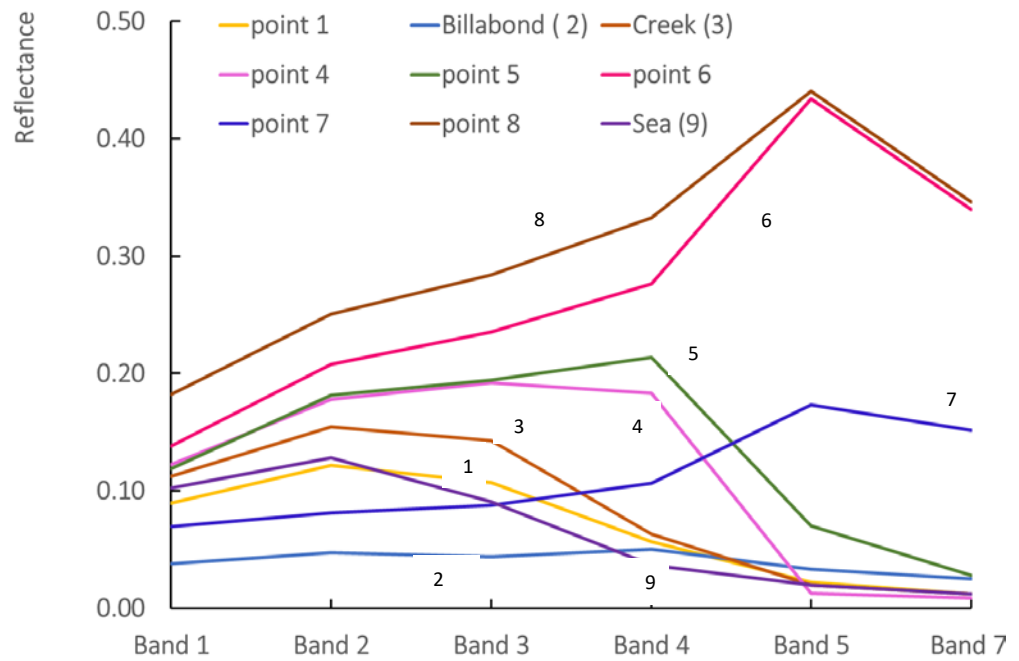


Figure 28 : Investigation of Spectral reflectance curves on 28 Oct 2003 image at different locations

4.2.2 Water extraction with different methods

The inundation areas extracted with different methods are shown in Figure 29. Supervised and unsupervised classification, and MNDWI show higher inundation area when compared to $NDWI_{DN}$, $NDWI_{ref}$ methods and extracted water area from EC JRC-GSW. This behaviour of different methods on the image of partially inundated area is similar to the behaviour in the image on 01 Feb 2010 with a higher inundation area almost over all the mud flat area.

In supervised classification and unsupervised classification, the billabong is classified as not-water. In MNDWI, $NDWI_{DN}$, $NDWI_{ref}$ and EC JRC-GSW the billabong appears as water. In all the methods, some area under the cloud shadow, as shown in Figure 28, has been classified as water.

The supervised classification gives the highest inundation area and the highest overall accuracy for the extraction of water from the image with partially inundated area.

4.2.3 Comparison of water extraction by different methods

The extraction methods with a higher overall accuracy were considered for further investigation. The comparison of inundation areas of unsupervised classification, MNDWI and $NDWI_{ref}$ with supervised classification is shown in Figure 29 and Table 6. The percentage of non-identified water pixels and newly identified water pixels is compared to the supervised classification. Unsupervised classification, MNDWI $NDWI_{ref}$ has not identified 7.51% 9.76% and 14.94% of area and has identified 0.62%, 2.19% and 1% of new area as water compared to the water area in supervised classification.

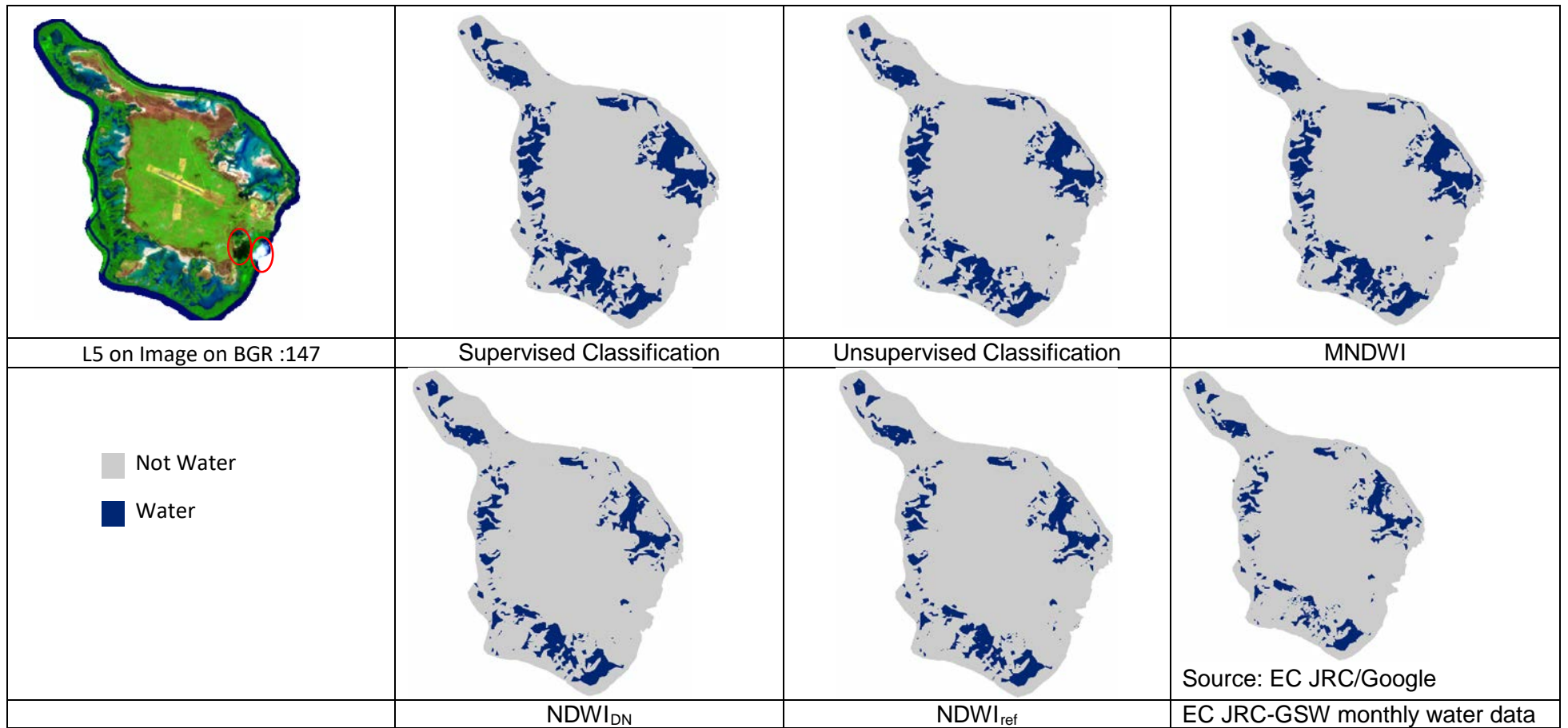


**Figure 28 : Extraction of water area on 28 Oct 2003
by different classifications and methods**

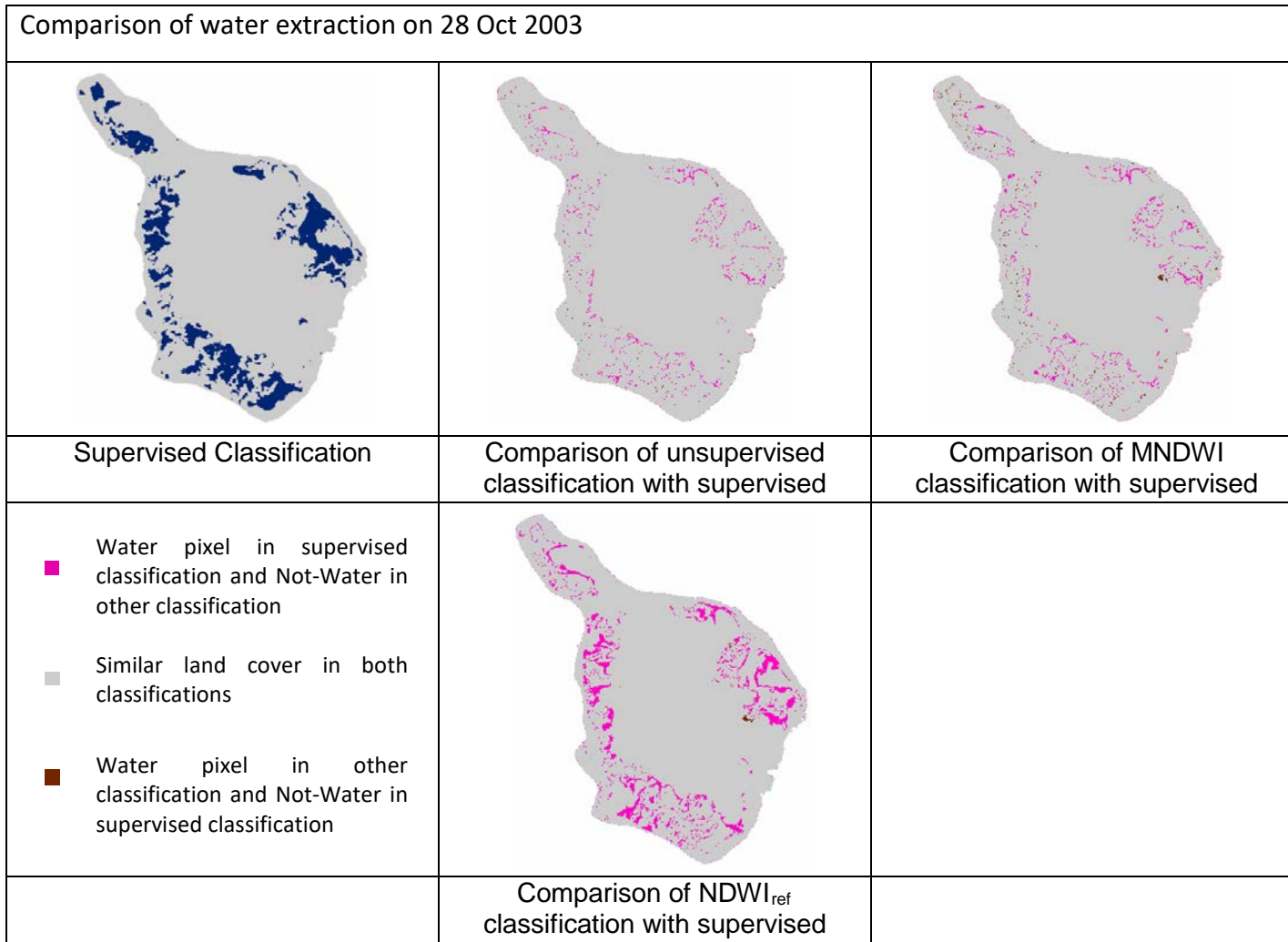


Figure 29 : Comparison of water area extracted on 28 Oct 2003 by different methods with supervised classification

Table 6. Comparison of extracted water area on 28 Oct 2003 by different methods with supervised classification

Type	Unsupervised Classification	MNDWI	NDWI _{ref}
Area not identified as water compared to water area in supervised classification (%)	7.51	9.76	14.94
Other area identified as water compared to water area in supervised classification (%)	0.62	2.19	1.00

4.2.4 Comparison of water extraction by supervised classification and NDWI_{ref}

The comparison of extracted inundation areas of supervised classification and NDWI_{ref} was considered due to the high difference of areas. The spectral reflectance of five pixels is shown in Figure 30. Accordingly, point 1, 2 and 3 are at pixels classified as water by supervised classification and as non-water in NDWI_{ref}. Point 4 and 5 are classified as water in both methods.

At point 1, 2 and 3 the spectral reflectance increases from band 1 to band 4 deviating the spectral reflectance curve of water. From band 4 to band 5 reflectance decreases drastically. The spectral reflectance at point 5 shows a similar behaviour as water in the area (Figure 27) though the reflectance values are marginally low. At point 4 the reflectance slightly increases from band 3 to band 4 deviating from behaviour of water. Then the reflectance is slightly lower in band 4 and much lower in band 5.

Though all the points are blue colour, the pixels visually appear heterogeneous. The water depth is shallow in the inundation area. Point 5 is located in a dark blue zone. It is located in the drainage path and the water depth could be comparatively higher. For visual comparison with the colour composite image it could be water at other points, however, the spectral reflectance does not comply with the behaviour of water.

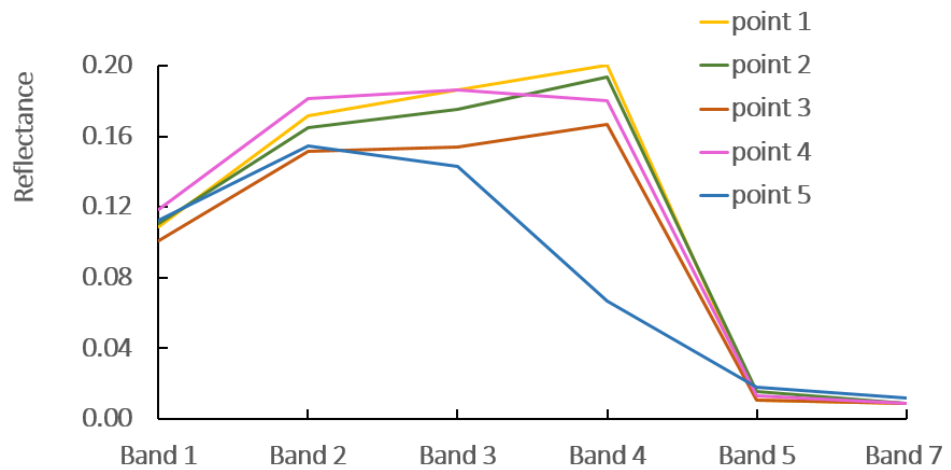


Figure 30 : Comparison of spectral reflectance curves on 28 Oct 2003 image at random points and water points

The water index NDWI compares reflectance in green and NIR. At point 4 the reflectance in NIR is slightly lower than in green. Therefore, pixels similar to the point 4 pixel is classified as water with positive NDWI values above the zero threshold. At point 1, 2 and 3 NIR reflectance is higher than green reflectance and NDWI is negative. Thus those pixels are classified as not-water.

4.3 Discussion on surface water extraction

In both images, some water inundation area according to the visual inspection, shows different spectral behaviour compared to pure water. A higher reflectance in band 1, 2, and 3 and a considerably higher reflectance in band 4 is observed in these areas. A closer look at the pixels in these locations shows heterogeneity in the colour in pixels around the considered pixel. These inundation areas are of shallow water depths. According to Van Der Meer and De Jong (2001), water colour is possibly affected by the constituents and the substrate.

The mud flats in the area are vegetated partly with low sparse samphire shrub lands (Woodgate 2013). This could be observed in the images during wet season and early dry season. It is apparent that there is a seasonal cycle of the vegetation. During the end of dry season, vegetation is not observed on mud flats. Vegetation may dry out due to low soil moisture and increasing salinity due to evaporation. During the wet season, vegetation blooms on the mud flats. These submerged vegetated mud flats may affect the increase in reflectance. According to Van Der Meer and De Jong (2001) the suspended sediments and the planktons in water increases the reflectance.

The spectral reflectance curve for pure water in Figure 2 and 3 show that the reflectance in band 1, 2, and 3 are well below 0.05. Figure 21 shows that the reflectance in band 1, 2, and 3 for water in the billabong are above 0.05 and are higher for band 4. According to Woodgate (2013) the billabong water has high salinity concentration. According to Lavery et al. (1993), Landsat TM band 4 is correlated with salinity. The higher reflectance in the water in the study area could be due to the sediments, salinity in water, shallow water depth, and the salty background.

The water area includes many small isolated water pockets. The areas smaller than 30 m by 30 m are most likely not classified as water due to the limiting spatial resolution of 30 m in Landsat. The mixed pixels near the boundaries contribute significantly to the difference in identifying water based on the behaviour of the index. The submerged weeds, sediments, bottom reflection, and overhanging trees could be reasons for mixed pixels.

In all methods used for water extraction, the creeks were not identified as water. The creeks paths were classified as vegetation in supervised and unsupervised classifications and as not-water in index methods. This could be due to the overhanging mangroves and the spatial resolution of 30 m in Landsat images. According to Woodgate (2013) tidal creeks are fringed by *Rhizophera* mangrove forest.

For $NDWI_{ref}$, zero threshold was used as proposed by McFeeters (1996) and the image was visually appealing without known not-water areas classified as water. For MNDWI and $NDWI_{DN}$, most images were visually not appealing at the land boundary and with many water pixels in not-water area at the zero threshold. However, the classified images visually showed similar pattern and distribution of water area. The overlay of 1 m or 0.5 m contours developed with SRTM 30 seconds data was not successful to distinguish low elevation areas to improve the threshold. Use of accurate elevations could improve the threshold in identifying possible lower elevation areas prone to inundations compared to adjacent higher elevations.

The permanent water feature, the billabong is a small area shown in the images by about six pixels. The inundation area changes for each image. The water depth is shallow, the bottom reflection is significant, and the spectral behaviour of water is

affected. The ground data of inundation area concurrent with an image is not available. Supervised classification is more appropriate for the study of changing shallow surface water inundations in this study area. The inland water area, which is classified in one class with seawater could be used to take training samples. Also, the training samples could be located at pixels of similar behaviour with water by investigating the spectral reflectance pattern. Unsupervised classification could be used to identify the spectral distinct classes before the supervised classification. Optimum results can be achieved using a combination of supervised and unsupervised classification (Erdas 1999).

4.4 Performance of water extraction on multiple images

The graph in Figure 31 shows the inundation area extracted from different methods on 13 images. According to the graph, the general performance of different water extraction methods showed consistent behaviour in each image.

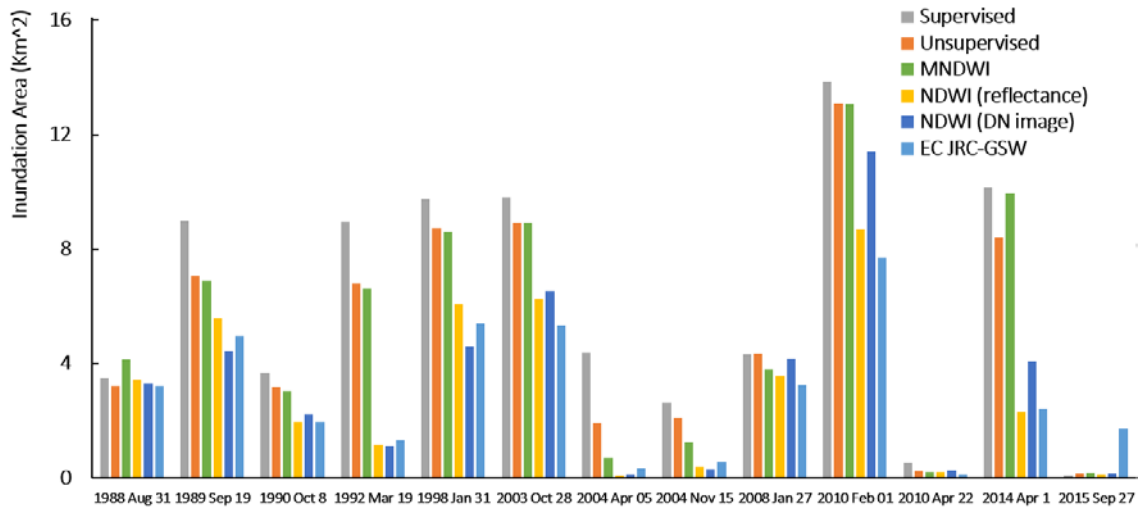


Figure 31: Extraction of inundation area on thirteen images with different methods

Except for the image of 31 Aug 1988, supervised classification shows the highest inundation area of all images. Unsupervised classification and MNDWI show closely matching inundation area but slightly higher with the unsupervised classification. The MNDWI inundation area of 31 Aug 1988 are higher than the supervised classification. Generally, unsupervised classification, supervised classification, and the index MNDWI show higher inundation areas for all images. The inundation area extracted from NDWI and EC JRC GSW is lower.

When comparing $NDWI_{ref}$ and $NDWI_{DN}$, the performance is not consistent. $NDWI_{ref}$ images have the variable atmosphere removed as well as normalised earth-sun distance and solar elevation normalised, where the $NDWI_{DN}$ images have not. Atmospheric attenuation can seriously affect the DN values of green wavelengths to the fourth power relative to NIR, thus the results from ratioing these two bands under

different atmospheres will produce vastly different results due to green bias. Also, the zero value used as the threshold will shift under different illumination and atmospheric conditions. All of this is normalised and robust comparisons over time can only be made using at surface reflectance data. $NDWI_{ref}$ extracts higher inundation areas for the images of 31 Aug 1988, 19 Sep 1989, 19 Mar 1992, 31 Jan 1998 and 15 Nov 2004 compared to $NDWI_{DN}$. However, the inundation area of $NDWI_{DN}$ on 01 Feb 2010 and 01 Apr 2014 is significantly higher than $NDWI_{ref}$. The inundation area of $NDWI_{ref}$ is extracted with a zero threshold according to the original proposal by McFeeters (1996). The water extraction at zero threshold shows consistent performance with visual inspection of the images. The billabong was mapped as water and no water areas appeared in higher elevation areas or in vegetation areas in the central part. Whereas the threshold values between 0.02 to 0.1 were used for $NDWI_{DN}$. According to Liu, Yao and Wang (2016) $NDWI_{ref}$ has better performance than $NDWI_{DN}$.

Both unsupervised and supervised classifications use spectral behaviour of the land cover types. The extracted inundation area in unsupervised classification was 5.6% (Table 5) and 7.5 % (Table 6) lower than supervised classification respectively on 01 Feb 2010 and 28 Oct 2003. ISO DATA method in the unsupervised classification use the straight Euclidean distance to measure the similarity in clustering (Sohn & Rebello 2002). ISO DATA method is iterative, hence, it is not geographically biased to the top of the data as it redefines the criteria for each class again in each iteration, so that spectral distance patterns in the data gradually emerge (Erdas 1999). The threshold is applied so that the patterns, which shows probabilities below the threshold, are not classified.

In supervised classification, taking appropriate training samples to represent the mean vector and the variability in the class is most important. The performance of the maximum likelihood method used for the supervised classification depends on the estimation of mean vector and the covariance matrix (Richards & Jia 1998). The decision rule of the maximum likelihood method is based on the probability that each pixel belongs to a particular class estimated on a weighted distance (Sohn & Rebello 2002). When the band shows normal distribution, equal probabilities are assumed for each of the classes (Erdas 1999).

Gautam et al. (2015) found that water extraction by MNDWI is closely matching with supervised classification, and that performance is similar in this study. Gao et al. (2016) found that NDWI is weak in extracting small water bodies.

4.5 Accuracy assessment

4.5.1 Overall accuracy

The overall accuracies of the accuracy assessment done by the interpretation of colour composite image as substitute for ground data, for the six methods of water extraction are shown in Figure 32.

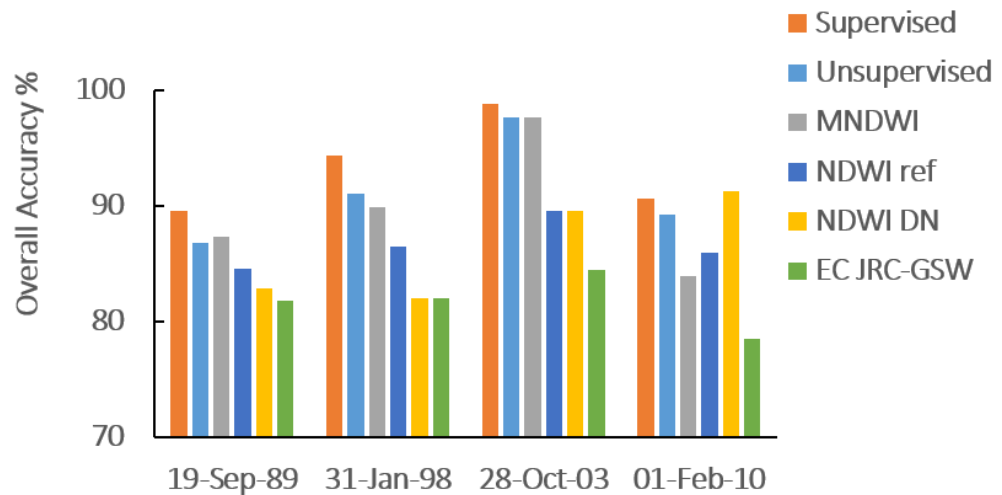


Figure 32: Overall accuracies of different methods of water extraction on four Landsat 5 images

The accuracy assessment is required to ascertain the best performing method for the study area and to evaluate the confidence for using the inundation area for developing a time series of inundations. According to the results, the overall accuracy varies from 81.77% to 98.80% for all the methods in different images. Both unsupervised and supervised classifications show overall accuracy greater than 85%,

which is widely accepted for image classifications with remote sensing data (Foody 2008).

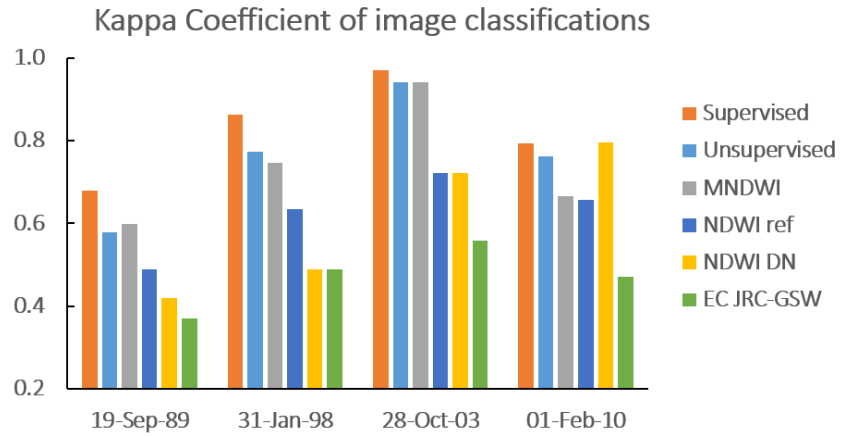
Supervised classification shows the highest accuracy in all the three images with a highest accuracy of 98.8% for 28 Oct 2008 and a lowest accuracy of 89.5% for the 19 Sep 1989 image. On 01 Feb 2010, the highest overall accuracy of 91.28% is in NDWI_{DN} whereas the value in supervised classification is 90.60%. The highest overall accuracy of unsupervised classification is 97.6 % for the 28Oct 2008 image and the lowest accuracy is 86.7% for the 19 Sep 1989 image. Overall accuracy of both supervised and unsupervised classification show similar patterns of change in performance in all four images.

The water index MNDWI shows a highest accuracy of 97.6%, however its lowest accuracy of 83.89% is below the widely accepted accuracy level. The comparison of performance of overall accuracy of NDWI_{DN} and NDWI_{ref} is inconsistent. The overall accuracy of NDWI_{ref} is higher in two images, and lower in one image compared to NDWI_{DN}. On the 28 Oct 2003 image, NDWI_{ref} is similar to NDWI_{DN}. EC JRC-GSW shows the lowest overall accuracy level in all the four images, and it is lower than 85%.

The overall accuracy is highest in supervised classification for three images. NDWI_{DN} shows the highest overall accuracy for the 01 Feb 2010 image, whereas this image shows the highest inundation area among the images used for this study.

4.5.2 Kappa coefficient

The kappa coefficients of the accuracy assessment for the six methods of water extraction are shown in Figure 33.



	Unsupervised	Supervised	MNDWI	NDWI _{DN}	NDWI _{ref}	EC_JRC-GSW
19-Sep-89	0.58	0.68	0.60	0.42	0.49	0.37
31-Jan-98	0.77	0.86	0.75	0.49	0.64	0.49
28-Oct-03	0.94	0.97	0.94	0.72	0.72	0.56
01-Feb-10	0.76	0.79	0.67	0.80	0.66	0.47

Figure 33: Kappa coefficients of different methods of water extraction for four Landsat 5 images

Kappa coefficient varies from 0.37 to 0.97 for all the classifications. Supervised classification shows the highest kappa coefficient for three images. For the 01 Feb 2010 image, NDWI_{DN} shows the highest kappa coefficient whereas NDWI_{ref} shows the highest overall accuracy on the same image and the image shows the highest inundation area among all the images. The kappa coefficient of 0.79 for supervised classification closely matches the highest value of 0.80 for NDWI_{DN}.

The kappa coefficient for 19 Sep 1989 is low for all the methods. Other than that, supervised, unsupervised and MNDWI methods show higher kappa coefficients than other methods. Similar to overall accuracy the comparison of performance of kappa coefficient in $NDWI_{DN}$ and $NDWI_{ref}$ is inconsistent. Both methods show good values and low values on different images. The kappa coefficients of EC JRC-GSW show the lowest values out of the six methods.

4.5.3 Figure of merits

4.5.3.1 Figure of Merits on 01 Feb 2010

The 'Figure of Merits' measure on comparing the spatial distribution is shown in Figure 34. The agreement between supervised and unsupervised classifications (0.86) is similar to the agreement between supervised and MNDWI method. It is a clearly better than the value of 0.58 between supervised and $NDWI_{ref}$ method.

4.5.3.2 Figure of Merits on 28 Oct 2003

According to the 'Figure of Merits' measure (Figure 34), the agreement between supervised and unsupervised classifications is the best with the value of 0.87. The agreement between supervised and MNDWI method (0.84) is closely matching with the best value. The poorest performance with an agreement value 0.77 is between supervised and $NDWI_{ref}$ method.

■ Water pixel in both images (intersection) ■ Water pixel in one image

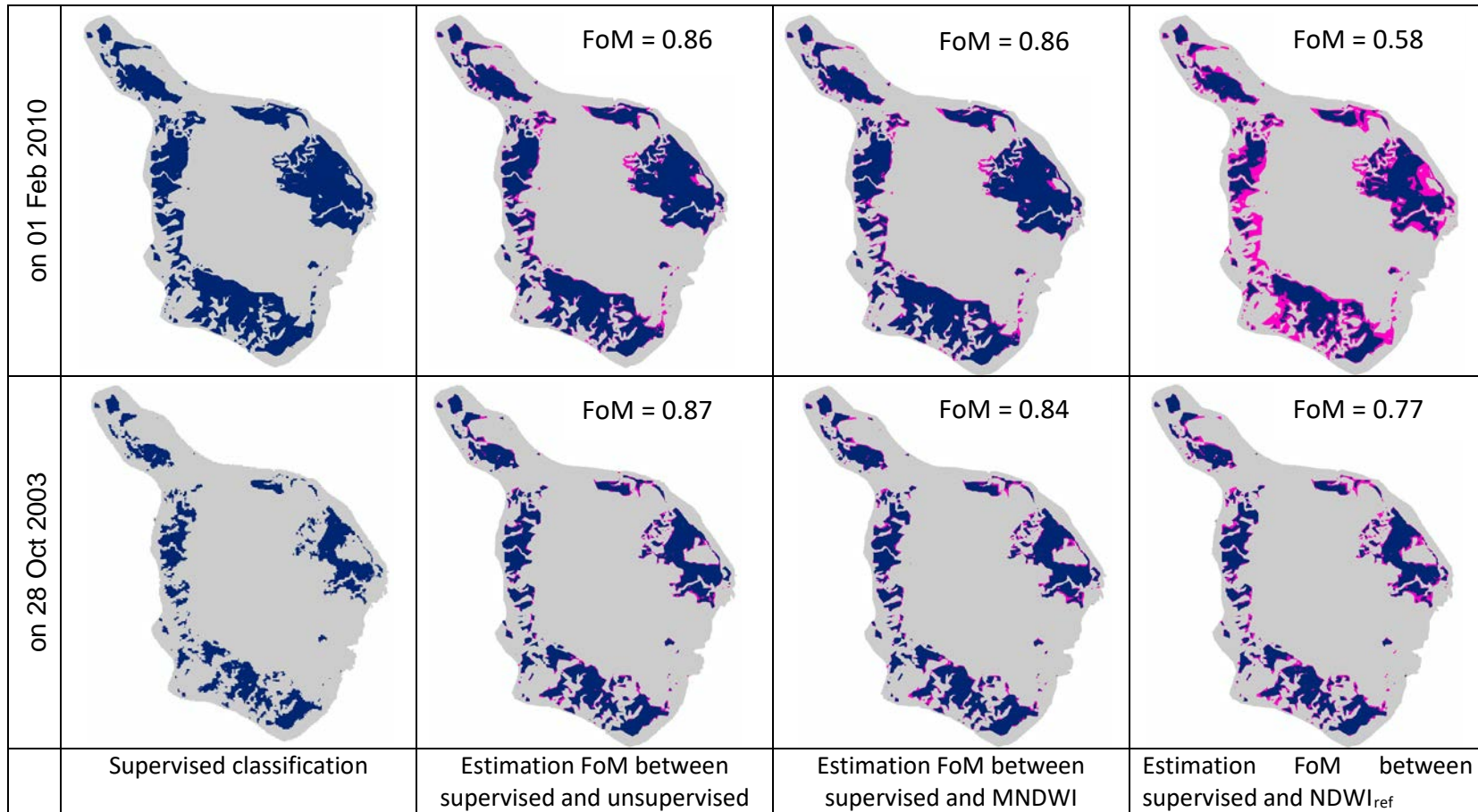


Figure 34: Estimation of Figure of Merits between different classification and methods on 01 Feb 2010 and 28 Oct 2003

4.5.4 Discussion on accuracy assessment

Overall accuracy and the kappa coefficient is non-site specific accuracy assessment. It considers only the total amount of water and not-water pixels without considering their spatial distribution. In this method of accuracy assessment, there is a possibility of balancing out the errors in different locations. It may lead to a misleading result of high accuracy. A better assessment would be achieved if the accuracies were assessed separately for different zones of inundation. Comber et al. (2012) use a geographically weighted regression to analyse the spatial variations in the accuracy of the classification.

In the accuracy assessment of the maps of low inundation area, with random sampling the number of sample points in the water area was very low. The random sampling is a weighted based method on the area. Selecting 200 sampling points was not adequate to represent the small class of water when compared to the bigger class of non-water in the images of partially inundated area particularly when the land area contains more points than the water area. In addition, ambiguous pixels in the water and non-water boundary were deleted without assigning them to a class. There was a possibility that the smaller number of points in the water class could not be adequately represented in the accuracy assessment.

Therefore, the accuracy assessment of the classification, especially for the images of low inundation area, could be improved by using a stratified random sampling approach. This could be achieved if the image is divided into grid cells and sample points were developed based on the grid cells. In a better way, the image could be considered in two thematic layers of water and non-water for the random sampling.

Then a near-similar number of random points could be chosen from each thematic class for the accuracy assessment.

During the accuracy assessment in this study, the areas used to train the classifier were excluded in generating the random ground data points to avoid overestimation of the accuracy and bias on the accuracy of the supervised classification. However, taking a homogeneous training area may not provide the variability within one cover type in individual pixel levels during the classification. Water inundation area in this study shows different characteristics of different salinity levels over salty flats, submerged weeds, and water under the overhanging vegetation along the creeks and mangrove forest. This may be reflected in the accuracy assessment.

In accuracy assessment, the error matrix is used based on the assumption of pure pixels and the perfectly located ground data points. The ground data set is considered as accurate. However, there could be mis-location of referenced ground data points and points in the thematic map. Foody (2008) says very large numbers of mixed pixels are in an image as a function of spatial resolution and the land cover mosaic. The accuracy assessment could be improved by using a high resolution image to collect ground data. As the inundation area is changing, it was not possible to find concurrent Google Earth images to collect ground data.

According to the accuracy assessments on the four images excluding the training area for random sampling to avoid bias, the supervised classification shows the best accuracy in three images. The supervised classification showed values close to those values with the highest accurate method of $NDWI_{DN}$ on the other image on 01 Feb 2010. The image on 01 Feb 2010 shows the highest inundation area and, for most of the time, that area is partially inundated. Supervised classification showed highest

accuracy in extracting water area in partially inundated maps. Therefore, supervised image classification was considered as the best performing method for extracting surface inundation areas according to the environmental conditions of the study area.

4.6 Correlation between rainfall and inundation area

The extracted inundation area by supervised classification for 24 selected images (Figure 35) with no clouds during the study period from 1987 to 2016 is plotted in Figure 36 with the daily rainfall. The inundations in the wet and dry season are distinguished by colours. It shows that there are large inundations in the dry season. The plots of inundation area against cumulative rainfall for 15 days, 30 days, 60 days, and 90 days are shown in Figure 37. According to the Figure 37, most of the inundation occurrences in the dry season have either zero rainfall or close to zero rainfall. It follows that there are areas being inundated during the dry season at times when there is no or very low rainfall in Milingimbi Island.

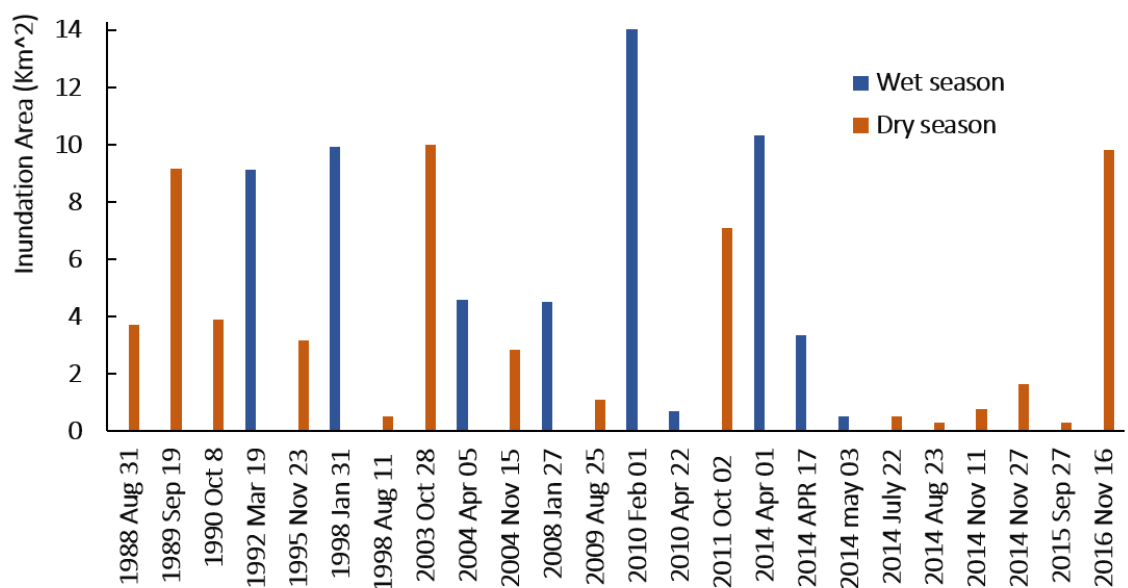


Figure 35 : Extracted surface water inundation areas by supervised classification on 24 images from 1987 to 2016

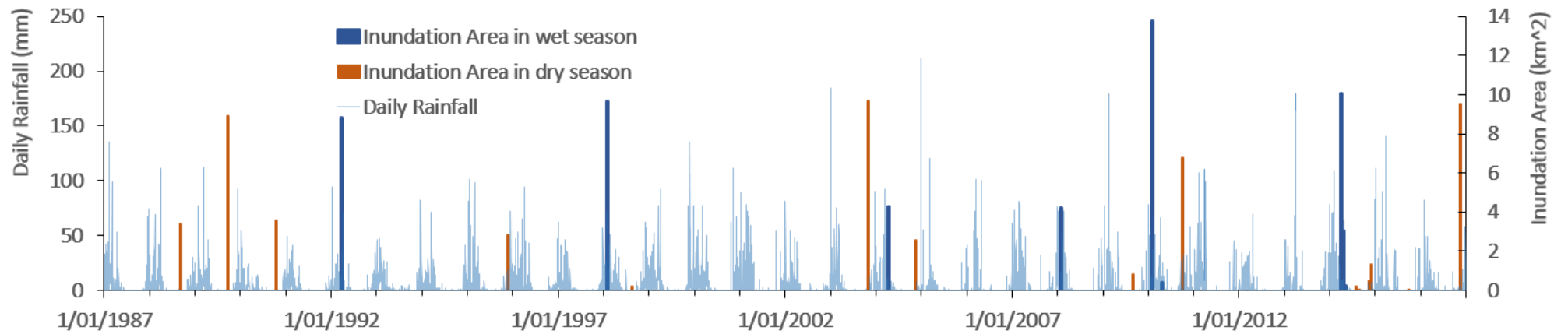
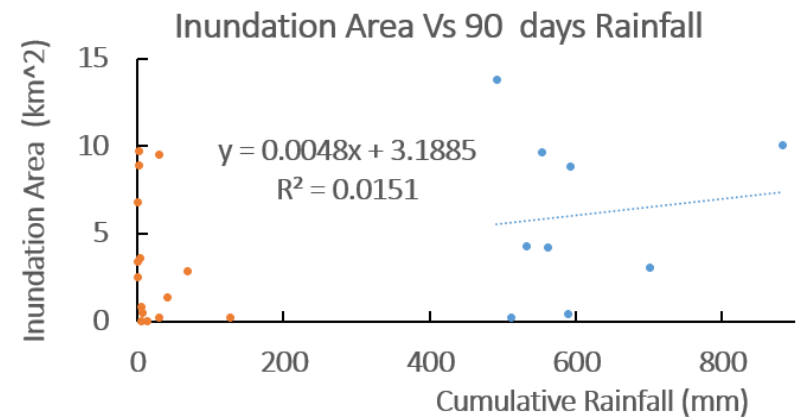
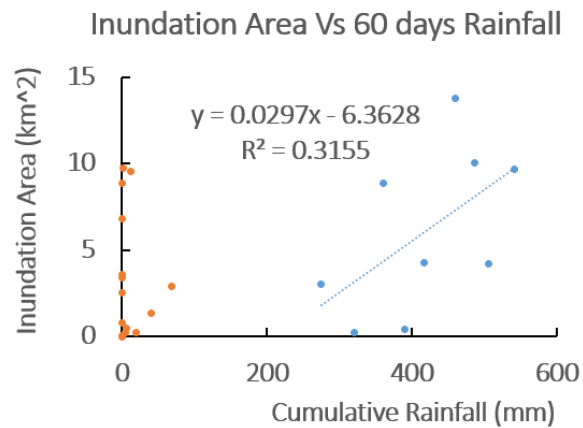
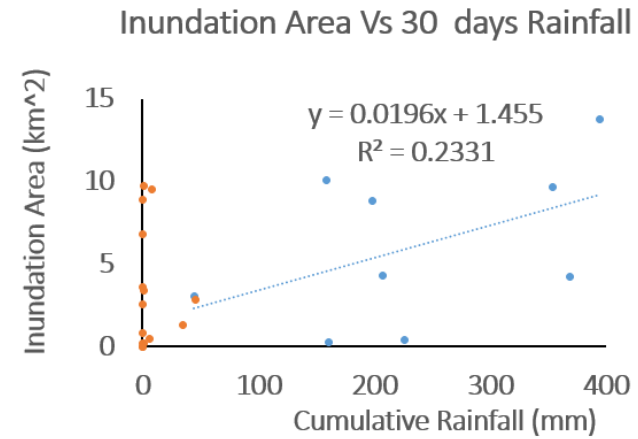
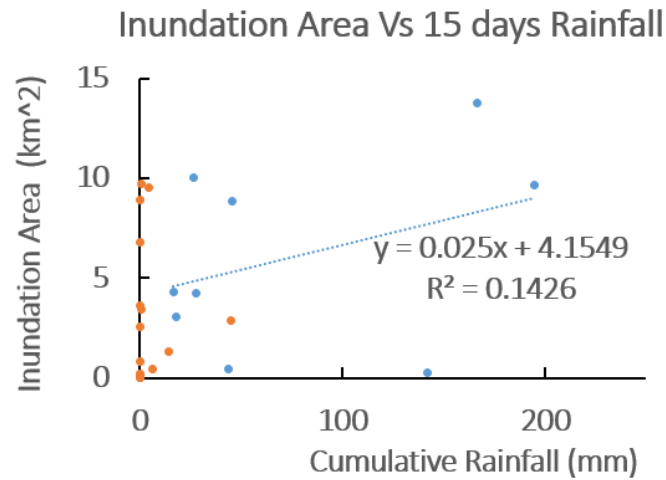


Figure 36 : Investigating surface water inundation areas and rainfall by comparing extracted inundation area on 24 images with daily rainfall from 1987 to 2016



● Inundation area in wet season ● Inundation area in dry season

Figure 37 : Correlation between inundation area and cumulative rainfall of 15, 30, 60 and 90 days

According to the plots of inundation area compared to an increasing number of days of cumulative rainfall (15, 30, 60, and 90 days), the best correlation of 31% is shown for 60 days cumulative rainfall. The low number of data points would have affected the correlation. In the wet season, there are two images, (22 Apr 2010 and 03 May 2014) at the end of the wet season, with high rainfall but low inundation areas. This small area of inundation could be a result of the inundation being very shallow and combined with a high evaporation rate reducing the extent of the inundation area.

To investigate the extent of inundation area during the dry season, all available images with surface inundation (3 in wet season and 4 in dry season) in 2014 were plotted with daily rainfall (Figure 38). In the months of June, August, September and October (dry season) no inundation areas were observed in the images. The rainy season finished in the month of April and during the months from May to December, there was no considerable rainfall other than a few minor daily events of less than 10mm. In the dry season, this rainfall is unlikely to generate surface runoff and areas of inundation due to rapid infiltration and high evaporation rates.

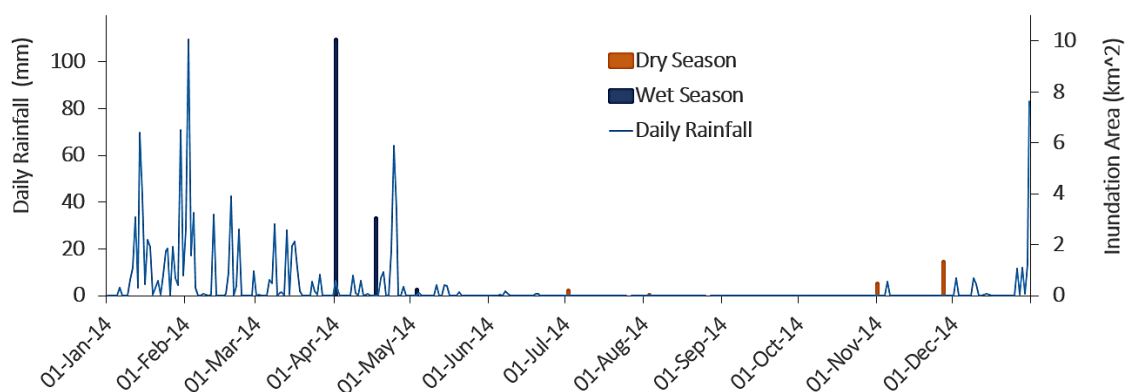


Figure 38 : Daily rainfall and extracted surface inundations in 2014 from seven images

4.7 Correlation between sea level and inundation area

The correlation between sea level variation recorded at Darwin and Groot Eylandt tidal gauge stations and inundation area on Milingimbi Island was investigated for the years 2003, 2011, and 2016 in which large areas of water inundation were observed in the dry season without periods of rainfall (Figure 39 and Figure 40).

At the Darwin tidal gauge the average monthly sea level is higher from January to April, and drops in May with a lower sea level recorded in June and July. The sea level increases from August and is high again in October and November. At Groote Eylandt, sea level is higher from January to March, becomes lower from March to November, and increases again in December.

If sea level variation at Milingimbi Island has a similar pattern to that of Darwin, there are higher tides during October and November and therefore the higher tide can cause inundation in the lower elevation coastal area of Milingimbi Island.

In the late dry season, larger areas of inundation on the island were observed in the months of October and November. Therefore, it is reasonable to suggest that the rise in sea level in Milingimbi Island in the months of October and November may be the cause for coastal inundation.

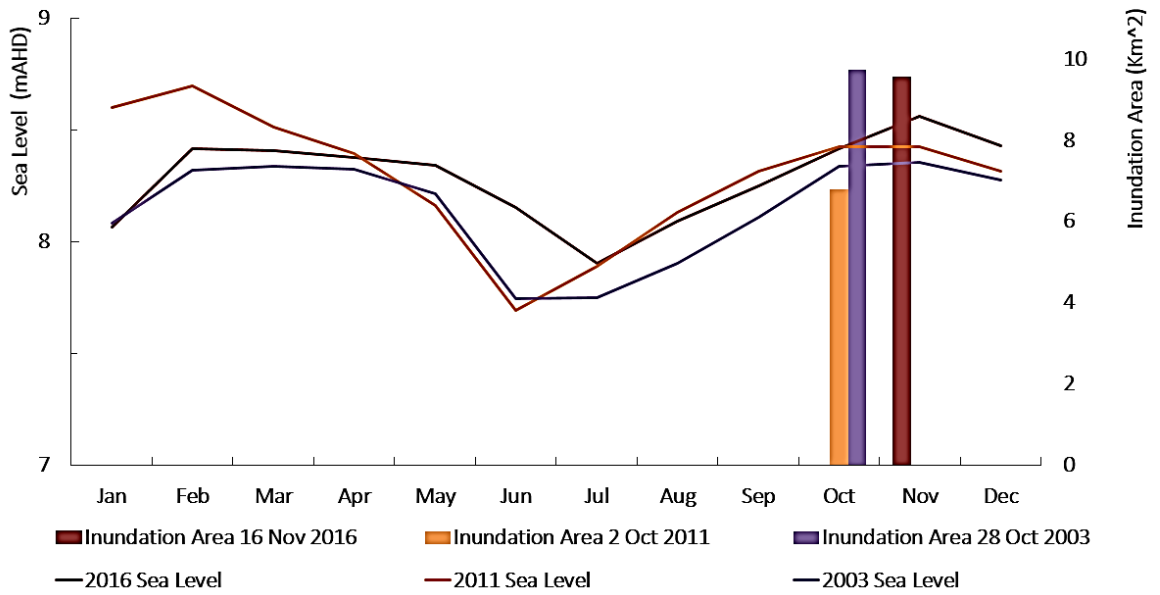


Figure 39 : Average monthly sea level variation recorded at Darwin tidal gauge and dry season surface water inundation area in Milingimbi Island for years 2003, 2011, and 2016.

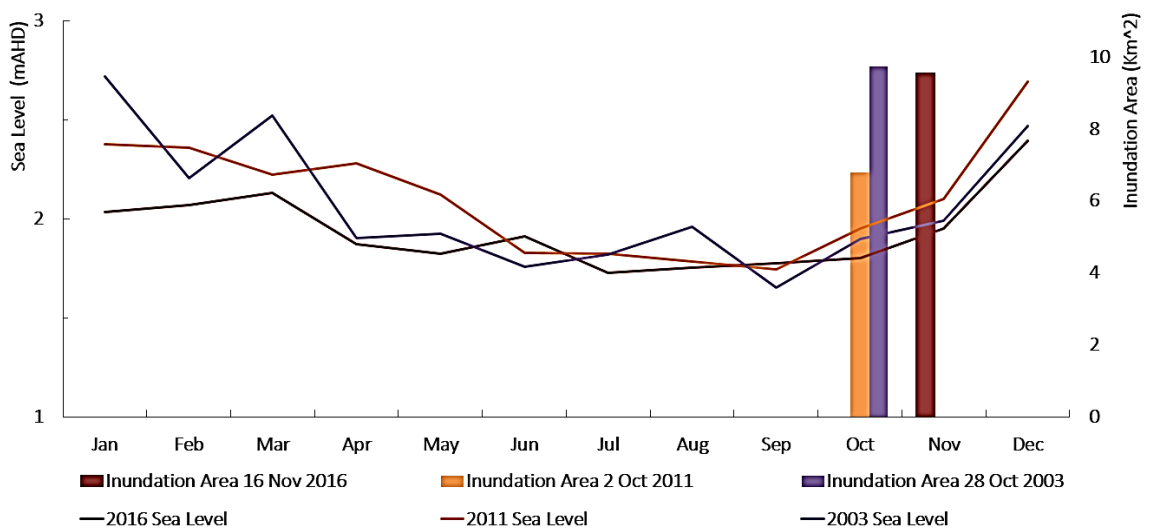


Figure 40 : Average monthly sea level variation recorded at Groot Eylandt tidal gauge and dry season surface inundations in Milingimbi Island for years 2003, 2011, and 2016

4.8 Frequency of inundation

4.8.1 Frequency of wet season inundation

The map in Figure 41 showing the inundation area during the wet season was prepared by stacking nine thematic maps of the wet season as shown in Figure 35. The frequency of inundation was assigned to each pixel with the ratio of number of times water was observed in the pixel compared to the total number of times of observations.

During the wet season 5.8 km² and 5.2 km² of area has the frequency of inundation between 25.1 -50 % and 0.1 – 25% respectively. The inundation area is low for the frequency above 50%.

4.8.2 Frequency of dry season inundation

Fifteen thematic maps of the dry season as shown, in Figure 35, were used to prepare the dry season inundation map shown in Figure 42. The frequency of inundation was assigned to each pixel with the ratio of number of times water was observed in the pixel compared to the total number of times of observations (15 for dry season map).

During the dry season, larger area of 6.8 km² has the frequency of inundation of 0.1 – 25%. The area is significantly reduced to 3.5 km² for the frequency of 25.1 -50 %. The land area of frequency of inundation above 50% is low (2.6 km²).

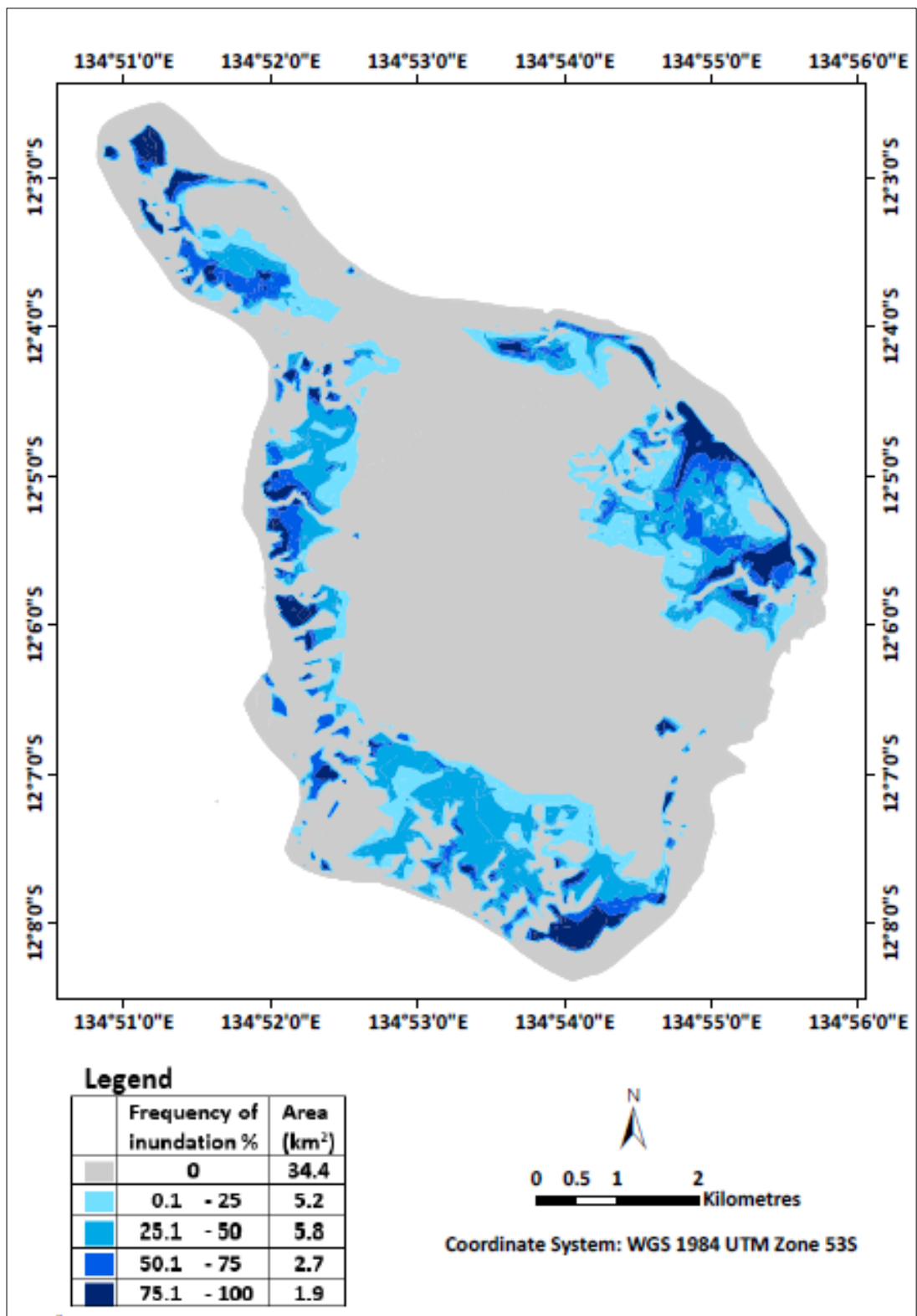


Figure 41 : Wet season inundation areas and the frequency of inundation mapped with nine wet season images

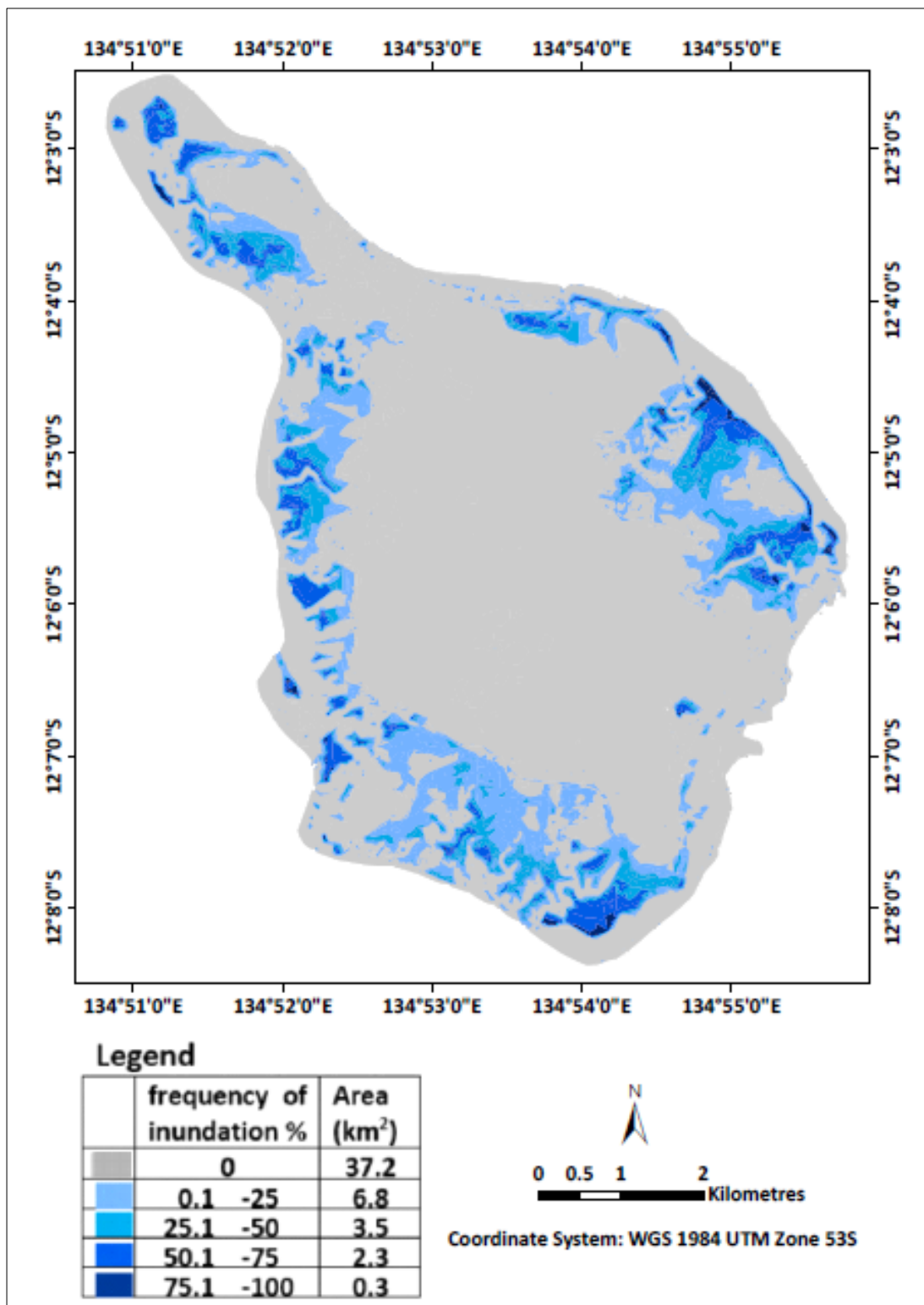


Figure 42 : Dry season inundation areas and the frequency of inundation mapped with nine dry season images

The given inundation area and the frequency may change both in wet and dry seasons, if the inundation area map is prepared with more images. For higher frequency of inundation over 50%, the area of inundation is significantly low in both wet and dry seasons. This could be affected by rapid surface runoff or high evaporation during the dry season.

5. CONCLUSION

5.1 Research findings

In this study, Landsat images were used to detect the surface inundation area in Milingimbi Island. Unsupervised classification, supervised classification, NDWI, MNDWI, and the water area from EC JRC-GSW data were used to extract the inundation area. Unsupervised, supervised classifications and MNDWI methods show similar values of inundations. This value has a significant difference with the areas of NDWI and EC JRC-GSW data. The inundations in this study area are of shallow water on salty flats and vegetated mud flats. The water constituents have affected the spectral characteristics and the performance of NDWI. The inundation area changes rapidly; therefore, use of prior knowledge of the area will improve the classifications. With the accuracy assessment of the classifications, and the above background conditions, supervised classification was found appropriate for extracting inundation areas in this study area.

There are no on-site records or previous studies done on the surface water in Milingimbi Island (Batelaan et al. 2015). This study demonstrates the capability of finding the inundations in the past using remote sensing which is required to investigate any changes in the inundation areas. EC JRC-GSW data gives the water area for each month from May 1987 to Sep 2015 for this study area. In addition to Landsat 5 and Landsat 8 images used for this study, EC JRC-GSW has used Landsat 7 ETM+ images for some months with scan line correction and for some months without the correction. EC JRC-GSW data has not proven a high accuracy in matching water areas with the classifications performed in this study. According to Huntington (2006) global and regional analyses are sometimes contradictory and variable to local

situations if not verified with local ground truth data, as there is a certain error in each classification. The use of EC JRC-GSW data as a monthly time series of surface water for investigating the surface inundation of Milingimbi Island is therefore not recommended.

According to this study, it is evident that there are areas of inundations on Milingimbi Island during the dry season when there is no or insignificant rainfall. The area of highest frequency of inundation between the wet and dry season is distinct and shows the possibility of different sources of inundation, which are either by rainfall or by higher tidal inflows. In the dry season, the cloud cover does not affect most of the images showing surface inundation. Therefore, remote sensed images of Landsat could be used to extract dry season inundations. Additionally, accurate onsite sea level monitoring in Milingimbi Island is required for further investigations of the inundation area and the effect of sea level rise.

The cloud cover has affected almost all wet season images in this study area. Use of optical remote sensing to observe the inundation area during the wet season is limited because of this factor. The hydrological characteristics of these small catchments are difficult to model especially with low temporal resolution optical remote sense images. The observed correlation between wet season inundation and cumulative rainfall in this study is poor. The result is highly affected by the low number of data points. In this study 60 days cumulative rainfall has shown the best correlation of R^2 0.31. Use of more data points by extracting inundations in more images will improve the correlation.

5.2 Limitations of the study

The cloud cover over the study area in the wet season has affected the extraction of inundation area.

The surface inundation on Milingimbi Island is seasonal and the area changes within a short duration. The possibility of observing different status of inundation under one significant rainfall event depends on many other factors, including repeat cycle of the Landsat satellite and the cloud cover. It also affects the possibility of using high-resolution image data for verification. Concurrent Google earth images were not found for the considered images during this study. Near-time data is not accurate for the verification of changing water area though could be used for accuracy assessment of permanent water features. Prior knowledge of the area provides limited information if the same inundation event is not observed. Therefore, collection of ground data of inundation for verification, concurrent with satellite passing time would improve the accuracy of the classification.

It was not possible to identify inundation areas that were smaller than 30 m by 30 m due to the 30 m spatial resolution of Landsat images. Most of the classifications were not able to pick up the creeks due to overhanging vegetation. At the boundaries of the creek lines, the submerged and the overhanging vegetation affected the water detection. Also due to the temporal resolution of satellite images, small water areas of short duration would not contribute to the possible inundation area in identifying the total inundation area under a certain sea level or cumulative rainfall. During the dry season, high evaporation may also affect the drying out of small, shallow

inundation areas. Use of better spatial and temporal resolution images or radar images would be an advantage for developing a time series of inundation data.

5.3 Outcome of the study

This study shows that there are surface inundations on Milingimbi Island during the dry season, which could be occurring due to the inland propagation of the tides.

For the first time, two maps of wet season and dry season inundation areas were developed for Milingimbi Island using extracted inundation area from eight images and sixteen images respectively. The maps show the frequency of inundation for each inundation area. The change in spatial distribution of dry season inundation was compared between Sep 1989 and Nov 2016 in which the total inundation area has closer values. The outcome has the limitation of unknown corresponding sea levels.

These maps could be used,

- To inform the Bureau of Meteorology to identify the requirement of establishing sea level monitoring station in Milingimbi.
- By Power and Water Corporation, NT for improving the water management plan for the island.
- By the Department of Environment, Water and Natural Resources to implement precautionary actions to protect the aquifer recharging area and to minimise the adverse impacts to the groundwater due to overland tidal flows.
- By Northern Land Council, NT to implement land management plans addressing control measures for land degradation.

- By the researchers for studies on surface water, and interaction between surface and groundwater in Milingimbi Island.

The outcome of this study provides a significant alert to the local community in the Milingimbi Island, water resources managers, and local and national administrators on the problem of land surface inundation from the tidal waves.

5.4 Recommendations for future researches

According to BoM (2016), the sea level in Northern Australia is rising at a greater rate than the global average. This would lead to increases in surface inundation due to tidal waves. However, this comparison of inundation area is more meaningful if the corresponding sea level is considered. Therefore, establishment of sea level monitoring on Milingimbi Island in co-operation with the local Indigenous community is a most important recommendation to investigate the impacts on the surface inundation due to sea level rise.

Erosion on the island due to runoff during the rainy season or the propagation of tidal waves can lead to an increase in degraded lands. Identifying the change in the low lying degraded salty mudflat land area would provide more understanding on the dynamics of this environment. The degraded land is easily identifiable in the dry season. This would require accurate ground data for training and verification in the classification process to overcome the challenges in distinguishing spectral characteristics of ground objects. This would be more prominent in distinguishing the boundary between salty flats and dry soil.

The increase in degraded low land area would increase the inundation area. Increased inundation with saline water has the possibility of affecting the only

drinking water source: the central aquifer. Identify the recharging area of the aquifer and precautionary measures to prevent intrusion of surface water in salty land area is the most important research recommended for the welfare and future livelihood of Indigenous people on Milingimbi Island.

Time of the highest inundation area and the satellite passing over the study area is not concurrent. Therefore, the area of inundation extracted from the images would not give the maximum inundation area corresponding to a sea level rise or rainfall. Establishing an accurate elevation data is important to identifying the inundation area correctly for each height of the sea level gauge. High vertical resolution elevation data would help to develop inundation maps for different tidal heights.

This study recommends accurate in situ sea level monitoring, identifying the groundwater recharge area, study of land degradation, and establishing accurate elevation data to project the future impacts on the limited land and water resources of Milingimbi Island. In the first instance, establishment of a tidal gauge on Milingimbi Island would help to identify the impact of sea level rise on areas of surface water inundation, particularly during the dry season. These recommendations form a valuable, strategic and timely approach to investigating and ultimately overcoming the problem of inundation and degradation of the environment of Milingimbi Island.

6. APPENDICES

Appendix 1 - Summary on literature review on different methods for detecting surface water

Method	Algorithm	Proposed by	Applied by	Satellite/ Sensor	Study Environment	Remarks
Threshold in band 5	Single band threshold		Haibo et al. (2011)	Landsat ETM ⁺	Small water features and reservoir in built-up environment.	Extraction with more noise, and need lot of visual comparison. Low accuracy. (in DN value image)
NDWI	$NDWI = \frac{Green - NIR}{Green + NIR}$	McFeeters (1996)	McFeeters (1996)	Landsat MSS	With both fresh and alkaline lakes and irrigated fields	Enhance water features. (proposed with reflectance)
			Xu (2006)	Landsat ETM ⁺	Three environments of lake, river and ocean with vegetation and built up lands	Noise of built up area is mixed with Extracted water features. (in DN value image)

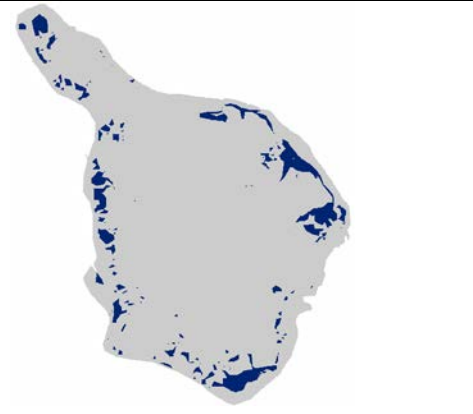
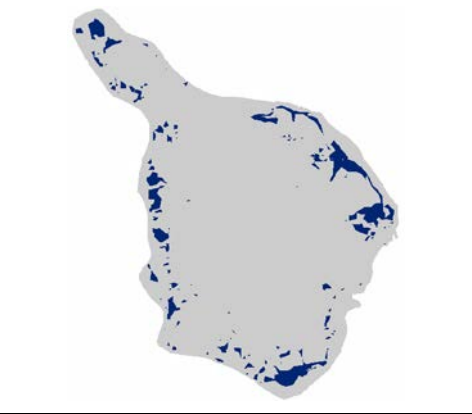
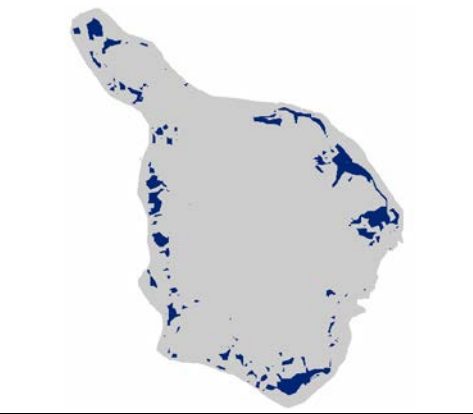
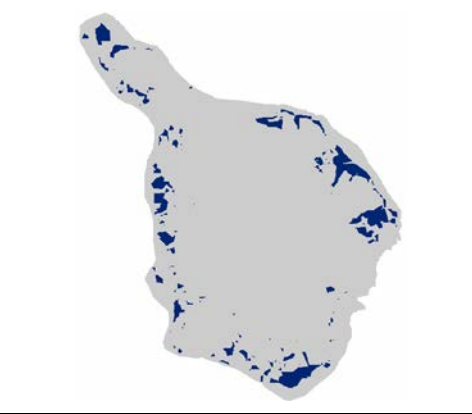
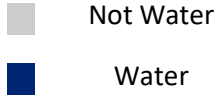
Method	Algorithm	Proposed by	Applied by	Satellite/ Sensor	Study Environment	Remarks
NDWI			(Haibo et al. 2011)	Landsat ETM	Small water features in built-up environment.	Water extraction is mixed with noise from non-water features buildings and soils. (in DN value image)
			Liu, Yao and Wang (2016)	Landsat 8 OLI	Highland area with many large lakes	NDWI35 with reflectance image is better compared to NDWI36 with DN value image.
			(Gao et al. 2016)	Landsat 8 OLI	Mountainous area and flat plateau area	Eliminate mountain shadow, weak in extracting small water bodies. (in DN value image)

Method	Algorithm	Proposed by	Applied by	Satellite/ Sensor	Study Environment	Remarks
MNDWI	$MNDWI = \frac{Green - MIR}{Green + MIR}$	Xu (2006)	Xu (2006)	Landsat ETM ⁺	Three environments of lake, river and ocean with vegetation and built up lands	Suppress or remove the noise of built up environment (in DN value image)
			Xu (2006)	Landsat ETM ⁺	River environment with vegetation	No major difference in water features between the MNDWI and NDWI images.(in DN value image)
			Haibo et al. (2011)	Landsat ETM	Small water features in built-up environment.	MNDWI has the highest accuracy in extracting small water bodies compared to NDWI and NWI (in DN value image).
			Liu, Yao and Wang (2016)	Landsat 8 OLI	Highland area with many large lakes	Performance of NDWI36 is better in DN value image.

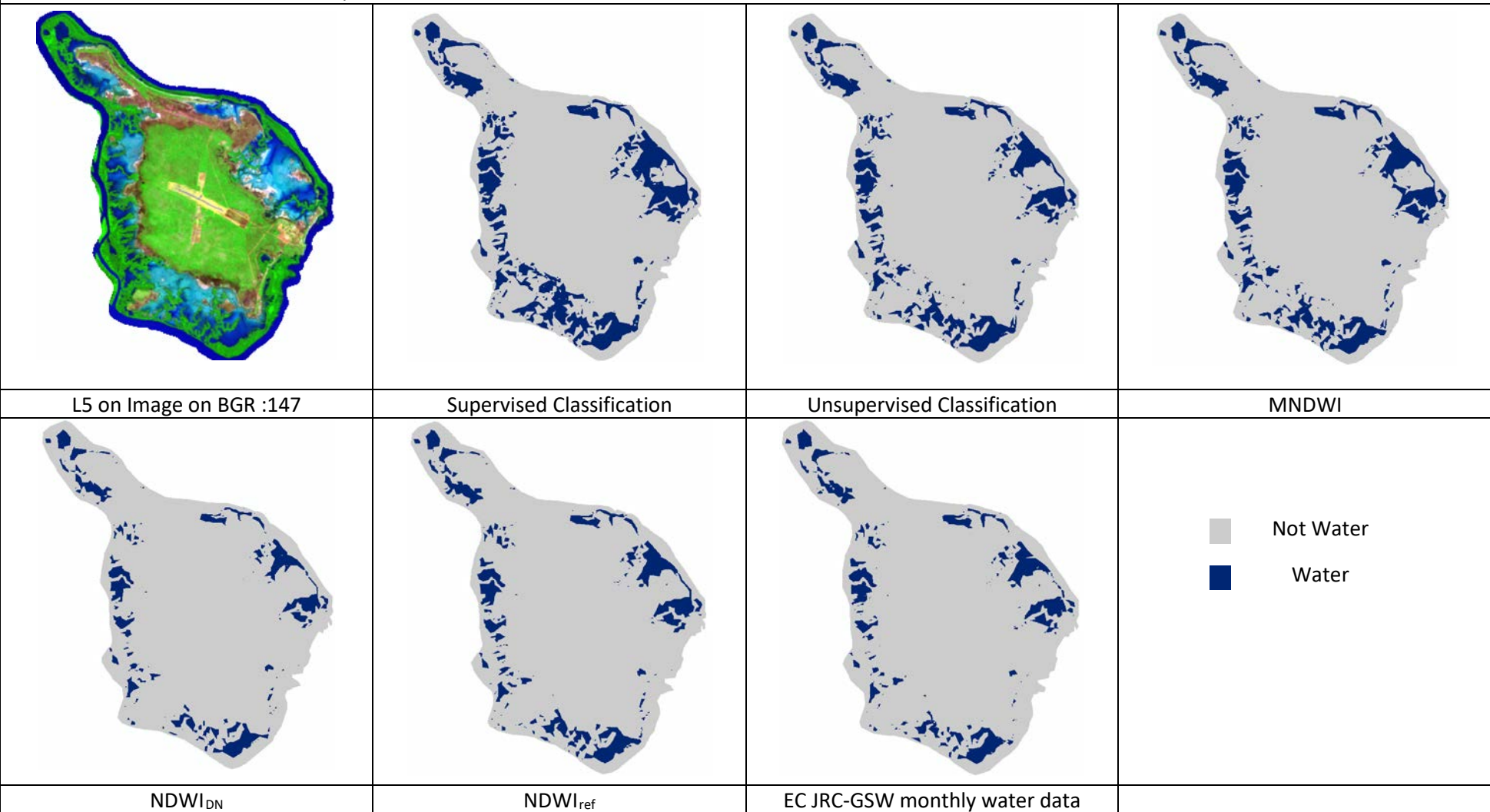
Method	Algorithm	Proposed by	Applied by	Satellite/ Sensor	Study Environment	Remarks
WRI	$WRI = \frac{\text{Green} + R}{\text{NIR} + \text{MIR}}$	Shen and Li (2010)		Landsat TM	Water features in built-up area in mountainous region.	WRI outcome is favourable with NDWI
NWI	$NWI = \frac{\text{Band 1} - (\text{Band 4} + \text{Band 5} + \text{Band 7})}{\text{Band 1} + (\text{Band 4} + \text{Band 5} + \text{Band 7})} * C$	Haibo et al. (2011)	Haibo et al. (2011)	Landsat ETM	Small water bodies in built-up area.	Not efficient to distinguish water and built up areas (in DN value image).
Image classification	Unsupervised Image classification		Haibo et al. (2011)	Landsat ETM	Small water bodies in built-up area.	Fast, easy and high accuracy (in DN value image).

Method	Algorithm	Proposed by	Applied by	Satellite/ Sensor	Study Environment	Remarks
Image classification	Supervised Image classification		Haibo et al. (2011)	Landsat ETM	Small water bodies in built-up area.	Used as the baseline to compare with different methods (in DN value image).
Tasseled cap transformation and wetness index		Wang et al. (2011)	Wang et al. (2011)	Landsat ETM+	Irrigated paddy fields in hilly area, water bodies with aquatic plants	Water classification accuracy was 79 %.
			Gao et al. (2016)	Landsat 8 OLI	Mountainous area and flat plateau area	Better in extracting small water bodies compared to NDWI. (in DN value image)
NDWI –DB	$NDWI - DB = \frac{DN_D - DN_S}{DN_D + DN_S}$	Li et al. (2016)	(Li et al. 2016)	Landsat 8 OLI	Natural mountainous area, plain city and plain country	NDWI –DB extracts small water bodies better when Compared with MNDWI, NEW, and AWEI

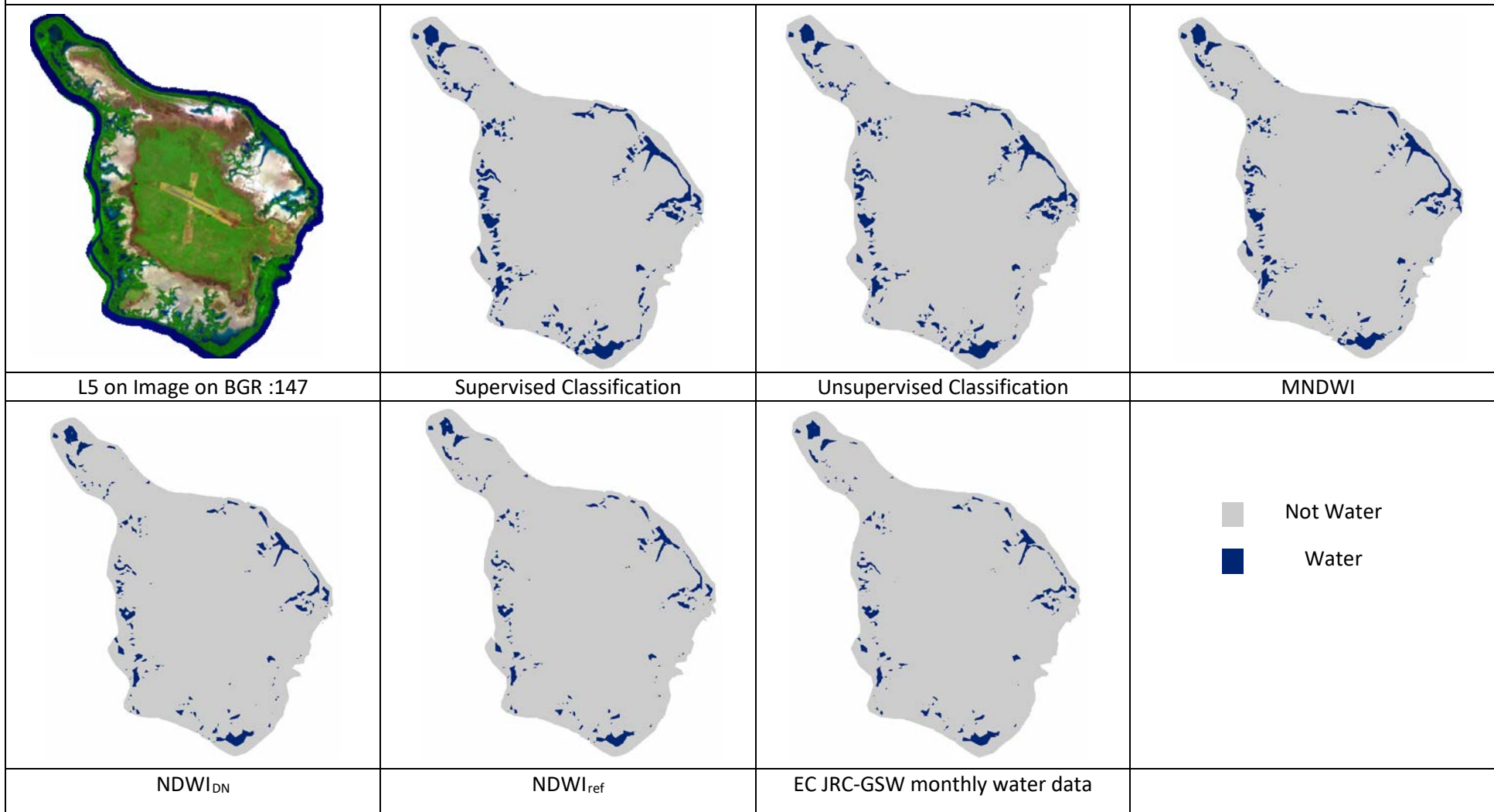
Appendix 2 – Extraction of inundation area by different methods

Extraction of water area on 31 August 1988			
			
L5 on Image on 31 Aug BGR :147	Supervised Classification	Unsupervised Classification	MNDWI
			
NDWI _{DN}	NDWI _{ref}	EC JRC-GSW monthly water data	

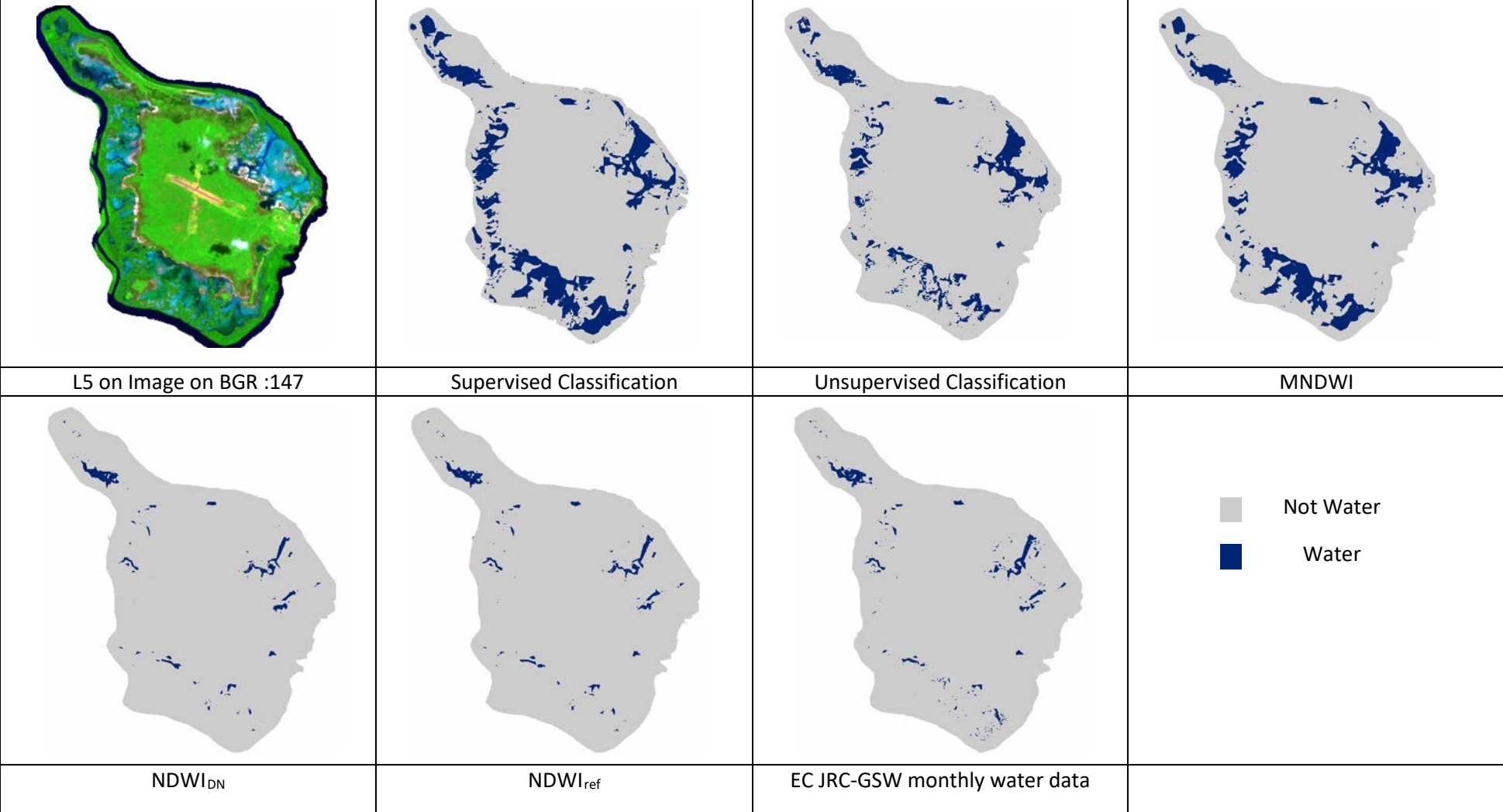
Extraction of water area on 19 Sep 1989



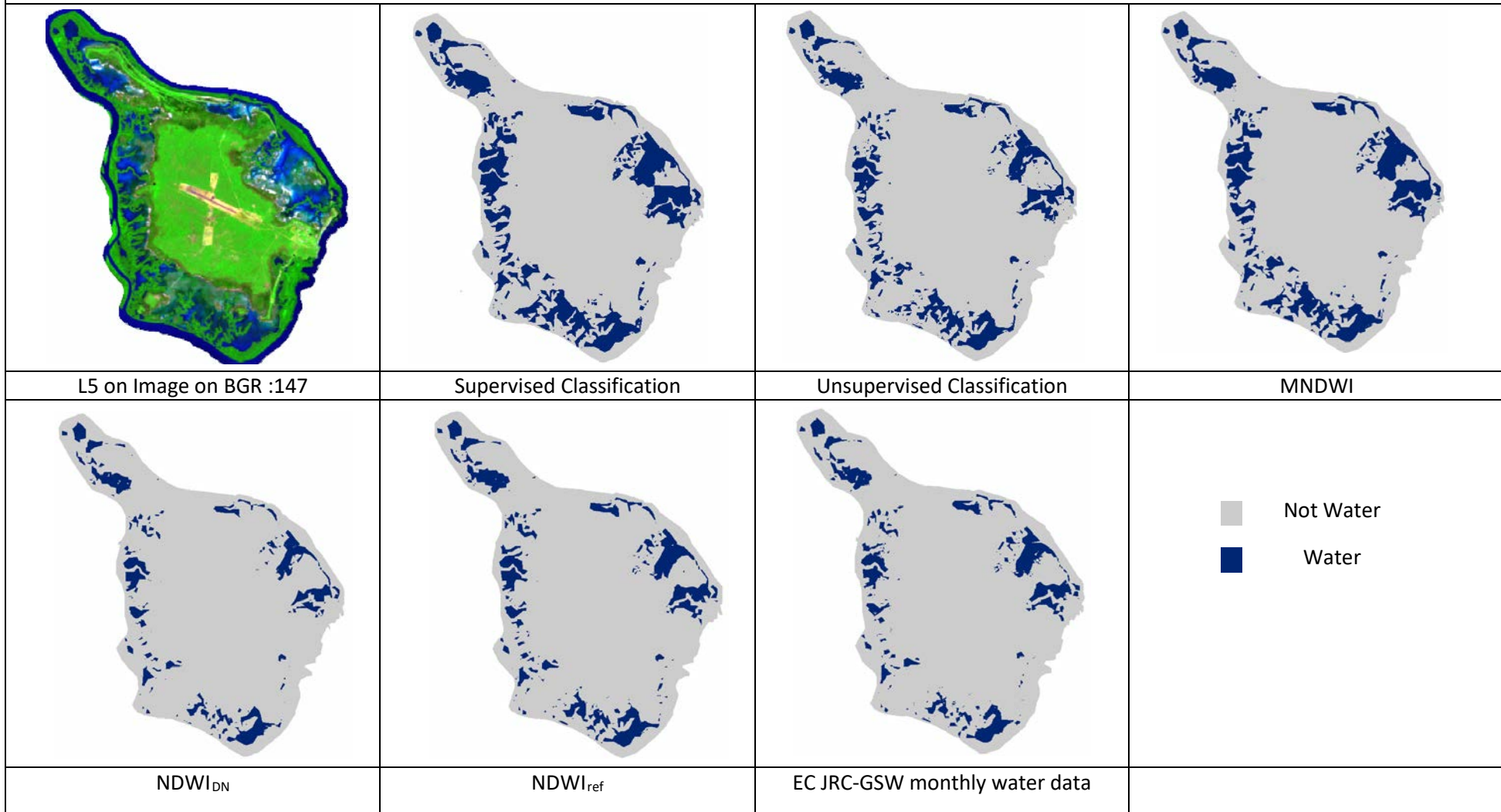
Extraction of water area on 8 Oct 1990



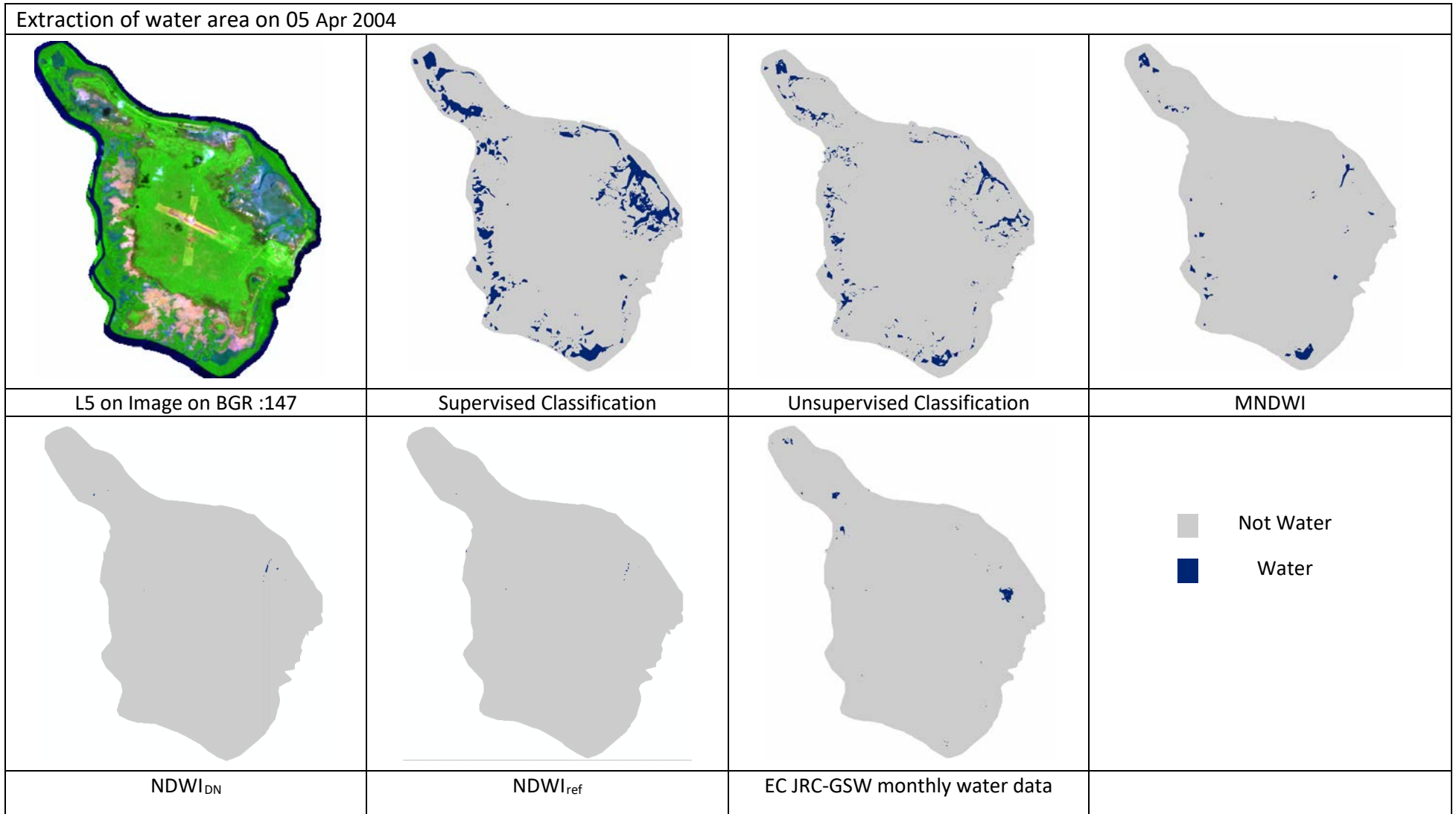
Extraction of water area on 19 Mar 1992



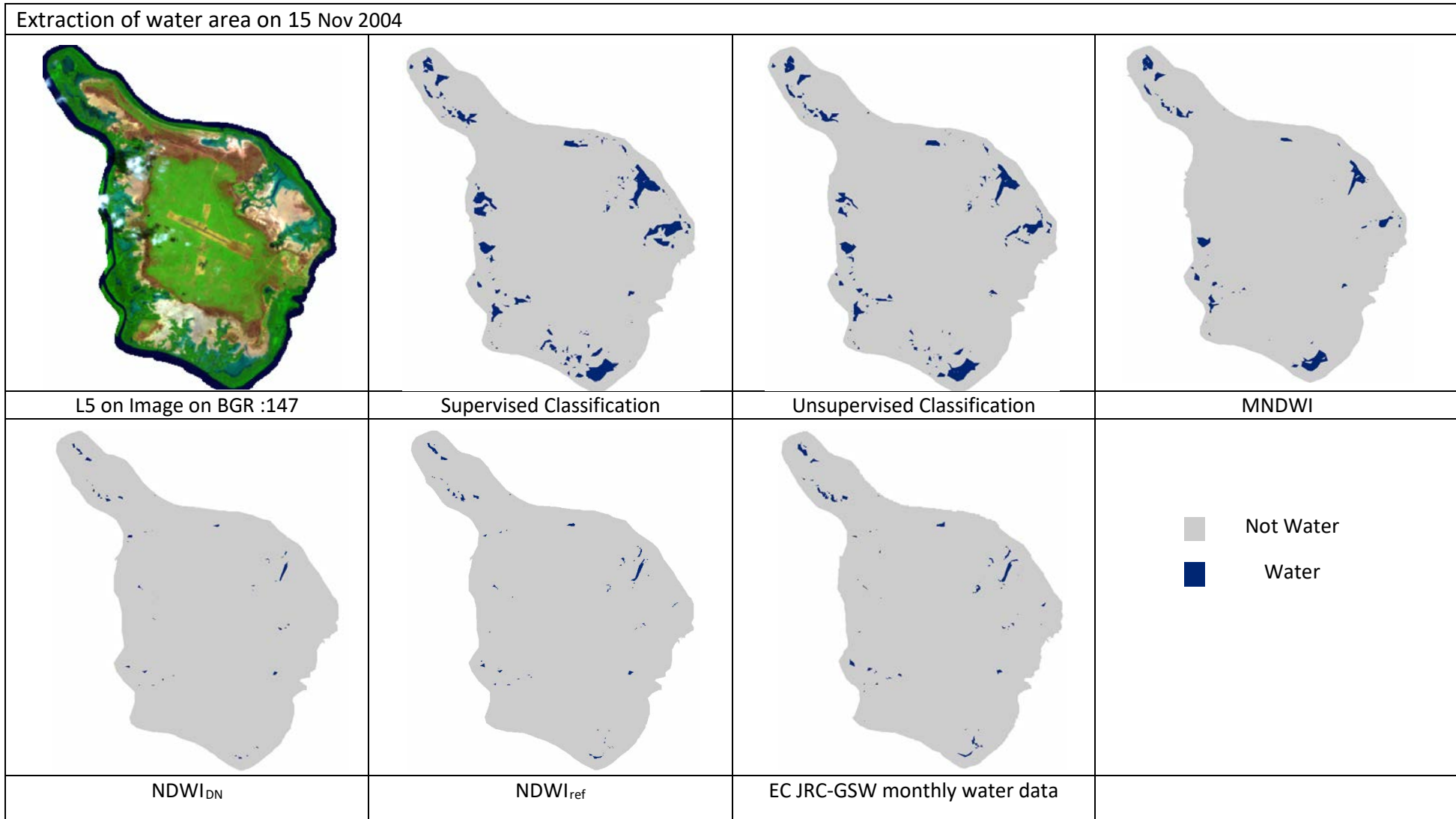
Extraction of water area on 31 Jan 1998



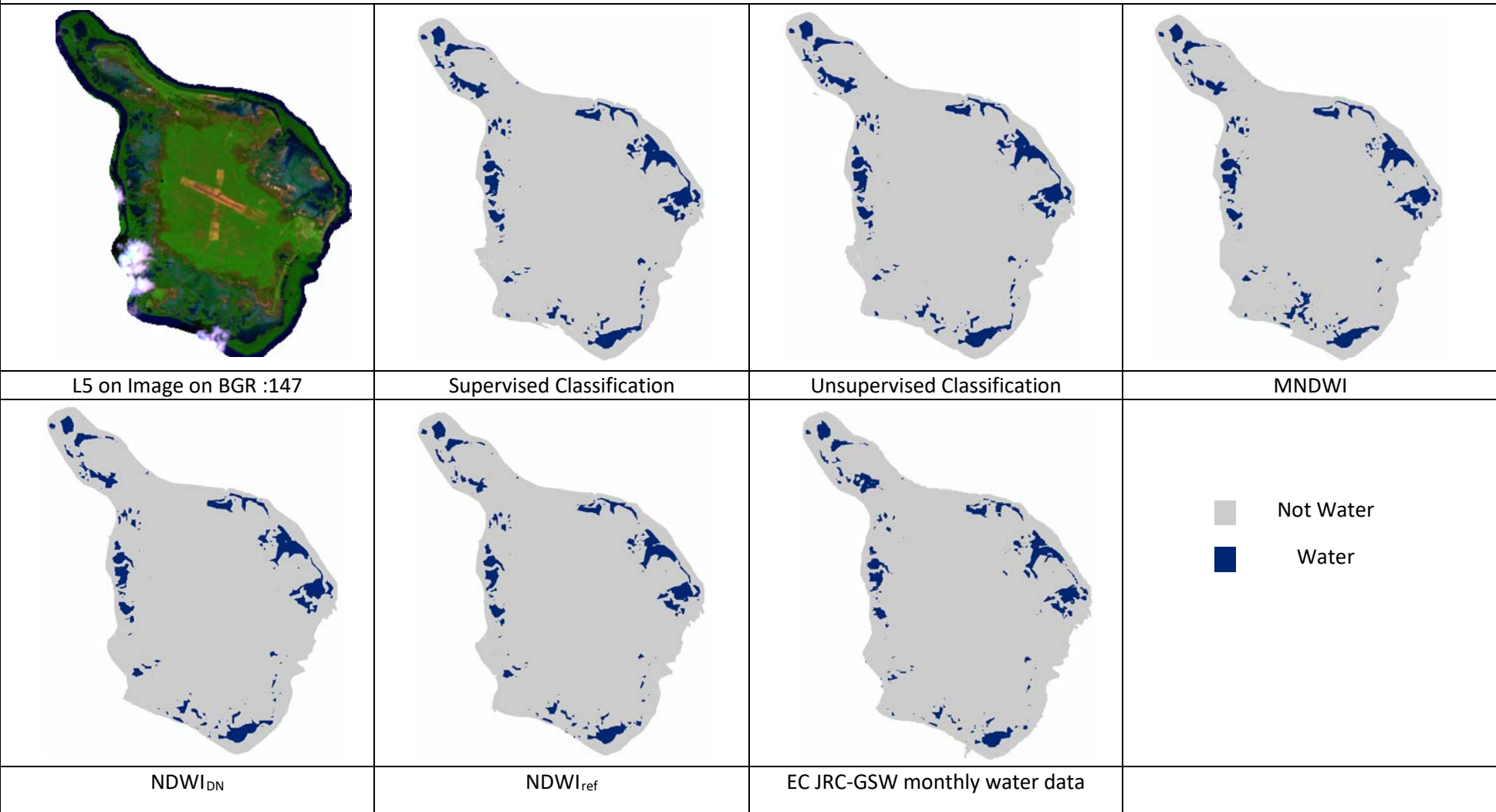
Extraction of water area on 05 Apr 2004



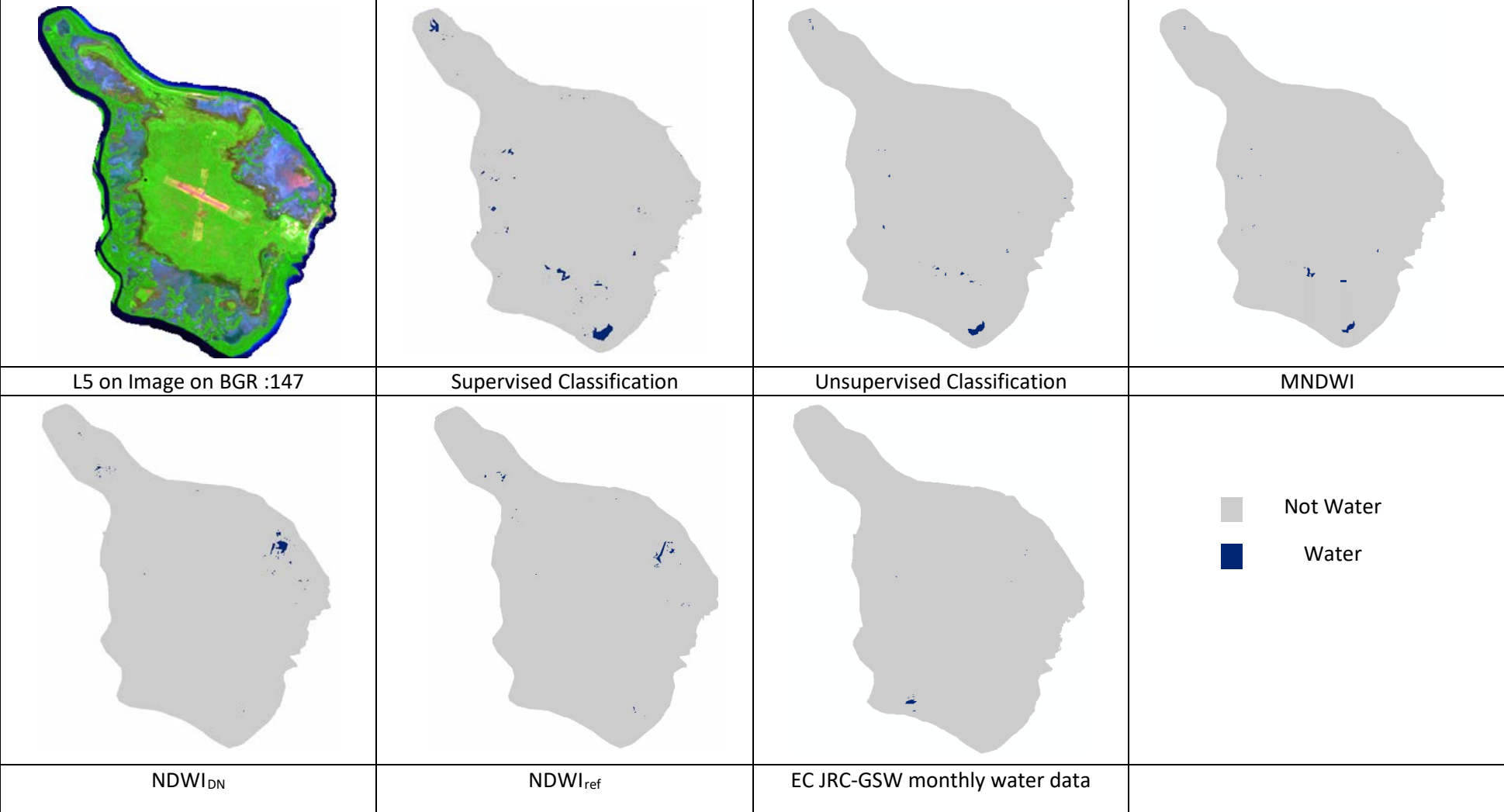
Extraction of water area on 15 Nov 2004



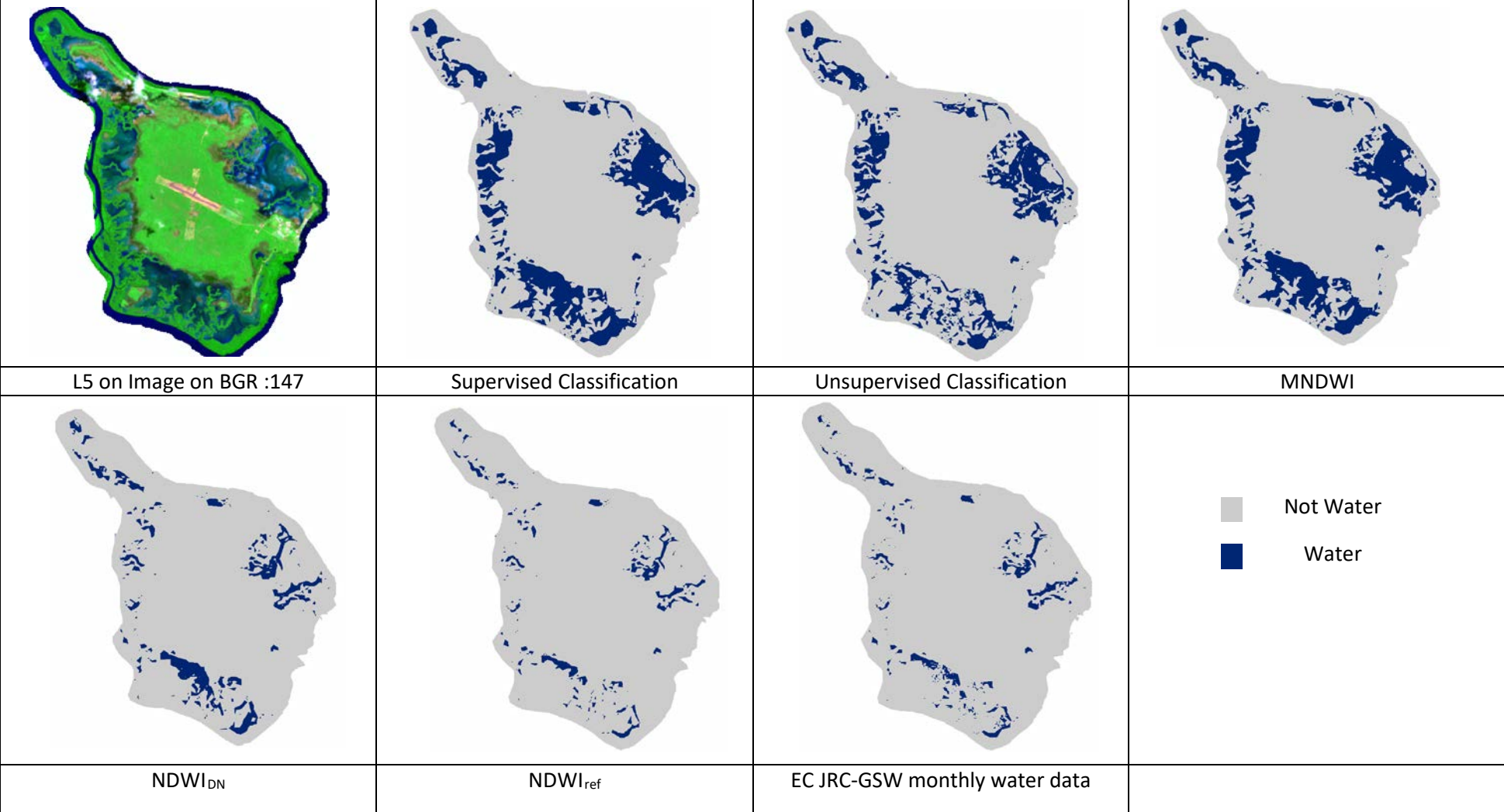
Extraction of water area on 27 Jan 2008



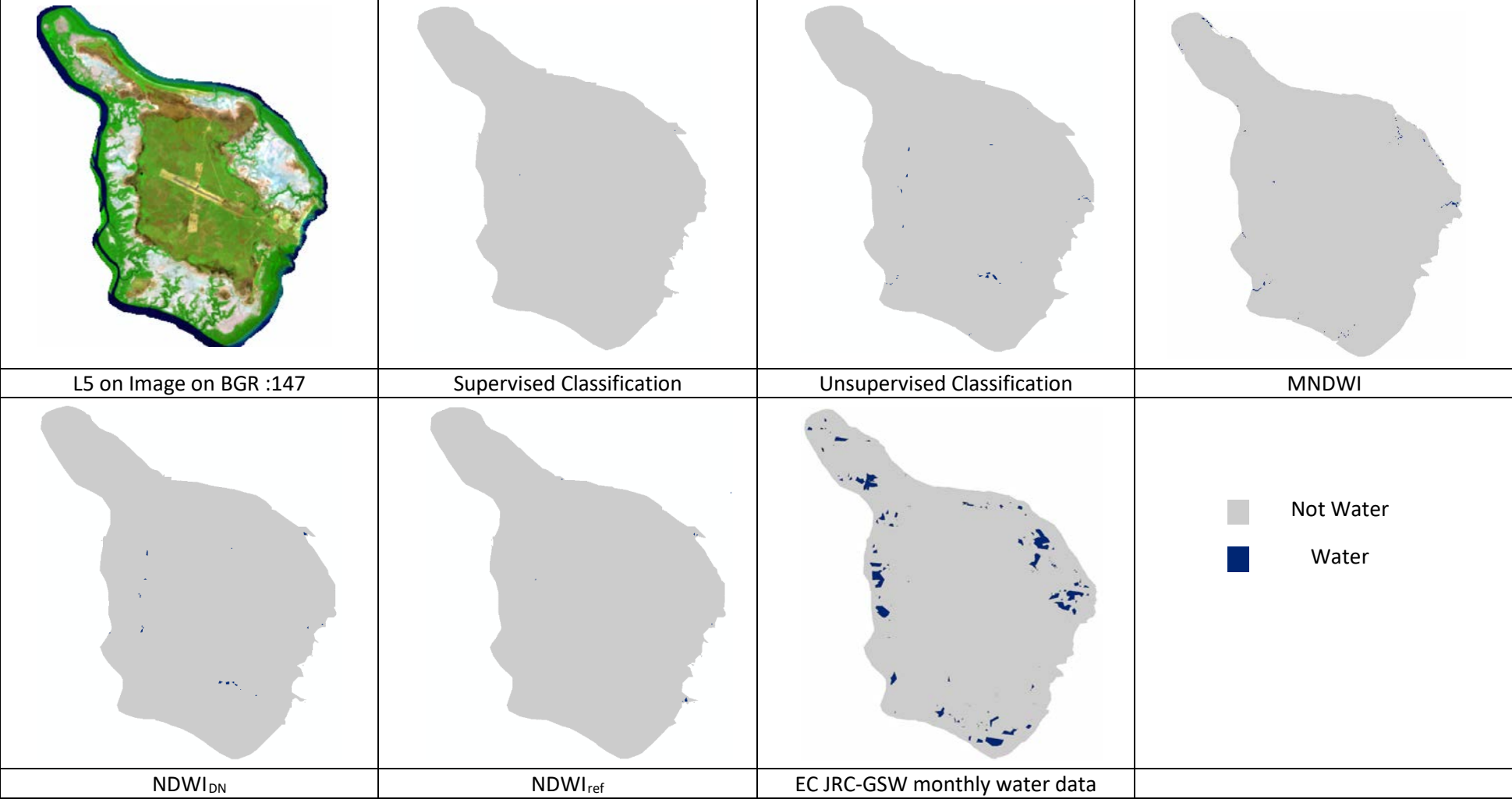
Extraction of water area on 22 Apr 2010



Extraction of water area on 01 Apr 2014



Extraction of water area on 27 Sep 2015



7. REFERENCES

Alparslan, E, Aydöner, C, Tufekci, V & Tüfekci, H 2007, 'Water quality assessment at Ömerli Dam using remote sensing techniques', *Environmental Monitoring and Assessment*, no. 135(1-3), pp. 391-8.

Alsdorf, DE, Rodríguez, E & Lettenmaier, DP 2007, 'Measuring surface water from space', *Reviews of Geophysics*, vol. 45, no. 2, pp. n/a-n/a.

Augustine, P 1960, *Milingimbi Mission Water Resources Survey Field officer's Report*.

Batelaan, O, Banks, E, Post, V, Dean, W, Ellis, J, Wilson, C & Cahill, K 2015, *Near-surface geophysics for water supply investigation for the water constrained aboriginal community of Milingimbi Island, Australia*, Flinders University.

BoM 2016, *Annual Climate Report 2015*, ed. Bo Meteorology, Melbourne, <http://www.bom.gov.au/climate/annual_sum/2013/>.

— 2017, *Australian baseline sea level monitoring project monthly sea level and meteorological statistics*, Bureau of Meteorology Commonwealth of Australia, viewed 15 May 2017, <<http://www.bom.gov.au/oceanography/projects/abslmp/data/monthly.shtml>>.

Chahine, MT 1992, 'The hydrological cycle and its influence on climate', *Nature*, vol. 359, no. 6394, pp. 373-80.

Charles Darwin University 2010, *Milingimbi Water*, Schools of Australian Indigenous Knowledge Systems and Education,.

Chen, X, Vierling, L & Deering, D 2005, 'A simple and effective radiometric correction method to improve landscape change detection across sensors and across time', *Remote Sensing of Environment*, vol. 98, no. 1, pp. 63-79.

Comber, A, Fisher, P, Brunson, C & Khmag, A 2012, 'Spatial analysis of remote sensing image classification accuracy', *Remote Sensing of Environment*, vol. 127, no. Supplement C, pp. 237-46.

Congalton, RG 1991, 'A review of assessing the accuracy of classifications of remotely sensed data', *Remote Sensing of Environment*, vol. 37, no. 1, pp. 35-46.

CRISP 2001, *What is Remote Sensing?*, Centre for Remote Imaging, Sensing and Processing, viewed 23 May 2017, <<https://crisp.nus.edu.sg/~research/tutorial/intro.htm>>.

Du, Y, Teillet, PM & Cihlar, J 2002, 'Radiometric normalization of multitemporal high-resolution satellite images with quality control for land cover change detection', *Remote Sensing of Environment*, vol. 82, no. 1, pp. 123-34.

Erdas 1999, *Erdas Field guide*, Georgia USA.

— 2010, *ERDAS IMAGINE Essentials Tour Guides*, USA.

Fang-fang, Z, Bing, Z, Jun-sheng, L, Qian, S, Yuanfeng, W & Yang, S 2011, 'Comparative Analysis of Automatic Water Identification Method Based on Multispectral Remote Sensing', *Procedia Environmental Sciences*, vol. 11, pp. 1482-7.

Feyisa, GL, Meilby, H, Fensholt, R & Proud, SR 2014, 'Automated Water Extraction Index: A new technique for surface water mapping using Landsat imagery', *Remote Sensing of Environment*, vol. 140, no. Supplement C, pp. 23-35.

Foody, G 2002, 'Status of land cover classification accuracy assessment', *Remote Sensing of Environment*, vol. 80, no. 1, pp. 185-201.

— 2008, 'Harshness in image classification accuracy assessment', *International Journal of Remote Sensing*, vol. 29, no. 11, pp. 3137-58.

Gao, H, Wang, L, Jing, L & Xu, J 2016, 'An effective modified water extraction method for Landsat-8 OLI imagery of mountainous plateau regions', *IOP Conference Series: Earth and Environmental Science*, vol. 34, no. 1, p. 012010.

Gautam, VK, Gaurav, PK, Murugan, P & Annadurai, M 2015, 'Assessment of Surface Water Dynamics in Bangalore Using WRI, NDWI, MNDWI, Supervised Classification and K-T Transformation', *Aquatic Procedia*, vol. 4, pp. 739-46.

Haibo, Y, Zongmin, W, Hongling, Z & Yu, G 2011, 'Water Body Extraction Methods Study Based on RS and GIS', *Procedia Environmental Sciences*, vol. 10, pp. 2619-24.

Henry, JB, Chastanet, P, Fella, K & Desnos, YL 2006, 'Envisat multi-polarized ASAR data for flood mapping', *International Journal of Remote Sensing*, vol. 27, no. 10, pp. 1921-9.

Herrick, JE, Sala, OE & Karl, JW 2013, 'Land degradation and climate change: a sin of omission?', *Frontiers in Ecology and the Environment*, vol. 11, no. 6, pp. 283-.

<https://www.e-education.psu.edu> 2017, *Spectral Response Patterns*, The Pennsylvania State University College of Earth and Mineral Sciences, <https://www.e-education.psu.edu/natureofgeoinfo/c8_p5.html>.

Huang, C, Zan, X, Yang, X & Zhang, S 2016, 'Surface water change detection using change vector analysis', in *36th IEEE International Geoscience and Remote Sensing Symposium, IGARSS 2016*, vol. 2016-November, pp. 2834-7.

Huntington, TG 2006, 'Evidence for intensification of the global water cycle: Review and synthesis', *Journal of Hydrology*, vol. 319, no. 1-4, pp. 83-95.

Idol, T, Haack, B & Mahabir, R 2015, 'Radar and optical remote sensing data evaluation and fusion; a case study for Washington, DC, USA', *International Journal of Image and Data Fusion*, vol. 6, no. 2, pp. 138-54.

Jensen, JR 2014, *Remote Sensing of the Environment, An Earth Resource Perspective*, Second edn, Pearson Education Limited, Essex, England.

Khawlie, M, Shaban, A, Abdallah, C, Darwish, T & Kawass, I 2005, 'Watershed characteristics, land use and fabric: The application of remote sensing and geographical information systems', *Lakes & Reservoirs: Research & Management*, vol. 10, no. 2, pp. 85-92.

Lavery, P, Pattiaratchi, C, Wyllie, A & Hick, P 1993, 'Water quality monitoring in estuarine waters using the landsat thematic mapper', *Remote Sensing of Environment*, vol. 46, no. 3, pp. 268-80.

Lawford, RG 2008, 'Observing surface waters for global change applications', in *Earth Observation of Global Change: The Role of Satellite Remote Sensing in Monitoring the Global Environment*, Springer Netherlands, pp. 169-87.

Leng, G, Huang, M, Voisin, N, Zhang, X, Asrar, GR & Leung, LR 2016, 'Emergence of new hydrologic regimes of surface water resources in the conterminous United States under future warming', *Environmental Research Letters*, vol. 11, no. 11.

Li, Y, Gong, X, Guo, Z, Xu, K, Hu, D & Zhou, H 2016, 'An index and approach for water extraction using Landsat-OLI data', *International Journal of Remote Sensing*, vol. 37, no. 16, pp. 3611-35.

Lillesand, T, Kiefer, R & Chipman, J 2004, *Remote sensing and image interpretation*, Fifth edition, edn, John Wiley & Sons, Inc., Hoboken, NJ.

Liu, Z, Yao, Z & Wang, R 2016, 'Assessing methods of identifying open water bodies using Landsat 8 OLI imagery', *Environmental Earth Sciences*, vol. 75, no. 10, p. 873.

Martinis, S, Kuenzer, C, Wendleder, A, Huth, J, Twele, A, Roth, A & Dech, S 2015, 'Comparing four operational SAR-based water and flood detection approaches', *International Journal of Remote Sensing*, vol. 36, no. 13, pp. 3519-43.

McFeeters, SK 1996, 'The use of the Normalised Difference Water Index (NDWI) in the delineation of open water features', *International Journal of Remote Sensing*, vol. 17, no. 7, pp. 1425-32.

McInnes, KL, Macadam, I, Hubbert, G & O'Grady, J 2013, 'An assessment of current and future vulnerability to coastal inundation due to sea-level extremes in Victoria, southeast Australia', *International Journal of Climatology*, vol. 33, no. 1, pp. 33-47.

Mereuta, M 2015., 'Using Landsat images in mapping and monitoring water bodies in Magura basin', *Aerul si Apa.Componente ale Mediului*, pp. pp. 217-25.

Mimura, N 2013, 'Sea-level rise caused by climate change and its implications for society', *Proceedings of the Japan Academy. Series B, Physical and Biological Sciences*, vol. 89, no. 7, pp. 281-301.

NASA 2013, *Landsat Science*, <<https://landsat.gsfc.nasa.gov/>>.

Oki, T & Kanae, S 2006, 'Global Hydrological Cycles and World Water Resources', *Science*, vol. 313, no. 5790, pp. 1068-72.

Pekel, J-F, Cottam, A, Gorelick, N & Belward, AS 2016, 'High-resolution mapping of global surface water and its long-term changes', *Nature*, vol. 540, no. 7633, pp. 418-22.

Perica, S & Foufoula-Georgiou, E 1996, 'Model for multiscale disaggregation of spatial rainfall based on coupling meteorological and scaling descriptions', *Journal of Geophysical Research: Atmospheres*, vol. 101, no. D21, pp. 26347-61.

Prigent, C, Papa, F, Aires, F, Jimenez, C, Rossow, WB & Matthews, E 2012, 'Changes in land surface water dynamics since the 1990s and relation to population pressure', *Geophysical Research Letters*, vol. 39, no. 8, pp. n/a-n/a.

Richards, JA & Jia, X 1998, *Remote Sensing Digital Image Analysis An Introduction*, Third edn, Springer Verlag, Germany.

Rokni, K, Musa, TA, Hazini, S, Ahmad, A & Solaimani, K 2015, 'Investigating the application of pixel-level and product-level image fusion approaches for monitoring surface water changes', *Natural Hazards*, vol. 78, no. 1, pp. 219-30.

Seyhan, E & Dekker, A 1986, 'Application of remote sensing techniques for water quality monitoring', *Hydrobiological Bulletin*, vol. 20, no. 1-2,, pp. 41-50.

- Shen, L & Li, C 2010, 'Water body extraction from Landsat ETM+ imagery using adaboost algorithm', in *2010 18th International Conference on Geoinformatics*, pp. 1-4.
- Sohn, Y & Rebello, NS 2002, 'Supervised and Unsupervised Spectral Angle Classifiers', *Photogrammetric Engineering & Remote Sensing*, vol. 68, no. 12, pp. 1271-80.
- Song, C, Woodcock, CE, Seto, KC, Lenney, MP & Macomber, SA 2001, 'Classification and Change Detection Using Landsat TM Data: When and How to Correct Atmospheric Effects?', *Remote Sensing of Environment*, vol. 75, no. 2, pp. 230-44.
- USGS 2016, *LANDSAT 8 (L8) DATA USERS HANDBOOK*, Department of the Interior U.S. Geological Survey, <<https://landsat.usgs.gov/>>.
- 2017, *Product guide Landsat 8 surface reflectance code (LASRC) product*.
- 2017, *What are the band designations for the Landsat satellites?*, viewed 02 July 2017, <<https://landsat.usgs.gov/>>.
- Van Der Meer, FD & De Jong, SM 2001, *Imaging Spectrometry Basic Principles and Prospective Applications*, vol. 4, Remote sensing and digital image processing, Kluwer Academic Publishers, The Netherlands.
- Vermote, E, Justice, C, Claverie, M & Franch, B 2016, 'Preliminary analysis of the performance of the Landsat 8/OLI land surface reflectance product', *Remote Sensing of Environment*, vol. 185, no. Supplement C, pp. 46-56.
- Vorosmarty, CJ, Green, P, Salisbury, J & Lammers, RB 2000, 'Global Water Resources: Vulnerability from Climate Change and Population Growth', *Science*, vol. 289, p. 284.
- Wang, Y, Ruan, R, She, Y & Yan, M 2011, 'Extraction of Water Information based on RADARSAT SAR and Landsat ETM+', *Procedia Environmental Sciences*, vol. 10, pp. 2301-6.
- Wen, X-P & Yang, X-F 2011, 'Monitoring of Water Quality Using Remote Sensing Data Mining', in K Funatsu (ed.), *Knowledge-Oriented Applications in Data Mining*.
- Woodgate, M 2013, *Millingimbi Island Hydrogeological Investigations 2013*, Territory Groundwater Services.
- Wu, G & Liu, Y 2014, 'Satellite-based detection of water surface variation in China's largest freshwater lake in response to hydro-climatic drought', *International Journal of Remote Sensing*, vol. 35, no. 11-12, pp. 4544-58.

Xia, J, Duan, Q-Y, Luo, Y, Xie, Z-H, Liu, Z-Y & Mo, X-G 2017, 'Climate change and water resources: Case study of Eastern Monsoon Region of China', *Advances in Climate Change Research*, vol. 8, no. 2, pp. 63-7.

Xu, H 2006, 'Modification of normalised difference water index (NDWI) to enhance open water features in remotely sensed imagery', *International Journal of Remote Sensing*, vol. 27, no. 14, pp. 3025-33.

Zhou, C, Luo, J, Yang, C, Li, B & Wang, S 2000, 'Flood Monitoring Using Multi-Temporal AVHRR and RADARSAT Imagery', *Photogrammetric Engineering & Remote Sensing*, vol. Vol. 66, , no. No. 5, , pp. pp. 633-8.

Zhou, Y, Dong, J, Xiao, X, Xiao, T, Yang, Z, Zhao, G, Zou, Z & Qin, Y 2017, 'Open Surface Water Mapping Algorithms: A Comparison of Water-Related Spectral Indices and Sensors', *Water (Switzerland)*, vol. 9, no. 4, p. 256.